Materials Advances

ROYAL SOCIETY OF CHEMISTRY

REVIEW

View Article Online
View Journal | View Issue

Cite this: *Mater. Adv.*, 2026, 7, 3031

Tailoring carbon nanomaterial architectures for CO_2 capture: structure–property relationships, surface engineering, and future perspectives

Jagdeep Singh, †*[a] Ashish Gupta, †[b] Zhiqi Zhu, [c] Santosh K. Tiwari [d] and A. S. Dhaliwal[e]

The rapid rise in atmospheric CO_2 concentrations, now exceeding 420 ppm, necessitates the urgent deployment of scalable carbon capture, utilization, and storage (CCUS) technologies to mitigate global warming. This review offers a comprehensive analysis of carbon nanomaterials (CNMs) as a transformative class of adsorbents, providing a sustainable alternative to energy-intensive amine scrubbing. CNMs span all dimensional regimes, ranging from zero-dimensional (0D) fullerenes and carbon dots, through one-dimensional (1D) carbon nanotubes and two-dimensional (2D) graphene, to three-dimensional (3D) hierarchical foams, which exhibit exceptional physicochemical properties, notably high specific surface areas and highly tunable pore architectures. Various surface engineering approaches, including tuning surface chemistry and pore architecture and heteroatom functionalization, have been explored to enhance adsorption capacity and selectivity, as well as enable multiple regeneration cycles. Through structure–property–performance analysis, it has been concluded that ultra-micropores (<0.7 nm) are favorable, which further enhance adsorption capacity at low pressures, the isosteric heat of adsorption (35–50 kJ mol^{-1}), and cycling stability. Furthermore, the surface modification of CNMs through nitrogen doping, amine functionalization, and hybrid composite engineering achieved CO_2 adsorption capacities of up to ~9 mmol g^{-1} at modest pressures, along with low-temperature regeneration (<100 °C), resulting in energy-efficient performance. This article also outlines ongoing challenges and research frontiers, emphasizing the need to enhance the CO_2/N_2 selectivity ratio, develop sustainable and scalable synthesis methods, incorporate techno-economic evaluations, and bridge laboratory-scale performance with industrial implementation. Later, a comparative analysis of the modified CNMs with standardized MOFs in terms of capacity is also discussed in detail. This analysis synthesizes current advancements and identifies knowledge gaps, offering a prospective outlook on the development and future trajectories of CNM-based adsorbents in greenhouse gas mitigation and achieving net-zero emission targets.

Received 3rd December 2025,
Accepted 7th January 2026

DOI: 10.1039/d5ma01408e

rsc.li/materials-advances

1. Introduction

The global energy needs are still mainly met by the burning of fossil fuels, which make up 65–70% of the world's energy use.[1–4] The substantial reliance on carbon-intensive energy sources, including power plants, biomass, and bioenergy, has led to an increase in CO_2 emissions, resulting in atmospheric CO_2 concentrations exceeding 420 ppm.[5–7] Such elevated greenhouse gas concentrations have intensified global warming, as reflected in an average rise in the Earth's surface temperature of ~0.06 °C, as shown in Fig. 1(a), underscoring an accelerating climate inequality driven by anthropogenic activities.[8,9] According to the Intergovernmental Panel on Climate Change (IPCC), limiting global warming to below 2 °C, preferably to 1.5 °C above pre-industrial levels, requires not only significant reduction in emissions but also the active removal of CO_2 from the atmosphere.[10–13]

Among the portfolio of negative emission technologies, carbon capture, utilisation, and storage (CCUS) has emerged as a foundation strategy for deep decarbonization.[14–17] CCUS integrates the capture of CO_2 from point sources or the atmosphere

[a] *Department of Physics and Materials Science, Thapar Institute of Engineering and Technology, Patiala, 147004, Punjab, India. E-mail: jagdeep.singh1@thapar.edu; Tel: +91-84279-04455*
[b] *Department of Physics, National Institute of Technology, Kurukshetra, Haryana, 136119, India*
[c] *School of Materials Science and Engineering, Central South University, Changsha 410083, China*
[d] *Centre for New Materials and Surface Engineering, Department of Chemistry, NMAM Institute of Technology, Nitte (Deemed to be University), Nitte, 574110, Karnataka, India*
[e] *Department of Physics, Sant Longowal Institute of Engineering and Technology, Longowal, 148106, Punjab, India*
† These authors contributed equally to this work.

with either its conversion into value-added products or its permanent isolation *via* long-term geological sequestration, thereby enabling substantial reduction in greenhouse gas emissions and supporting net-zero or even net-negative carbon trajectories.[18–23] Reflecting its growing strategic importance, the global CCUS sector has expanded rapidly across all stages of development as shown in

Jagdeep Singh

Dr. Jagdeep Singh received his Bachelor of Science (BSc) degree in 2013 from Panjab University, Chandigarh, followed by a Master of Science (MSc) degree, awarded with a Gold Medal, and a Doctor of Philosophy (PhD) degree from Sant Longowal Institute of Engineering and Technology (SLIET), Longowal, a Deemed-to-be University under the Ministry of Education, Government of India. He is currently serving as an Assistant Professor at the Thapar Institute of Engineering and Technology (TIET), Patiala, India. His research expertise lies in the rational design, scalable synthesis, and functional integration of advanced carbon-based nanomaterials, sustainable biopolymer-derived nanocomposites, and two-dimensional (2D) materials. His work is primarily directed toward next-generation applications in energy storage and conversion, environmental remediation, wearable and flexible electronics, innovative sensing platforms, and multifunctional hybrid devices. His research integrates solid-state physics, nanoscale engineering, and device-level optimization to address critical challenges in sustainability, performance, and scalability.

Ashish Gupta

Dr. Ashish Gupta received his PhD in Engineering Sciences from AcSIR, CSIR National Physical Laboratory, New Delhi, in 2018. He held multiple research positions at the CSIR-NPL and NIT Kurukshetra. His research interests include carbon nanomaterials, electrospun nanofibers, graphene/MXene-based composites, and their applications in energy storage, water purification, sensing, and EMI shielding. He has authored over 45 peer-reviewed journal articles, holds two international patents, and has an h-index of 23.

Santosh K. Tiwari

Dr Santosh K. Tiwari holds a PhD in graphene-based polymer nanocomposites from IIT Dhanbad, India. He has over five years of international research experience at leading labs, including HSCL in South Korea, the Guangxi Institute of Technology, at Guangxi University, China, and the University of Warsaw, Poland, where he served as a Scientist NAWA Fellow. He has published more than 90 SCI indexed articles (h-index 32) and four patents. His academic contributions also include guest-editing special issues, delivering invited talks, chairing conference sessions, and presenting his work at numerous national and international scientific platforms. Dr Tiwari currently serves as an associate professor and heads the Centre for New Materials and Surface Engineering (CNMSE) at NMAMIT, Nitte. In addition, he is a visiting faculty member at Guangxi University, Nanning, China. His research interests span Carbon materials, large scale nanosizing strategies, 2D nanomaterials, materials for extreme environments, and polymeric nanoscale systems.

A. S. Dhaliwal

Dr. A. S. Dhaliwal is a Professor and Head of the Department of Physics at the Sant Longowal Institute of Engineering and Technology (SLIET), Longowal, Punjab, India. He obtained his MSc in Physics (1985) and MPhil (Materials Science, 1986), and PhD (Atomic Physics, 1991) from Punjabi University, Patiala. His research spans nuclear and experimental physics, materials synthesis and characterization, polymers, nanocomposites, radiation detection, protection, and spectroscopy. He has published extensively in peer-reviewed journals and has received the Career Award for Young Teachers from AICTE, New Delhi (2001). He has authored over 100 peer-reviewed journal articles and has an h-index of 27.

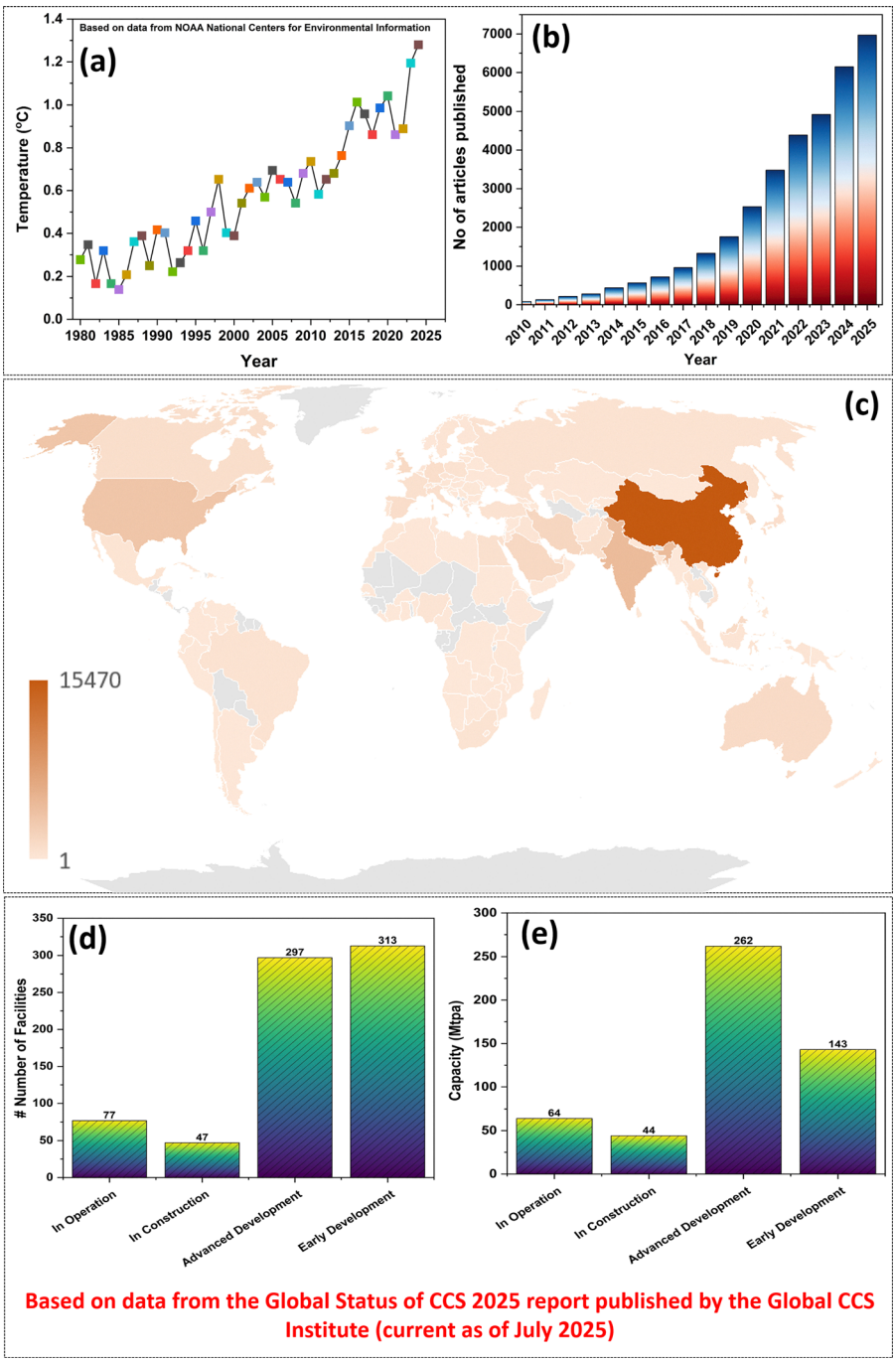

Fig. 1 (a) Global average upsurge in surface temperature (data taken from NOAA National Centers for Environmental Information), (b) annual trend (15 years) in the number of publications based on data retrieved from Scopus with keywords "CO_2 capture using carbon-based nanomaterials" and (c) global heat map showing the distribution of CO_2 capture and sequestration-related publications by the top countries over 25 years, (d and e) significant expansion in the number of facilities and total capture capacity across operational, construction, and advanced development stages (analysis draws on data reported in the Global Status of CCS 2025 by the Global CCS Institute, current as of July 2025).

Fig. 1(d and e).[24] As of July 2025, 77 facilities were operational worldwide, with a combined capture capacity of 64 Mtpa. The broader project pipeline included 734 facilities with a total capacity of 513 Mtpa. Notably, capacity at the FEED stage increased from 180 to 262 Mtpa, while 44 Mtpa was under active construction, signalling a clear shift toward large-scale deployment. Keeping the importance in mind, researchers marked a global surge in publications on CCUS, as depicted in Fig. 1(b), which highlights the country-wise distribution and temporal evolution of research in this domain.

Various materials, including liquid sorbents (chemical solvents such as amines, monoethanolamine, and diethanolamine), solid adsorbents (alumina, zeolites, and metal–organic frameworks (MOFs)), and membranes (*e.g.*, polysulfone and polyimides), are

being utilised in CCUS. Among these, CNMs have emerged as strong alternatives to the materials mentioned above for CO_2 capture due to their exceptionally high surface area, superior structural engineering, lower energy demands for regeneration, enhanced operational flexibility, and cost-effectiveness.[25–27] Unlike zeolites with rigid topologies and limited performance, they offer a useful platform where pore structures and functionalities can be precisely engineered for diverse capture needs.[28–31] Their performance advantages are evident across key parameters, including surface areas of up to 2688 $m^2\ g^{-1}$, a CO_2 uptake of ~8–9 mmol g^{-1}, and superior adsorption capacity.[32,33] They also achieve exceptional CO_2/N_2 selectivity and enable low-energy regeneration at temperatures below 100 °C, compared to 300–500 °C required for zeolites. Additionally, their tolerance to humidity levels below 5% contributes to increased reliability in practical applications.[34,35] These materials exhibit superior cycling stability and effective thermal conductivity, facilitating efficient heat management and ensuring reliable long-term performance. These attributes lead to energy savings, lower operational costs, and improved process stability. CNMs demonstrate cost-effectiveness and scalability due to their ability to be synthesised from readily available precursors, including biomass and polymers.[36] Their customizable pore structures and functional groups enable the tailoring of adsorption energetics and kinetics, while their chemical inertness and mechanical strength ensure that they can withstand harsh industrial environments.

Researchers have explored a broad spectrum of CNMs with different dimensionalities, ranging from 0D to 3D, for CCUS.[37–43] The dimensionality of these materials fundamentally governs key performance parameters, such as specific surface area, pore size distribution, surface functionality, diffusion pathways, and adsorption energetics. While 0D carbons (carbon dots and fullerenes) lack intrinsic porosity and contribute mainly through surface functionalization and 1D carbons (CNTs) suffer from bundling-induced porosity loss and diffusion limitations, 2D materials (graphene, GO, and rGO) offer improved surface accessibility and CO_2/N_2 selectivity. Still, they are constrained by irreversible restacking and moisture sensitivity. In contrast, 3D hierarchical carbon architectures effectively combine ultra-micropores for strong CO_2 confinement with meso- and macroporous networks for rapid mass transport, resulting in superior adsorption capacity, selectivity, and low regeneration energy. Consequently, although lower-dimensional carbons provide valuable chemical tunability, 3D hierarchical CNMs emerge as the most promising platforms for scalable and industrially relevant CO_2 capture, particularly under flue gas and direct air capture (DAC) conditions.

Advanced functionalization techniques, including nitrogen doping, surface oxidation, and amine grafting, are extensively employed to improve CO_2 capture in CNM-based adsorbents by modifying surface chemistry and adsorption energetics.[44–46] Nitrogen doping introduces Lewis basic sites, which enhance CO_2 interactions, thereby improving capacity, selectivity, and cycling stability.[47] The controlled surface oxidation enhances CO_2 selectivity, although excessive oxidation increases the sensitivity to moisture.[32] Amine functionalization enables the highest CO_2 uptake through reversible carbamate formation.[48,49] However, it is constrained by pore blockage and stability challenges at elevated loadings.[50] Consequently, synergistic combination of heteroatom doping with moderate oxidation or reduced amine loading on hierarchical carbon frameworks offers the most balanced and scalable CCUS performance.

In response to international climate agreements, numerous governments have made CCUS a key component of their plans to reduce carbon emissions. The US has endorsed its commitment to the Paris Agreement and plans to reach net-zero emissions by 2050.[51] The federal government is investing a significant amount of money in the research and development of CCUS. China, which releases the most carbon dioxide into the atmosphere, aims to be carbon neutral by 2060 and has begun constructing large-scale collection facilities.[51] India aims to reduce the emission intensity of its GDP by 45% by 2030 and achieve net-zero emissions by 2070. The emphasis will be on biomass-derived carbon sources, including biochar.[51] The European Union, Japan, and South Korea also aim to accelerate the adoption of CCUS by implementing stringent rules and regulations.[51]

It is prominent that there has been an exponential increase in research papers related to CNM-based materials for CO_2 collection and conversion in recent years, as illustrated in Fig. 1(b). This increase suggests that an increasing number of academics and businesses are interested in developing multifunctional absorbents that can effectively capture CO_2 and convert it into valuable products, such as fuels, chemicals, and construction materials.[52–54] However, turning new ideas from the lab into business remains a significant challenge. Some of the main problems are improving pore structures for selective CO_2 uptake at low partial pressures, enhancing the durability of materials in real-world conditions (such as moisture and temperature fluctuations), reducing the costs of synthesis and regeneration, and improving cycling stability over time.[55] A significant obstruction is the lack of a holistic structure–property–performance paradigm, which hinders the predictive design of materials and their scalability.[52,56] Additionally, a systems-level approach is necessary for successful integration into industrial processes.[38] This approach includes process engineering, techno-economic analysis, and life cycle evaluation. It is essential to determine how much these materials can genuinely benefit the environment and how much carbon they emit throughout their entire life cycle.

The number of review articles on CCUS in the literature has grown substantially, presenting a chronological overview of various reviews published over the past four years, along with their primary focus areas, as shown in Table 1.

Previously published articles in the literature provide insight into process-level engineering, offering detailed technological summaries. However, these studies offer limited specific information about materials. Along with zeolites and MOFs, CNM-based adsorbents such as activated carbon, biochar, CNTs, MWCNTs, fullerenes, GO, rGO, and carbon dots are emerging nanomaterials with structural diversity and tunability. The existing literature reveals a significant gap in the absence of a dimensionality-driven (0D–3D) framework that systematically correlates diffusion behaviour, adsorption kinetics, and CO_2 affinity with the underlying architecture of CNMs. Furthermore,

Table 1 Chronological overview of key CCUS review articles (2021–2024), highlighting their primary technological focus and application domains

Year	Focus of the article	Source
2021	Critical technology review: an in-depth update on post-combustion technologies (absorption, adsorption, membrane, and cryogenic), emphasizing hybrid systems and future directions for decarbonization	Raganati *et al.*[57]
2021	Adsorption-based post-combustion capture: a focused review on adsorption technologies, specifically evaluating adsorbent materials (activated carbons, zeolites, and MOFs), gas–solid contacting systems (fixed/fluidized beds), and regeneration strategies (PSA and TSA)	Raganati *et al.*[58]
2022	Amine-functionalized solid materials: solid porous supports (silica, carbons, MOFs, and polymers), comparing their CO_2 adsorption capacities and regeneration performance	Hack *et al.*[59]
2022	Energy sector applications: a review of capture technologies (pre-combustion, oxy-fuel, and post-combustion) explicitly applied to energy sectors, with a particular focus on thermoelectric plants and bioenergy (ethanol plants).	Sílvio *et al.*[60]
2023	20-year reflective: an examination of CO_2 capture methods developed over the last two decades, covering absorption, gas–solid reactions, adsorption, cryogenic processes, membrane processes, and natural inclusion	Kammerer *et al.*[61]
2023	Process intensification: a review focusing on novel technologies to reduce costs in post-combustion capture, including rotating packed beds, loop reactors, mop fans, and advanced solvent developments	Joel *et al.*[62]
2023	Power plant scenarios: an assessment identifying post-combustion capture as the best option for retrofitting power plants and proposing future scenarios such as ultrasound regeneration and synergistic solvent effects	Alalaiwat *et al.*[63]
2024	Capture and mineral storage: a review linking CO_2 capture (liquid, solid, microencapsulated) directly with mineral storage solutions (*in situ* and *ex situ* mineralization)	Liu *et al.*[64]
2024	Hybrid configurations: a review of process developments in post-combustion capture from power plant flue gases, identifying combined two-stage hybrid configurations as the optimal route for efficiency and purity	Obi *et al.*[65]
2024	Environmental assessment: a comprehensive review of direct and indirect capture methods (including reforestation) with a strong focus on environmental impact assessment (*e.g.*, global warming potential) and economic sustainability	Goren *et al.*[66]

the integration of capture-to-utilization remains underexplored, particularly in existing reviews, and is notably absent in the catalytic conversion of captured CO_2 using metal-free carbon-based catalysts, which are predominantly focused on capture or storage alone. Despite their importance for low-pressure and DAC applications, key mechanistic aspects, including the role of ultra-microporosity (<0.7 nm), optimal adsorption enthalpy (35–50 kJ mol^{-1}), and heteroatom-induced Lewis acid–base interactions, remain insufficiently explored. Moreover, many existing reviews continue to rely on pre-2020 paradigms, overlooking recent advances in functionalized, hybrid CNMs.

Hence, by addressing these gaps, the present review adopts a materials science-centric perspective that explores the fundamentals and current advancements in CNM-based materials for CO_2 capture, with a focus on nanostructured carbon families (0D to 3D). We have extensively studied their structural, surface, morphological, and functional attributes and connected these behaviors with CO_2 adsorption efficacy. We also discussed more advanced techniques for modifying materials, such as physical activation, heteroatom doping, and surface functionalization, and gained an understanding of the mechanisms that improve CO_2 capture efficiency. Moreover, in real-world situations, the detailed comparison of different CNMs for CO_2 capture performance has been explored. The complicated challenges and their portable solutions are also discussed in detail to align with global decarbonization objectives. This approach positions CNMs as versatile platforms for global carbon dioxide management and next-generation CCUS technologies.

2. CCUS: a historical perspective and a key climate mitigation strategy

The foundations of CO_2 capture and climate science were laid as early as 1896, when Svante Arrhenius published the first quantitative study linking atmospheric CO_2 levels to global temperature increases.[67] Later, in the 1920s and 1930s, industrial interests arose around this issue and secured the first patents focused on removing CO_2 from natural gas streams. A breakthrough 1930 patent on amine-based chemical absorption, which laid the groundwork for modern CO_2 capture technologies, led to the first large-scale use of captured CO_2 in the 1970s. In 1972, the world's first commercial enhanced oil recovery (EOR) project (SACROC) using injected CO_2 was developed in Texas. In 1980, pilot-scale studies scientifically validated the feasibility of injecting CO_2 into geological formations. In 1988, the Intergovernmental Panel on Climate Change (IPCC) was established to address the challenge of reducing CO_2 emissions.[68,69] The timelines for CO_2 capture, utilization, and storage technologies are shown in Fig. 2(a). In 1996, the Sleipner Project in Norway became the world's first industrial-scale CCUS operation, successfully storing CO_2 in deep saline aquifers and proving that large-scale climate mitigation was technically achievable. Between 2000 and 2008, global R&D efforts, such as the Salah storage site in Algeria, significantly advanced capture, transport, and storage technologies. Globally, CCUS projects store over 45 million tons of carbon dioxide, equivalent to the emissions of approximately 10 million passenger vehicles, every year. The International Energy Agency (IEA) predicts that CCUS may contribute to a 17% reduction in CO_2 emissions by 2025.

From a materials perspective, the field of CNM-based adsorbents for CO_2 capture has undergone a significant transformation from 1985 to 2025, as shown in Fig. 2(b), transitioning from basic activated carbons, which primarily rely on weak physisorption, to sophisticated, multifunctional systems designed for low-energy and DAC. Initial activated carbons, while chemically stable, exhibited restricted uptake (<1.5 mmol g^{-1}), thereby underscoring the significance of ultramicroporosity. The discovery of CNTs and fullerenes in the 1990s introduced nanoscale carbon architectures, thereby illuminating the impact of

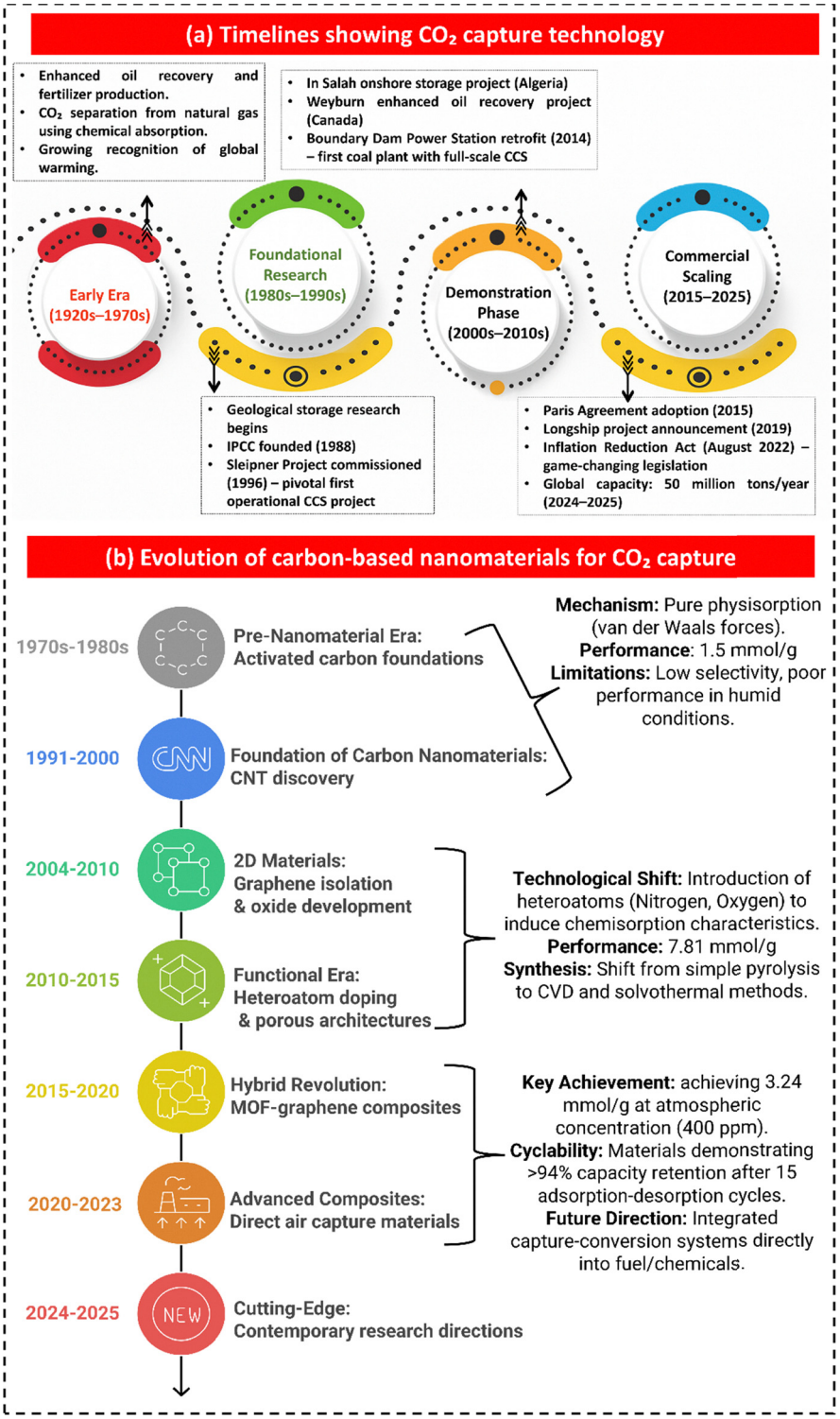

Fig. 2 (a) Chronological overview of the evolution of CO_2 capture technologies (1920–2025), highlighting the accelerated emphasis on CCUS strategies in recent decades for large-scale emission mitigation; (b) Timeline depicting the progression of CNM-based materials for CO_2 capture, emphasizing key material innovations, mechanistic transitions, and performance milestones from activated carbons to advanced direct air capture (DAC) oriented systems (1970–2025).

dimensionality on adsorption processes.[70] Furthermore, the isolation of graphene and the subsequent development of graphene oxide between 2004 and 2010 facilitated the creation of atomically thin, functionalized surfaces with enhanced CO_2 affinity, despite the performance limitations imposed by restacking.[71] The period from 2010 to 2015 witnessed further progress, particularly in heteroatom doping and hierarchical porosity, marking a functional era and resulting in record capacities. Based on research spanning from 2015 to 2020, especially on carbon–MOF composites, it was found that these composites significantly improved

Table 2 Evolution of key CO_2 capture performance metrics, highlighting improvements in capacity, energy efficiency, selectivity, stability, cycling speed, and cost with the transition to advanced CNM-based and hybrid materials

Metric	Year					
	1990	2000	2010	2015	2020	2025
CO_2 capacity (mmol g^{-1})	<1	0.8–1.2	2–3	4–5	6–8	9+
Energy (kJ mol^{-1})	150–185	120–160	60–100	40–50	25–40	12–20
CO_2/N_2 selectivity	2–5	3–8	10–25	30–50	60–85	100–150
Cycle time	Hours	Hours	30–60 min	10–30 min	5–15 min	<5 min
Thermal stability	Limited	Moderate	Good	Good-excellent	Excellent	Excellent
Humidity tolerance	Poor	Poor	Moderate	Good	Excellent	Excellent
Cost ($ per ton CO_2)	>500	300–500	100–200	80–150	150–300	100–300

both adsorption capacity and kinetics, achieving values as high as 9.02 mmol g^{-1} (GrO@HKUST-1 composites) and simultaneously enhancing stability and regenerability.[72] Subsequently, from 2020 onwards, CNMs have been re-engineered for DAC. The comparative analysis of key performance metrics for CO_2 capture materials is highlighted in Table 2.[57,59,73–84]

The CCUS process consists of three main steps and is illustrated in Fig. 3. The described process functions as a continuous chemical looping system, wherein an amine-based solvent selectively sequesters CO_2 from flue gas, followed by its release for subsequent compression and storage.[85–87] The primary stages, as depicted in the accompanying figure, along with their respective technical difficulties, are outlined below:

Flue gas intake and cooling: initially, the flue gas, which exits the power plant and primarily consists of N_2, CO_2, water vapor, and minor impurities (SO_x, NO_x, and particulates), is cooled to approximately 40–50 °C.[88] This cooling step is crucial for optimizing the amine/CO_2 reaction, as its efficiency diminishes significantly at higher temperatures. Significant challenges encompass solvent poisoning due to SO_x/NO_x, which leads to the formation of heat-stable salts, and particulate fouling, which intensifies pressure drop and increases maintenance requirements.

CO_2 absorption (absorber column): following cooling, the gas ascends through the absorber column, while a lean amine solution is introduced from the top. CO_2 is chemically absorbed through chemisorption, resulting in a CO_2-saturated solvent and a processed flue gas. Significant challenges stem from the oxidative breakdown of amines when exposed to oxygen, corrosion caused by the byproducts of this degradation, and reaction kinetics that necessitate large column dimensions and substantial capital expenditures.[89]

Solvent regeneration (stripper/regenerator): the CO_2-laden amine is subjected to heating (generally between 100 and 120 °C) to reverse the absorption process, thereby releasing

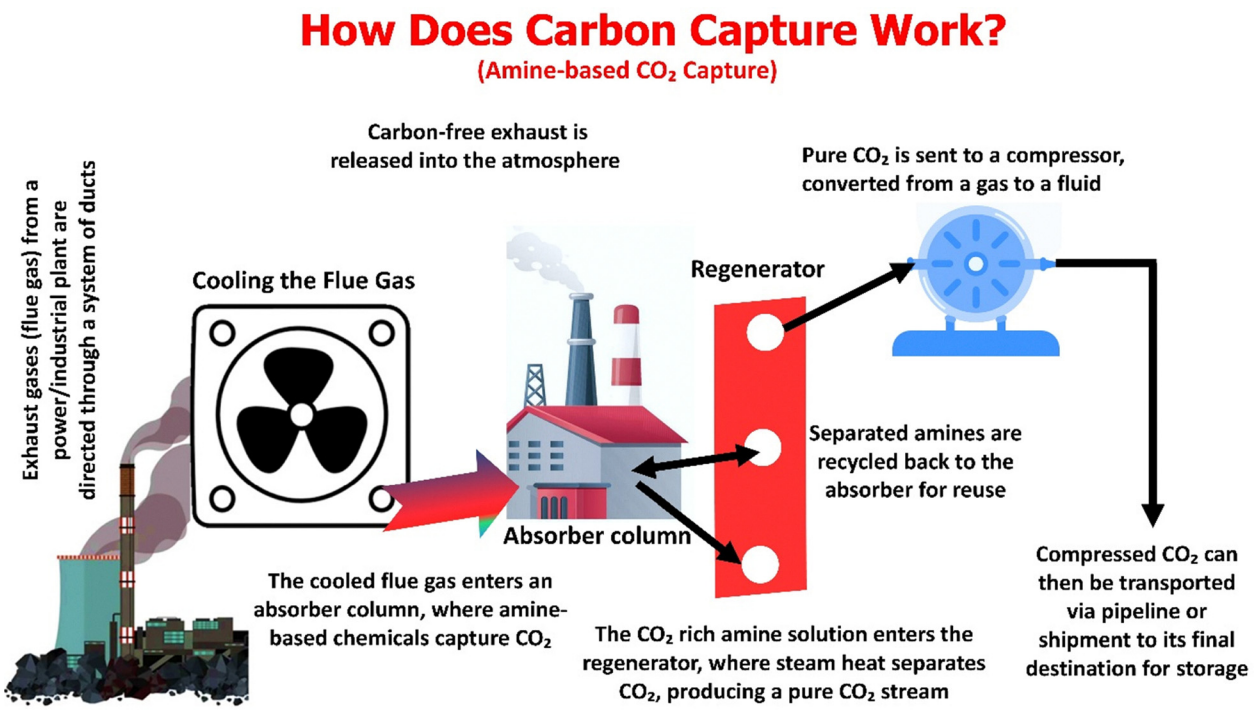

Fig. 3 Schematic of amine-based post-combustion CO_2 capture, showing flue-gas cooling, CO_2 absorption in an amine scrubber, thermal regeneration of the solvent, amine recycling, and compression of purified CO_2 for transport and storage.

high-purity CO_2 and regenerating the lean solvent for subsequent use. The primary obstacle is the considerable parasitic energy requirement for steam production, which can account for 20–30% of the plant's total output. Furthermore, the thermal degradation of the solvent and losses of amine *via* vapor slip diminish both operational efficiency and the solvent's operational lifespan.[87] Moreover, the high energy penalties associated with solvent regeneration (stripping), significant equipment corrosion requiring expensive metallurgy, and the oxidative degradation of amines, which leads to the emission of toxic byproducts, are also concerns.

CO_2 compression: the liberated CO_2 undergoes compression to supercritical pressures to facilitate efficient transport.[90] This process requires rigorous dehydration protocols to prevent the formation of carbonic acid and subsequent corrosion, alongside multistage compression that incorporates intercooling to regulate both heat generation and energy expenditure.

Regarding transport and geological storage, supercritical CO_2 is conveyed through pipelines or vessels and subsequently injected into deep geological formations, including saline aquifers and depleted oil or gas reservoirs located 2500 feet below ground.[66] Such storage reduces the likelihood of atmospheric leakage and ensures safer long-term containment. CCUS will be a key part of this plan to help lower greenhouse gas emissions from cement, steel, and chemical manufacturing, which are hard to decarbonize and fix. Pipeline corrosion may be a possible risk if the purity of CO_2 (absence of moisture, H_2S, SO_2, N_2, O_2, *etc.*) is compromised. In summation, despite the technological maturity of amine-based carbon capture and storage, its substantial energy requirements, solvent degradation, corrosion susceptibility, and long-term storage risks continue to drive research into advanced materials and alternative capture methodologies.

3. Methods of CO_2 capture

The three primary methods of CO_2 capture are depicted in Fig. 4: (i) pre-combustion, (ii) oxyfuel combustion, and (iii) post-combustion, which are further subdivided into different categories.[91–93]

In the pre-combustion process, the fuel (coal or natural gas) is pre-treated before combustion.[94] To prepare coal for use, it is gasified at low oxygen levels, producing syngas that is primarily composed of carbon monoxide and hydrogen gas and relatively free from other harmful gases.[95] The steam-water gas shift process that occurs in the syngas converts the CO gas into CO_2, producing more hydrogen gas. The high CO_2 concentration ($>20\%$) in the H_2/CO_2 fuel gas combination facilitates the extraction of CO_2.[96] The hydrogen is then burnt in an air atmosphere to produce mostly nitrogen gas and water vapour. Coal-fueled Integrated Gasification Combined Cycle (IGCC) power plants may employ this pre-combustion capture technique to increase efficiency by 7–8%. Two examples of physical solvents that work well for CO_2 separation are Rectisol (based on methanol) and Selexol (polyethylene glycol ethers). While these are effective, they are expensive and often require complex thermal management. CNM-based materials offer a compelling alternative here due to their tunable surface chemistry and pore structures. Unlike Rectisol and Selexol, which rely on bulk liquid handling, solid-state carbon-based adsorbents (such as activated carbon, GO, and CNT-based filters) can potentially reduce the energy penalty associated with solvent circulation and regeneration. Furthermore, these adsorbents exhibit excellent material compatibility in these reducing syngas environments, resisting the chemical degradation that can plague organic solvents over time. This approach helps to generate syngas for chemical

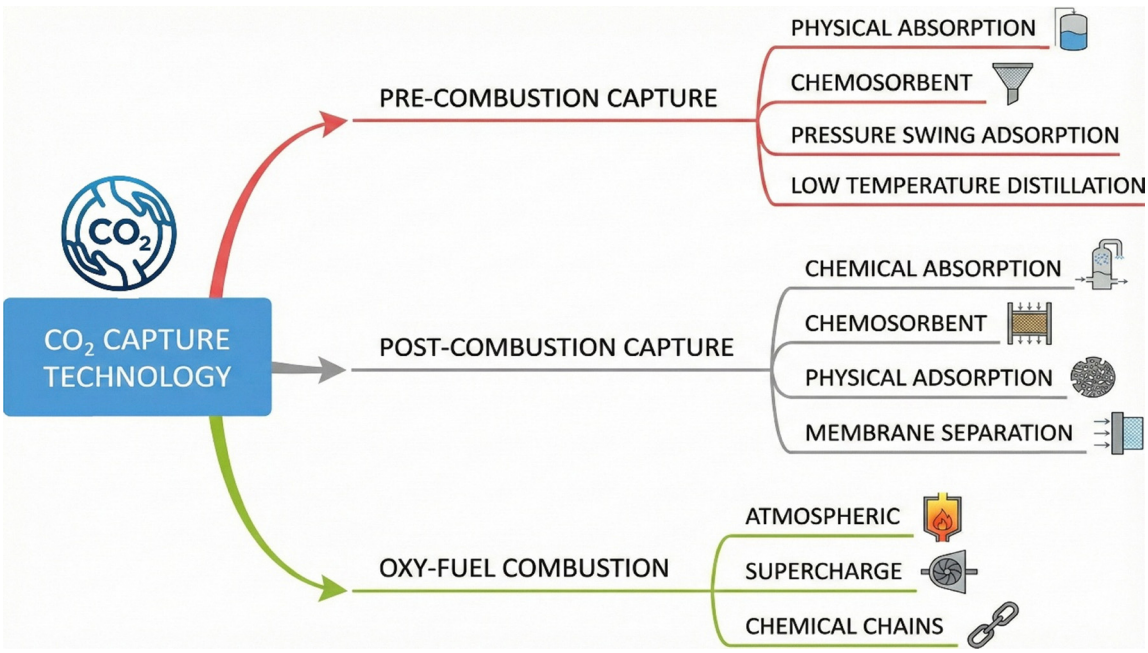

Fig. 4 CO_2 capture pathways and primary capture techniques in pre-combustion, post-combustion, and oxy-fuel processes.

synthesis and carbon-free fuels. Although high costs limit its wider adoption, it is primarily employed in the fertilizer and hydrogen production sectors (Fig. 5).

Whereas, burning fuel with extremely pure oxygen ($\geq$95%) instead of air is known as oxy-fuel combustion capture.[97,98] As a result, the exhaust gas contains negligible nitrogen, which significantly reduces thermal NO_x.[99] Using highly pure oxygen for combustion results in exhaust gases mainly composed of CO_2, H_2O, and SO_2.[100] Electrostatic precipitator and flue gas desulphurization techniques may remove particulates and sulfur dioxide. The residual gases contain a high percentage of CO_2 (80–98%), which can be compressed, transported, and stored.[101] Nevertheless, this approach consumes a significant amount of oxygen from the air separation unit, which increases expenses and requires substantial energy.[102] Additionally, oxygen poses risks and impacts boiler performance.[103] Moreover, flue gas recycling is necessary to control boiler temperature due to the higher combustion rate of oxygen-rich flue gas. Oxyfuel combustion remains a promising CO_2 capture technique, despite these obstacles, with area for improvement.

However, post-combustion CO_2 capture is a commonly used technology in the chemical industry because it captures CO_2 after fuel combustion and can be retrofitted into existing power plants with minimal modifications.[104,105] Monoethanolamine (MEA) and diethanolamine (DEA) are utilized in amine-based chemisorption, a widely used method that has drawbacks including solvent loss, corrosion, hazardous byproducts, and expensive regeneration.[106] CNMs are gaining a significant role in post-combustion scenarios to address these specific drawbacks. In terms of energy efficiency, solid sorbents based on graphene or functionalized CNTs typically require significantly lower regeneration heat (1.2–2.5 GJ per ton CO_2) compared to the latent heat of water vaporization inherent in aqueous amine systems (3.5–4.5 GJ per ton CO_2).[32] From a cost perspective, while pristine graphene is expensive, biomass-derived activated carbon and biochar offer a low-cost, sustainable route to high-surface-area materials that can compete economically with amine solvents on a large scale. Additionally, CNMs demonstrate superior chemical stability against oxidative degradation and corrosion, issues that severely limit the lifespan of amine solvents in oxygen-rich flue gas streams.

Chemical looping, which captures CO_2, is another promising method for capturing CO_2. However, it has high operational costs.[107] Adsorption using novel solid sorbents is gaining interest as an alternative due to its efficiency. Similarly, oxy-fuel combustion, where fuel burns with pure oxygen and recycled flue gas, is another critical approach for CO_2 capture. Key advantages include ease of integration, operational flexibility without plant disruption, and broad industrial adaptability. This method remains a promising, cost-effective solution for large-scale CO_2 reduction. A detailed comparative summary highlighting the key differences between these technologies, along with their respective advantages and disadvantages, is presented in the accompanying figure (Fig. 6 and Table 3).

4. Key requirements of various CNMs for CO_2 adsorption materials

In recent years, solid adsorbents based on carbon (activated carbons, carbon nanotubes, graphene-based materials, and biochar) have gained significant attention over conventional

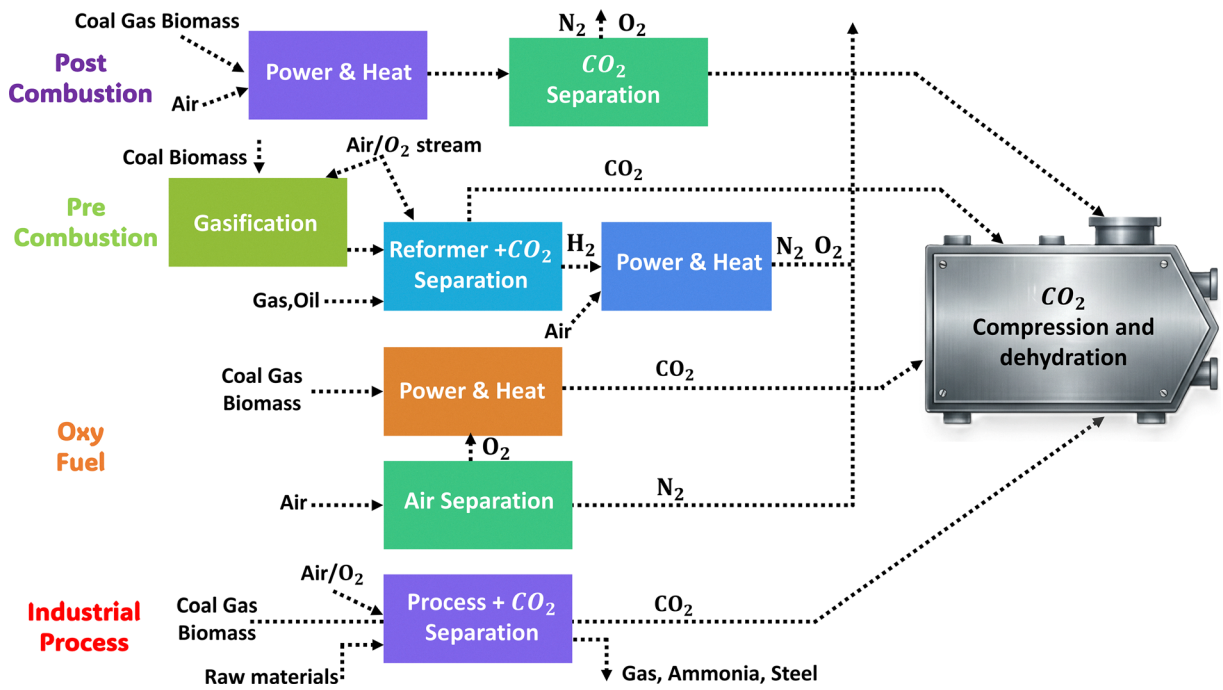

Fig. 5 Graphical representation of major CO_2 capture routes with integrated energy and industrial systems before transport, storage, and utilization.

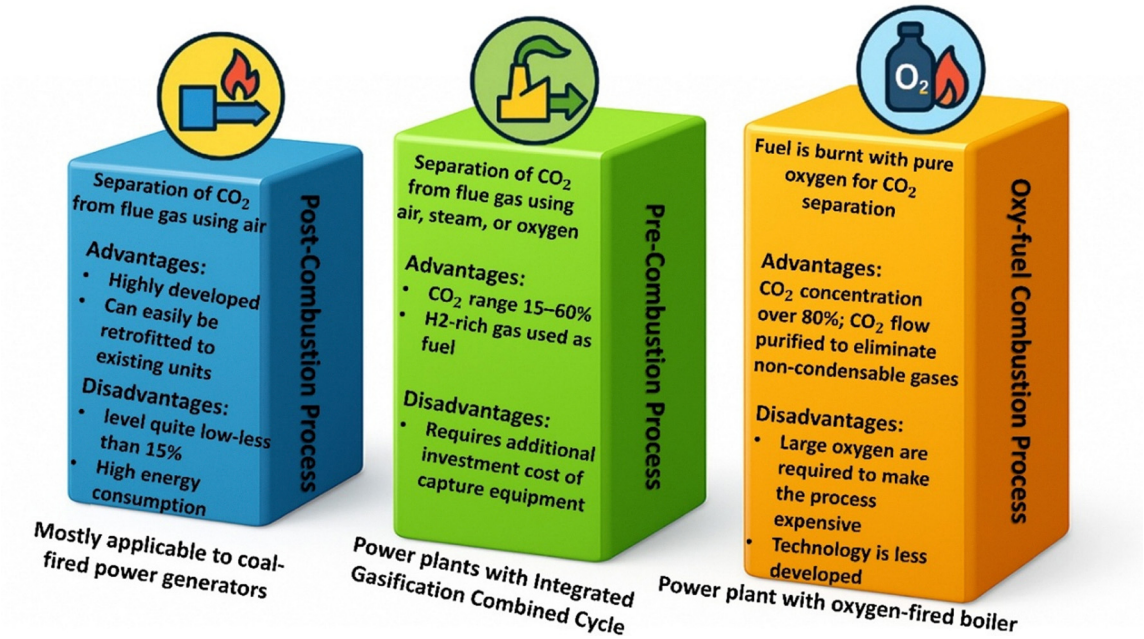

Fig. 6 Comparison of major carbon capture routes, post-combustion, pre-combustion, and oxy-fuel combustion, highlighting their operating principles, key advantages, limitations, and typical applications.

Table 3 Thermodynamic and energetic comparison of industrial CO_2 capture strategies, illustrating inherent efficiency limitations and opportunities for disruption through CNM-enabled separation technologies

Metric	Pre-combustion capture	Oxy-fuel combustion	Post-combustion capture
Thermodynamic driving force	Pressure-driven separation: elevated CO_2 partial pressure enables low-energy physical separation processes	Phase-change–driven separation: near-pure CO_2 streams allow condensation-based capture	Chemically driven separation: dilute CO_2 streams require high-energy chemical bond formation and cleavage
Specific energy demand	$\sim$2.5 MJ kg^{-1} CO_2 (lowest): energy is primarily associated with syngas generation and CO_2 compression	$\sim$3.0–4.0 MJ kg^{-1} CO_2: energy consumption is primarily driven by the electricity demand of the air separation unit (ASU)	$\sim$3.5–4.5 MJ kg^{-1} CO_2 (highest): substantial steam input required for solvent regeneration (reboiler duty)
Efficiency	High: CO_2 separation occurs upstream of expansion, minimizing irreversibility and exergy destruction	Moderate: significant combustion-related exergy losses, partially mitigated through latent heat recovery	Low: high entropy generation arising from CO_2 separation from nitrogen-diluted flue gas
CNM integration potential	Transformative: membrane reactors enable simultaneous reaction and separation, shifting equilibrium, and eliminating intermediate cooling steps	High: membrane-based oxygen separation can replace cryogenic ASUs, substantially reducing parasitic energy losses	Incremental to moderate: advanced solid sorbents reduce sensible heat penalties, but the fundamental entropy constraint remains

solvent-based systems due to their several advantages, such as high efficiency, lower energy penalties, and operational flexibility.[108–110] Due to their large surface areas, diverse pore architectures, chemical stability, and cost-effectiveness, these materials are beneficial for post-combustion and DAC applications.[111] Recent breakthroughs in material synthesis, such as the creation of hierarchically porous carbons and nitrogen-doped frameworks, have significantly enhanced CO_2 absorption and selectivity compared to other gases, including N_2 and H_2O.[112]

Adsorption occurs when gas-phase molecules adhere to a nearby solid surface due to interactions between the gas-phase molecules and the solid surface.[113] It can be categorized into two main types: physisorption (physical adsorption) and chemisorption (chemical adsorption). Physisorption occurs when molecules adhere to the surface of an adsorbent through weak van der Waals forces, with an enthalpy of approximately 10 kJ mol^{-1}.[114,115] The process could be over quickly because these interactions are weak. Chemisorption refers to the interaction between adsorbed molecules and the solid surface, where the interaction is stronger.[116] These interactions can involve sharing electrons and atoms or the creation of new chemical species or radicals. The hydroxyl (–OH) and carboxyl (–COOH) groups enhance hydrogen bond interactions, leading to significant chemisorption, and exhibit an adsorption enthalpy of more than 100 kJ mol^{-1}.[117] It is also more difficult to reverse, which makes regeneration of the sorbent involved in chemisorption more challenging. For applications that utilize adsorption, the type of adsorbent material is crucial because it directly impacts the effectiveness of these processes. When selecting the right materials, key factors to consider are their performance under post-combustion conditions, where CO_2 pressure is low, as well as their associated costs. The adsorbent's structure, including

its pore structure, surface chemistry, and overall design, also significantly impacts its ability to capture CO_2 effectively. The following is a detailed explanation of the main features (Fig. 7).

Surface area: the large surface area and high pore volume significantly affect the CO_2 adsorption capacity of porous materials.[118] An increased surface area results in a higher number of active sites available for CO_2 molecule binding, thereby enhancing the overall uptake capacity.[119] The balance between surface area and pore volume is essential for optimizing adsorption efficiency. The optimization of pore structure holds significant importance, and an optimal pore network ensures that active sites are easily accessible to CO_2 molecules, thereby avoiding diffusion limitations that may impede adsorption.[119] Efficient penetration of CO_2 into the material occurs when pores are optimally distributed and possess suitable sizes, allowing for effective interaction with the available adsorption sites. The optimized pore architecture directly enhances CO_2 capture efficiency. Porous materials, including activated carbon, graphene, and carbon nanotubes (CNTs), serve as prime examples of these principles. Activated carbons are characterized by their extensive pore networks and can exhibit surface areas that range from 400 to over 3000 $m^2\ g^{-1}$. Graphene possesses a two-dimensional structure that provides an exceptionally high theoretical surface area. When engineered into porous configurations, it can achieve remarkable structure. Similarly, carbon nanotubes (CNTs), characterized by their hollow, tubular structures, offer high surface areas and adjustable interlayer spacing, allowing for precise control over pore size and accessibility. The ability of these materials to be engineered with extensive surface areas and customized pore volumes renders them highly effective and suitable candidates for the advanced CO_2 capture process. Ongoing research on the development of these materials aims to optimize their characteristics further to achieve enhanced adsorption capacities and efficiencies.

Pore size, volume, and adsorption mechanism: a well-developed microporous structure is essential for efficient CO_2 adsorption. The adsorption behavior depends on the pore size, affecting how different materials perform under various pressure conditions. Due to the strong molecular interactions in confined spaces, microporous materials are particularly effective for low-pressure adsorption. In contrast, mesoporous structures are more suitable for high-pressure adsorption, where physical adsorption dominates. Micropores (<2 nm) serve as active sites for CO_2 capture through physisorption, where CO_2 molecules interact with the surface *via* weak intermolecular forces, including hydrogen bonding and ionic interactions. Research indicates that CNM-based materials with a high ultra-micropore concentration exhibit significantly improved CO_2 uptake even at low pressures ($\sim$0.15 bar).[32] The optimal pore size for CO_2 physisorption is slightly larger than the kinetic diameter of CO_2 molecules (0.33 nm), ensuring efficient molecular trapping and adsorption.[120]

Adsorption–desorption efficiency: the efficiency of adsorption and desorption depends on the pore structure of the material. Adsorption and desorption cycles must be accelerated for large-scale industrial applications, and a well-engineered adsorbent with an optimized pore structure guarantees effective mass transfer and quick kinetics.

In addition to the above-stated surface properties, the various other criteria for high-performance CO_2 adsorbents for industrial applications are described below:

4.1. Heat of adsorption in CO_2 capture

The heat of adsorption (Q_{st}) is a critical factor in determining the interaction strength between CO_2 molecules and adsorbent materials, directly influencing the feasibility of CO_2 capture. In post-combustion scenarios, where CO_2 concentrations are

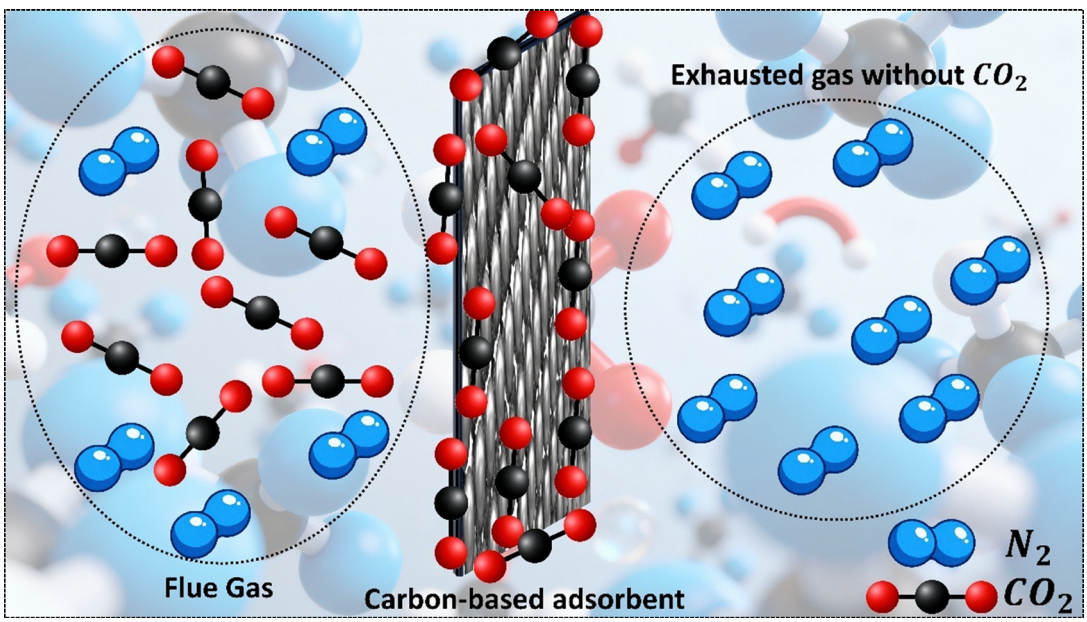

Fig. 7 Adsorption mechanism of CO_2 capture from flue gas *via* a carbon-based adsorbent.

relatively low, adsorption based on physisorption is weaker.[121] In physisorption, porous carbon materials exhibit Q_{st} values ranging from 15 to 50 kJ mol^{-1}, ensuring low energy consumption for regeneration. In contrast, chemisorption-based adsorbents (Q_{st} > 80 kJ mol^{-1}), such as amine-functionalized carbons or doped materials, are better suited for post-combustion CO_2 capture due to their ability to form stronger covalent or ionic bonds with CO_2. For industrial-scale CO_2 capture, achieving an optimal balance between adsorption efficiency and regeneration energy consumption requires a Q_{st} range of 35–50 kJ mol^{-1}. Functionalizing porous materials with amine groups can also enhance CO_2 adsorption by increasing Q_{st} to approximately 50 kJ mol^{-1}. Conversely, mesoporous and macroporous adsorbents are more suitable for pre-combustion CO_2 capture due to their larger pore sizes, which enable efficient gas diffusion and removal. The optimal Q_{st} range for industrial use is 25–50 kJ mol^{-1}, striking a balance between high adsorption capacity and energy-efficient regeneration.

4.2. Chemical, thermal, and mechanical stability in CO_2 capture

To achieve effective CO_2 capture in practical applications, adsorbents must demonstrate outstanding chemical, thermal, and mechanical stability. In post-combustion environments, characterized by flue gases with elevated temperatures ranging from 40 to 80 °C and a low CO_2 pressure of approximately 15 bar, maintaining the structural integrity of the adsorbent is essential. Exposure to water vapor in flue streams can lead to swelling and subsequent degradation, compromising the efficiency of the adsorbent. CNMs exhibit significant advantages attributed to their elevated thermal and chemical stability, ensuring prolonged durability and reusability. Certain carbon frameworks have demonstrated the capability to adsorb and desorb CO_2 for over 100 cycles, exhibiting a capacity loss of less than 10%, which highlights their durability. Contaminants present in flue gas, including N_2, NO_2, and SO_2, can adversely affect CO_2 selectivity, thereby complicating the performance of adsorbents.[122] To resolve these challenges, it is essential to design adsorbent materials that can endure humid environments while preserving mechanical and thermal stability, ensuring that optimal performance is not compromised.

4.3. Surface chemistry and functionalization

The surface chemistry of adsorbent materials is crucial for controlling the adsorption of CO_2 and the selectivity of the process.[122] Adding functional groups to different heteroatoms (such as nitrogen and boron) or chemical groups can significantly improve the ability to adsorb. Nitrogen doping (*via* amines, amides, or pyrrolic/pyridinic N) makes chemisorption stronger by making acid–base interactions stronger. Studies show that CO_2 absorption is 20–50% higher in nitrogen-doped carbon materials as compared to undoped. Nitrogen-doped graphene aerogels are better at capturing CO_2 because they have basic nitrogen sites that interact well with CO_2 molecules. Adding carboxyl, phenolic, and carbonyl groups to the surface also makes it more polar, which facilitates the bonding of CO_2 to hydrogen, thereby increasing the surface's effectiveness in adsorption.[123] Adding sulfur or phosphorus atoms to the material, instead of nitrogen, creates more active sites and alters the distribution of electrons. Including metals like Mg, Ca, or transition metals in these materials can also boost the adsorption effectiveness by increasing CO_2 binding affinity through Lewis acid–base interactions.

4.4. CO_2 adsorption capacity

The adsorption capacity is a crucial factor in determining how effectively CO_2 can be collected, as it directly influences the rate at which CO_2 is absorbed from gas mixtures. For CO_2 capture to work well, rapid adsorption kinetics are necessary. This means that porous materials can swiftly trap CO_2 molecules. However, in other cases, microporous materials may hinder the movement of CO_2, potentially impairing overall efficiency. Physisorption allows CO_2 molecules to enter small gaps in microporous materials (with pore diameters $\leq$0.33 nm), thereby accelerating diffusion at low pressures. At higher pressures, both micro- and macropores increase in volume, significantly altering the adsorption process. It typically takes only 2 to 4 minutes for materials to absorb a significant amount of CO_2 to reach complete equilibrium. Amine-functionalized adsorbents may be engineered to enhance CO_2 adsorption rates by reinforcing hydrogen bonding interactions with CO_2. Chemical activation using KOH, $ZnCl_2$, or H_3PO_4 has also been found to improve the ability of CNM-based adsorbents to capture CO_2.

4.5. Adsorbent costs and the synthesis process

Choosing the appropriate adsorbent requires carefully weighing several key criteria. For industrial-scale applications, the production and synthesis processes must be both cost-effective and environmentally friendly, while also being resource-efficient. CNM-based materials must be affordable and easily produced in large quantities to enable widespread use.[124] Using biochar and other abundant, renewable materials offers a low-cost way to capture CO_2. Additionally, new technologies have enabled the large-scale production of materials like graphene oxide, thereby facilitating their practical use.[125]

4.6. Material regeneration and recyclability after CO_2 capture

A key part of CCUS is the excellent regeneration of adsorbent materials, which makes them usable for an extended period while using less energy. The last stage of the CCUS cycle, CO_2 desorption from the sorbent, is equally as critical as the first step, *i.e.*, adsorption. Traditional CCUS techniques rely on the chemical absorption of CO_2, followed by thermal desorption from aqueous alkanolamine solvents at 100–120 °C.[126] This method requires a significant amount of energy and causes amine degradation, making it less affordable to reuse. Solid nanoporous materials may be used instead of amine-based solvents, especially those that include N-donor functional groups, such as pyridine, imidazole, and tetrazole.[127] Dipole–quadrupole interactions between CO_2 molecules and nitrogen sites enhance the adsorption capacity of these materials for CO_2, requiring lower regeneration temperatures compared to water-based solutions. Additionally, the strong interactions between CO_2 molecules and both the

surface and interior pores enhance adsorption efficacy, thereby decreasing material degradation across multiple cycles. Therefore, porous materials rich in nitrogen offer a long-term, cost-effective method for absorbing a significant amount of CO_2. They are also more recyclable and can be utilized in CCUS applications for an extended period.[128]

4.7. Resistance to moisture and impurities in flue gas

In addition to CO_2 and NO_2, industrial flue gas contains water vapor and trace amounts of other pollutants, such as NO_x and SO_x.[129] An ideal adsorbent must exhibit high tolerance to these impurities to maintain the efficiency and cost-effectiveness of the CO_2 capture process. Common sorbents, such as activated carbon and zeolites, often face reduced adsorption capacity in humid environments, creating a significant challenge. To address this, adsorbents are designed to minimize competitive adsorption of H_2O and other contaminants, thereby improving CO_2 selectivity.[130] Developing materials with inherent moisture resistance eliminates the need for pre-drying or additional purification steps, simplifying the process and making large-scale carbon capture more economically viable.[131]

4.8. Selectivity

In this way, along with the above-discussed points, selectivity is a crucial concern that permits further exploration. The purity of captured CO_2 is significantly influenced by the selectivity of the sorbent, which refers to its ability to preferentially adsorb CO_2 over other gases present in the flue gas mixture. Selectivity is commonly quantified as the ratio of CO_2 adsorption capacity to that of competing gases, such as N_2. A high CO_2/N_2 selectivity ensures efficient separation, leading to high-purity CO_2 for further utilization or storage.[132]

4.9. Comparative performance of CNMs in CO_2 capture

CNMs exhibit superior performance compared to other materials in CO_2 capture. With surface areas of up to 2688 $m^2\ g^{-1}$ and pore volumes of 0.6–1.5 $cm^3\ g^{-1}$, they offer higher capacity and enhanced molecular sieving through ultra-micropores (<0.7 nm). Their tunable heats of adsorption (15–40 kJ mol^{-1}) enable efficient regeneration, while capacities reach 5–8 mmol g^{-1} at 1 bar and up to 15 mmol g^{-1} at 5 bar, well above industrial benchmarks. The detailed performance matrix of these materials compared to the industry standard is highlighted in Table 4.

5. Utilization of captured CO_2

Currently, the predominant use of captured CO_2 is enhanced oil recovery (EOR), where CO_2 is injected into oil reservoirs to facilitate the extraction of additional crude oil.[133] In addition to EOR, there is growing interest in using CO_2 to make fuels, chemicals, and industrial materials through catalytic and electrochemical processes.[134] In contrast to liquid amines, which necessitate energy-intensive desorption processes, functionalized carbons, such as nitrogen-doped porous carbons and CNTs, can serve a dual purpose. They can both seize CO_2 and facilitate the direct conversion of CO_2 into methane or syngas through the support of metal catalysts, including nickel and ruthenium, thus mitigating overall energy expenditures.

Furthermore, developing globular pathways facilitates the conversion of captured CO_2 into valuable products. These include polymers, construction materials, and advanced CNMs, such as CNTs and graphene, which can be produced *via* electrochemical or chemical vapor deposition methods.[135] Biological approaches, employing algae or bacteria, present an additional utilization strategy. In these methods, CNMs, such as GO scaffolds, augment CO_2 absorption and biomass production. Consequently, these sophisticated utilization strategies collectively underscore the potential of CNMs to enhance the economic feasibility and environmental impact of carbon capture and storage.[136–138]

Table 5 highlights recent progress in CNM-based catalysts enabling the electrochemical conversion of CO_2 into value-added C_2^+ hydrocarbons, alcohols, and N-containing products through C–C and C–N coupling pathways. A key feature across these systems is the use of metal-free or heteroatom-doped carbon frameworks, which overcome limitations associated with metal catalysts, such as high cost, scarcity, and susceptibility to poisoning, while offering tunable electronic structures and abundant active sites.

6. CNM-based adsorbents for CO_2 capture

Materials intended for CO_2 capture must combine cost-effectiveness, wide availability, and high performance to satisfy global demands. Among potential candidates, carbon stands out as an exceptionally versatile element, offering a wide array of allotropes and the ability to form structures across all

Table 4 Comparative performance metrics of CNMs *versus* industry-standard sorbents for CO_2 capture

Performance metrics	Industry standard	Performance of CNMs	Advantage
Optimal surface area range	800–1500 $m^2\ g^{-1}$	1500–2688 $m^2\ g^{-1}$	Higher surface area
Critical pore size distribution	70% micropores (<2 nm)	60–85% ultra micropores (<0.7 nm)	Enhanced molecular sieving
Required pore volume	0.4–0.8 $cm^3\ g^{-1}$	0.6–1.5 $cm^3\ g^{-1}$	Higher volume
Target heat of adsorption	25–35 kJ mol^{-1}	15–40 kJ mol^{-1}	Tunable energy requirements
Minimum CO_2 capacity (1 bar)	3–5 mmol g^{-1}	5–8 mmol g^{-1}	High capacity
Maximum CO_2 capacity (5 bar)	6–10 mmol g^{-1}	8–12 mmol g^{-1}	Improvement
CO_2/N_2 selectivity target	10–50	15–200	High selectivity
Cycling stability requirement	>100 cycles	>300 cycles	Longer cycle life
Regeneration temperature	<120 °C	<100 °C	Lower regeneration temperature
Maximum material cost	<$100 per kg	$20–200 per kg	Cost-competitive at scale
Production scalability	Moderate	Good to excellent	Superior for most types
Environmental stability	Good under dry conditions	Excellent chemical stability	Enhanced durability

dimensional scales from zero-dimensional (0D) carbon dots and fullerenes, to one-dimensional (1D) carbon nanotubes, two-dimensional (2D) graphene sheets, and three-dimensional (3D) architectures such as carbon foams and activated carbon.[144–147] 0D materials (fullerenes and carbon dots) represent the lowest dimensional limit with cage-like sp^2-carbon frameworks and high theoretical surface-to-volume ratios.[148] However, pristine fullerenes interact weakly with CO_2 *via* physisorption, and their strong tendency to aggregate into fullerite crystals drastically reduces accessible surface area. Although ionization or functionalization can theoretically enhance CO_2 binding, electronic instability, aggregation, and prohibitively high synthesis costs restrict 0D carbons to significant roles as functional additives rather than practical sorbents.[149,150] 1D materials, such as carbon nanotubes (CNTs), offer dual adsorption domains on their inner lumen and outer surfaces.[110] While confinement within nanotube interiors can enhance CO_2 binding, mass-transfer resistance and weak interactions with smooth graphitic walls limit practical uptake. Chemical functionalization (*e.g.*, amine grafting) improves selectivity and capacity but introduces trade-offs by blocking pores and slowing kinetics. 2D materials (graphene and GO) provide extremely high theoretical surface areas and tunable surface chemistry.[32,39] Their primary limitation is irreversible restacking driven by π–π interactions, which collapses porosity. Structural engineering strategies, such as pillaring with CNTs, metal oxides, or MOFs, successfully preserve interlayer spacing and enhance CO_2 diffusion. 3D hierarchical porous carbons represent the most technologically mature and scalable class of materials. By integrating micro-, meso-, and macropores into a continuous framework, these materials overcome diffusion limitations inherent to lower-dimensional systems. Micropores offer high adsorption potential, while meso- and macropores facilitate rapid mass transport.[151]

As discussed in the earlier section, this study focuses on specific CNM-based adsorbents for the collection and subsequent transformation of CO_2 into value-added products. To provide a comprehensive picture, we discuss some materials in depth and then summarize their comparison with other essential CNMs. This method facilitates easier comparison of their performance, benefits, and drawbacks in the context of CO_2 capture. Table 6 provides a summary of several CNMs discussed, focusing on their structural characteristics, physicochemical properties, and specialized functions in CO_2 adsorption. Some of the main benefits, including a large surface area, adjustable porosity, and the capacity to transform with functional groups, are also included, along with some of the drawbacks, such as the difficulty of regeneration and expense. This comparison enables us to identify the most suitable candidates for CCUS applications that are both effective and long-lasting.

6.1. Activated carbon-based adsorbents

Porous materials, particularly activated carbon, have attracted significant global research interest owing to their tunable pore architecture, exceptionally high surface area, and remarkable chemical and thermal stability.[162,163] These attributes contribute to activated carbon's high CO_2 adsorption capacity, complemented by excellent selectivity and ease of regeneration. A key advantage of activated carbon is its sustainable production, as it can be derived from waste biomass and agricultural residues, making it both cost-effective and environmentally friendly.[164,165] This section of the review discusses the various precursor materials employed in the synthesis of activated carbon and subsequently applied for CO_2 adsorption.[166–171]

Sawdust, a common byproduct of woodworking, is traditionally used in rural areas as a fuel source for heat and light. However, it has shown significant promise as a precursor for producing activated carbon or biochar for CO_2 adsorption applications[172–176] Foorzinezhad *et al.*[177] recently synthesized activated carbon from Iranian sawdust using a pure CO_2 activation process. Sawdust was activated at six different temperatures, ranging from 700 °C to 1100 °C. SEM images (Fig. 8) show the morphological evolution of carbon with increasing temperature. The unactivated carbon (Fig. 8a and b) exhibits a smooth, amorphous surface with minimal porosity. At 700 °C (Fig. 8c), initial pore formation is observed, although it is partially filled with ash. Increasing temperature (800–1100 °C) significantly improves porosity due to byproduct removal. At 1000 °C, smaller pores merge within larger structures (inset, Fig. 8f), attributed to the formation of tunnel-like channels through the volatile gasification process. However, above 1000 °C, the structure becomes irregular and heterogeneous, potentially reducing surface area and CO_2 adsorption capacity.

BET surface area increased with temperature, reaching a maximum of 1651 $m^2\ g^{-1}$ at 1000 °C before declining to 1163 $m^2\ g^{-1}$ at 1100 °C, as shown in Fig. 8(j). This trend directly influenced CO_2 uptake, with the highest adsorption capacity observed in samples treated at 1000 °C, attributed to the optimized surface area. Fig. 8(k) shows the pore size distribution curve for the 1000 °C-treated sample, obtained using non-linear Density Functional Theory (DFT), which demonstrates the presence of

Table 5 CNM-based catalysts for CO_2 conversion to C_2^+ and N-containing products *via* C–C and C–N coupling

Catalyst type	Catalyst material	Coupling reaction	Final products	Performance metrics (faradaic efficiency/yield)	Ref.
Metal-free	N-doped graphene quantum dots (NGQDs)	C–C (CO_2, H_2O)	C_2H_4, C_2H_5OH	FE = 90% at −0.74 V, I = 46 mA cm^{-2} at −0.86 V	139
	N-doped carbon (c-NC) with ordered cylindrical mesopores	C–C (CO_2, H_2O)	C_2H_5OH	FE = 77% at −0.56 V, selectivity 100%	140
	B and N codoped nanodiamonds (BND)	C–C (CO_2, H_2O)	C_2H_5OH	FE = 93.2% at −1.0 V, Y = 90 mg h^{-1} cm^{-2}	141
	F-doped CNTs	C–N (CO_2, NO_3^-)	$CO(NH_2)_2$ (Urea)	FE = 18.0% at −0.65 V, I = 3.5 mA cm^{-2} Y = 6.36 mmol g^{-1} h^{-1}	142
	N-doped carbon	C–N (CO_2, NO_3^-)	$CO(NH_2)_2$ (Urea)	FE = 62% at −0.5 V, Y = 596.1 μg mg^{-1} h^{-1}	143

Table 6 Average surface area, pore structure, functional properties, and CO_2 capture characteristics of commonly used carbon materials and their derivatives

Carbon material	Surface area (m^2 g^{-1})	Pore structure	Functionalization/ modification	CO_2 adsorption characteristics	Notes	Ref.
Activated carbon	500–2500	Microporous with some mesopores	Physical (steam or CO_2) or chemical (KOH, H_3PO_4) activation	High capacity at high pressure; low selectivity without functional groups	Inexpensive, scalable, sensitive to humidity	152
Carbon nanotubes	100–1000	Mostly mesoporous; can be microporous	Acid/base treatment; amine or metal doping	Moderate CO_2 uptake; fast kinetics; tunable properties	Excellent thermal/ mechanical stability	153
Graphene oxide	300–700	Layered, meso-porous/microporous	Oxygen groups (–OH, –COOH, and epoxy) naturally present	Moderate uptake; improved selectivity due to polar groups	Good dispersion in composites; lower conductivity	154
Reduced graphene oxide	500–1200	Less oxidized than GO; microporous/ mesoporous	Partially removed O-groups by chemical or thermal reduction	Increased capacity due to the restoration of the π-conjugated network	Hydrophobic; can be used in composite adsorbents	154
Carbon aerogels	400–1500	Highly porous (micro–meso)	Controlled sol-gel synthesis; surface functionalization is possible	High capacity; excellent regeneration due to open structure	Fragile; high synthesis cost	155
Carbon xerogels	400–1200	Micro- and mesoporous	Like aerogels, ambient drying	Comparable to aerogels but with more practical processing	Useful for large-scale applications	156
Ordered mesoporous carbon	1000–2000	Highly ordered mesopores	Can be doped with N, amines, or metals	High CO_2 uptake; tunable pore architecture	Made using mesoporous silica templates	157
Biochar	200–900	Microporous and mesoporous	Depends on the pyrolysis temperature and the feedstock	Low-to-moderate CO_2 uptake; potential for amine grafting	Renewable; cost-effective; environmental benefit	158
MOF-derived porous carbon	1000–3000	Microporous, hierarchical, and possible	Direct carbonization; N-doping from ligands	Very high surface area; high selectivity with N-doping	Retains structural features of MOFs; thermal stability is enhanced	159
Activated carbon fibers	1000–2500	Predominantly microporous	Surface oxidation, amine impregnation	High CO_2 capture rate and capacity due to fiber morphology	Excellent for rapid adsorption/desorption cycles	152
Hard carbon	300–600	Microporous with closed pores	N-doping or physical activation	Moderate uptake; cost-effective	Commonly used in energy and storage devices	160
Soft carbon	<100	Mostly nonporous	Not typically used for CO_2 capture	Poor adsorption performance	Used more for electrodes than adsorption	161

ultra-micropores (0.4–1.76 nm). Specifically, as the activation temperature increased from 700 °C to 1000 °C, CO_2 adsorption capacity increased from 3.3 to 9.2 mmol g^{-1} after 35 minutes but slightly declined to 8.6 mmol g^{-1} at 1100 °C, likely due to the loss of active sites, functional groups, and structural alterations that weakened the adsorbent–adsorbate interactions. Moreover, operational parameters influenced the adsorption performance, with the highest uptake recorded at a low flow rate of 50 mL min^{-1}. Temperature also played a crucial role; the 1000 °C heat-treated sample captured 10.64 mmol g^{-1} of CO_2 at 0 °C, compared to 9.2 mmol g^{-1} at 50 °C.

Dry fruit shells, a significant byproduct of agro-industries, have been effectively utilized as precursors for the production of activated carbon (AC), with applications in CO_2 adsorption.[179–182] Koli *et al.*[178] employed *Terminalia catapa* (Indian almond) shells to synthesize AC through acid activation, followed by heat treatment under air (HPC) and nitrogen (HPAC) atmospheres. The resulting materials were utilized for CO_2 capture. The surface area and pore structure play a significant role in determining their CO_2 capture capacity. Fig. 8(l) shows the nitrogen adsorption–desorption curve for HPC and HPAC, demonstrating a small hysteresis at p/p_0 = 0.4. This confirms the presence of meso- and micro-pore structures in both samples.[178] Notably, HPAC exhibited a higher surface area (~616 m^2 g^{-1}) and CO_2 adsorption capacity (2.3 mmol g^{-1}) compared to HPC, which showed low CO_2 uptake (1.7 mmol g^{-1}) owing to a lower surface area (244 m^2 g^{-1}). Similarly, Xu *et al.*[180] developed K_2CO_3-activated porous carbon from peanut shells, achieving a remarkable CO_2 adsorption capacity of 5.7 mmol g^{-1} at 273 K, which significantly outperformed unmodified peanut shells (1.54 mmol g^{-1}) and sunflower seed shells (1.46 mmol g^{-1}).[179,180] In another study, activated carbon derived from walnut shells exhibited a CO_2 adsorption capacity of 2.1 mmol g^{-1}.[170] Olive tree pruning residues have also been explored as a biomass source for AC synthesis aimed at CO_2 capture.[183,184] AC derived from this biomass has shown impressively high surface areas, ranging from 786 to 1985 m^2 g^{-1}.

Recently, Ramos *et al.*[185] developed a high-performance CO_2 adsorbent by using olive mill waste through chemical activation with potassium hydroxide (KOH). The optimized activated carbon (designated OMW-1) exhibited an impressive CO_2 uptake performance of 2.4 mmol g^{-1} in pure CO_2 and, critically, 0.84 mmol g^{-1} in 15% vol CO_2, making it suitable for realistic industrial applications. SEM analysis reveals that activation parameters critically govern pore development and CO_2 adsorption behavior of OMW-derived activated carbon (Fig. 9). Activation at 650 °C (OMW-1) yields well-distributed, uniform cavities with a stable micro–mesoporous framework, whereas 950 °C (OMW-2) causes excessive thermal decomposition of cellulose, hemicellulose, and lignin, leading to enlarged, non-uniform pores and partial structural collapse. Increasing activation time from 45 to 75 min promotes gradual formation of interconnected pores. However,

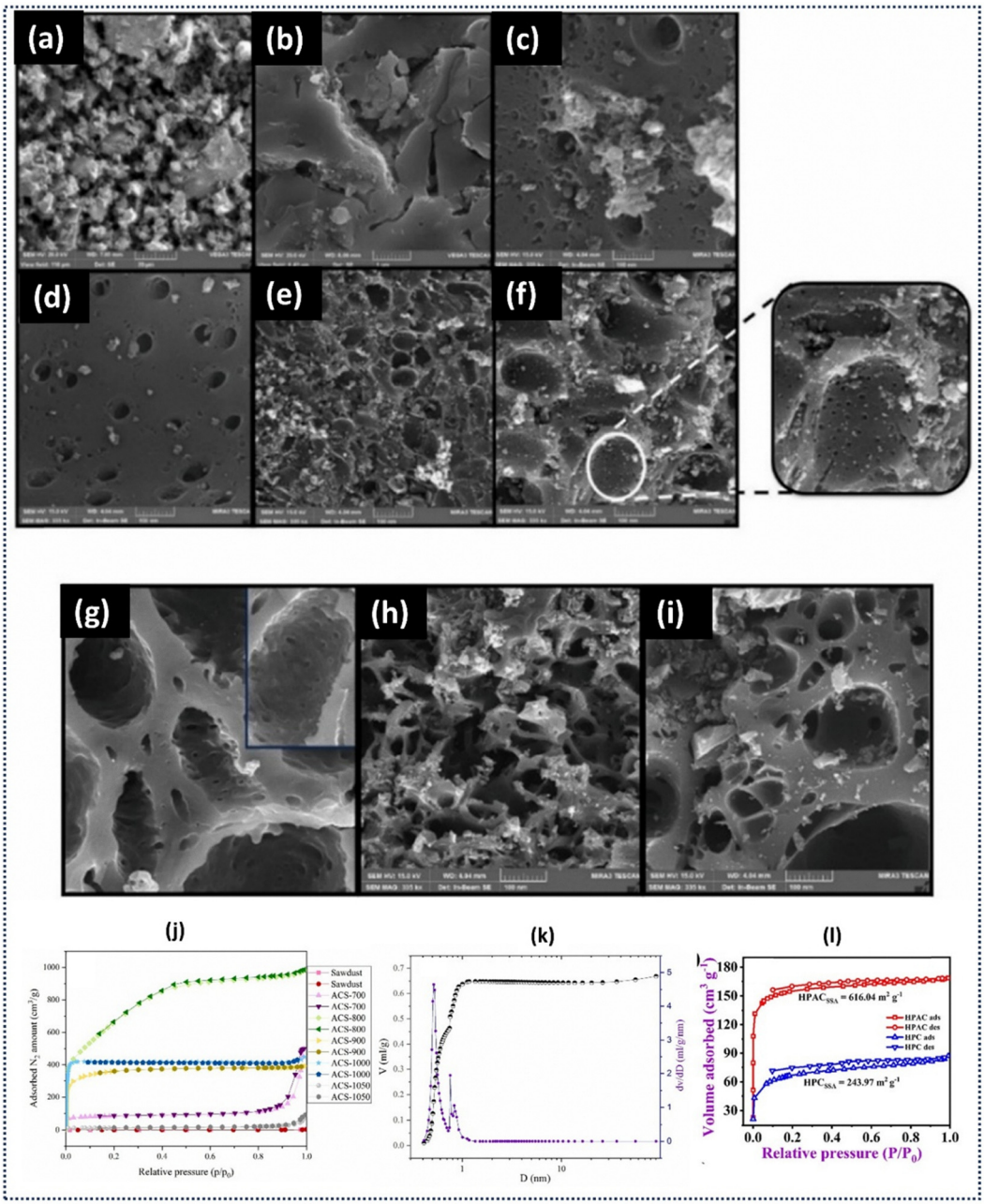

Fig. 8 FE-SEM micrographs of (a, b) untreated sawdust, (c) A-CWO-700, (d) A–CS–800, (e) A–CS–900, (f, g) A–CS–1000, (h) A–CS–1050, and (i) A–CS–1100; (j) Nitrogen adsorption–desorption isotherms and (k) corresponding pore size distribution of A–CS–1000 calculated using NLDFT (reproduced from ref. 177 under the Creative Commons Attribution (CC BY) license); (l) BET adsorption–desorption isotherm of activated carbon (HPAC and HPC) (reproduced from ref. 178 with permission from [Springer Nature], copyright [2023]).

prolonged treatment (120 min) induces surface cracking and degradation, especially at higher temperatures. The KOH/biochar ratio further modulates pore architecture. The 2:1 ratio (OMW-1) provides a balanced micro–mesopore network optimal for CO_2 capture, while higher ratios (4:1 and 6:1) progressively increase microporosity (up to 96.3%) but reduce total pore volume and accessibility, diminishing practical adsorption efficiency. These morphological trends directly explain adsorption performance: OMW-1, with 94.6% microporosity and a narrow average pore size of $\sim$4.8 Å, exhibits the highest CO_2 uptake (105.7 mg g^{-1}), whereas OMW-3, despite its ultra-high surface area (2577 m^2 g^{-1}), shows inferior uptake due to excessive meso/macropore contribution.

Thus, based on the above studies, it can be concluded that increasing activation temperatures generally reduces surface area and pore volume due to structural collapse. However, CO_2 adsorption capacity improved when the activation temperature was raised from 500 °C to 600 °C, before declining at even higher temperatures. The highest CO_2 uptake (265.8 mg g^{-1} at 0 °C) was reported for the AC sample activated at 600 °C with a carbon-to-KOH ratio of 1:3 (AC600 3/1).[183]

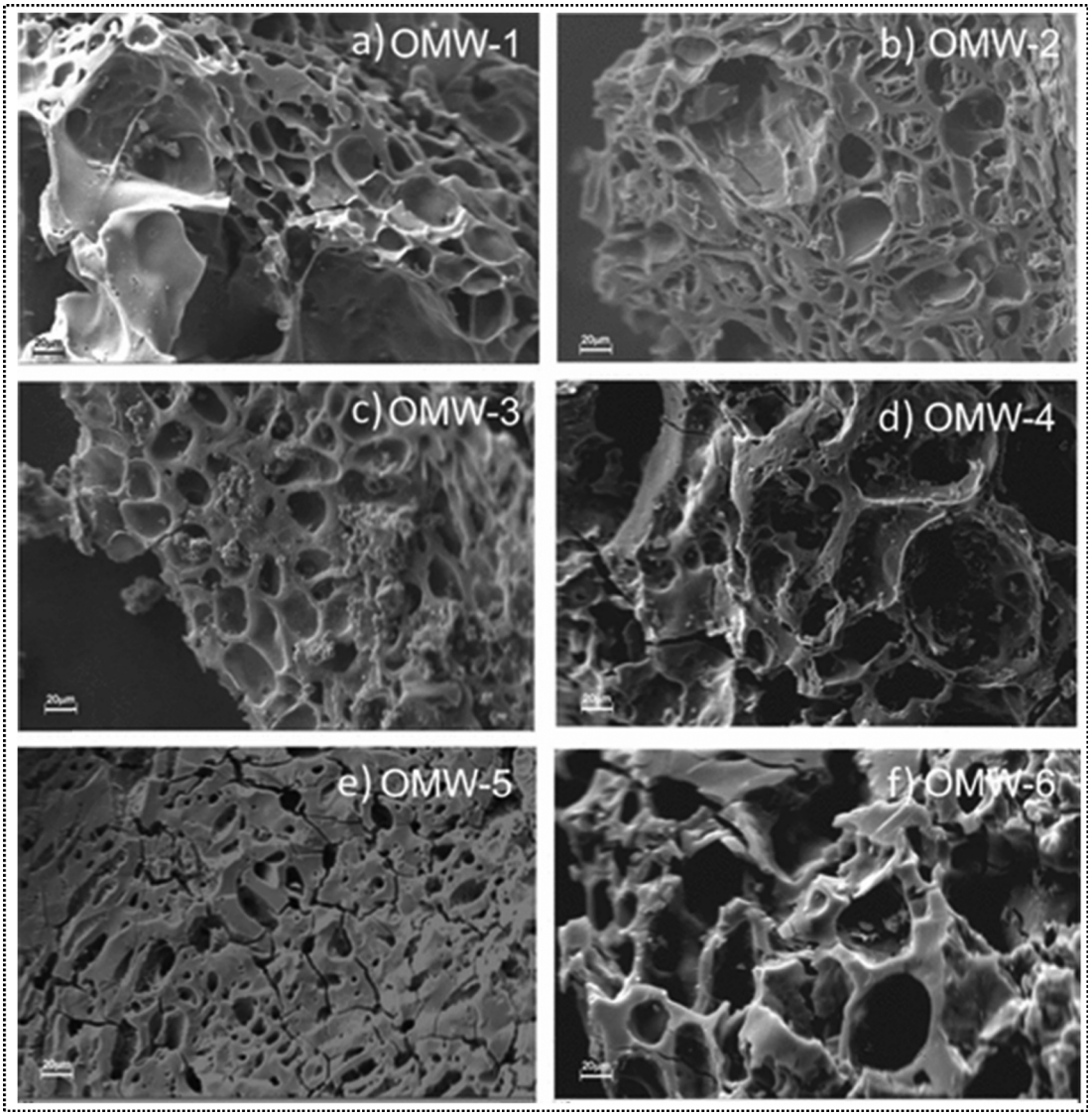

Fig. 9 SEM micrographs recorded at 1000× magnification for the activated carbon samples: (a) OMW-1, (b) OMW-2, (c) OMW-3, (d) OMW-4, (e) OMW-5, and (f) OMW-6, illustrating the evolution of surface morphology under different activation conditions (reproduced from ref. 185 under the Creative Commons Attribution (CC BY 4.0) license).

A clear performance pattern is observed across various biomass feedstocks. Precursors with inherently high lignocellulosic content, such as coconut and walnut shells, consistently exhibit superior microporosity compared to soft biomass, including leaves and stalks, when activated under identical conditions.[186,187] Nevertheless, the synthesis method often has a greater influence on the final performance than the origin of the feedstock. Chemical activation with KOH or H_3PO_4 generally yields surface areas 1.5–2 times higher than those achieved through physical activation with CO_2 or steam, thereby enabling higher CO_2 gravimetric uptake, despite the trade-off of broader pore size distributions, which may compromise selectivity at low partial pressures.

In recent years, significant attention has been directed toward modifying and functionalizing AC materials to enhance the availability of active adsorption sites for CO_2 capture. The incorporation of heteroatoms, such as nitrogen, oxygen, and sulfur, into the carbon framework has emerged as an effective strategy to enhance CO_2 uptake. Since CO_2 is inherently acidic, it can strongly interact with materials containing basic surface functionalities, such as amine groups.[167] Amine-functionalized AC exhibits superior CO_2 adsorption capacities compared to pristine or unmodified AC (SAC). Functionalization with various amine compounds, such as diethylenetriamine (DETA), triethylenetetramine (TETA), and tetraethylenepentamine (TEPA), has been explored in the literature, where TETA introduces both primary and secondary amine groups.[188] Due to its shorter chain length, DETA facilitates a higher degree of amine functionality incorporation into the AC structure.

Additionally, the pore architecture plays a critical role in determining adsorption performance, as it governs the accessibility of adsorbate molecules to the adsorbent surface. While

amine functionalization can generate mesoporous structures, as evidenced by type IV hysteresis loops, it often reduces surface area due to pore blockage by the relatively large molecular weight of organic amines. Fig. 10(a) presents FTIR analysis of SAC composites modified with varying concentrations of DETA and TEPA, while Fig. 10(c) illustrates the proposed reaction mechanism. This mechanism involves the formation of a zwitterionic intermediate upon interaction between the lone pair of electrons in the amine and the carbon atom present in CO_2, followed by deprotonation by a free amine group to yield carbamate species, as confirmed by FTIR spectra (Fig. 10a and b) after CO_2 adsorption.[189] Remarkably, a 30% DETA–SAC composite achieved an adsorption capacity of 78.62 mg g^{-1} under 20% CO_2 concentration conditions and at a gas flow rate of 800 mL min^{-1}.

Further advancements include the work conducted by Lotfinezhad *et al.*, who employed nitrogen doping on jujube and date seed-derived activated carbon using urea as the nitrogen source following KOH activation. Nitrogen incorporation occurs through the thermal decomposition of urea, which releases free amine radicals that interact with hydroxyl groups on the activated carbon surface, forming nitrogen-functional groups and creating a microporous architecture.[190] Ospino *et al.* reported that nitrogen doping enhances CO_2 capture capacity and selectivity but compromises AC's textural properties. A notable drawback of nitrogen-doped activated carbon is its diminished CO_2 adsorption performance under humid conditions, attributed to the strong water affinity of the nitrogen-functionalized surfaces.[191]

It has been observed that the CO_2 adsorption capacity increases significantly as the CO_2 pressure increases. For example, at 90 vol% CO_2, the adsorption reached 2.33 mmol g^{-1}, while at 10 vol% CO_2, it dropped to 1.16 mmol g^{-1}. This improvement at higher pressures is due to CO_2 molecules interacting more with the accessible adsorption sites on the material's surface. Even when the same synthesis circumstances and procedures are used, the choice of precursor is crucial in determining the effectiveness of the final adsorption. For instance, nitrogen-doped activated carbon made from date seeds exhibited better CO_2 absorption (2.93 mmol g^{-1}) compared to activated carbon made from jujube seeds. This was mainly because the microporous structure of the date seeds was more developed. Another important aspect that affects how things adsorb is temperature. A rise in CO_2 capture temperature typically makes it more challenging to collect CO_2 while all other factors remain constant. Specifically, increasing the temperature from 25 °C to 50 °C for date-seed-derived AC resulted in a significant 42.7% decrease in adsorption capacity.[190]

Composites, compared to activated carbon alone, have shown significant improvements in their ability to capture CO_2. MXenes, a class of two-dimensional transition metal carbides and nitrides, are one of the most promising materials to be added to activated carbon matrices. They have lately gotten

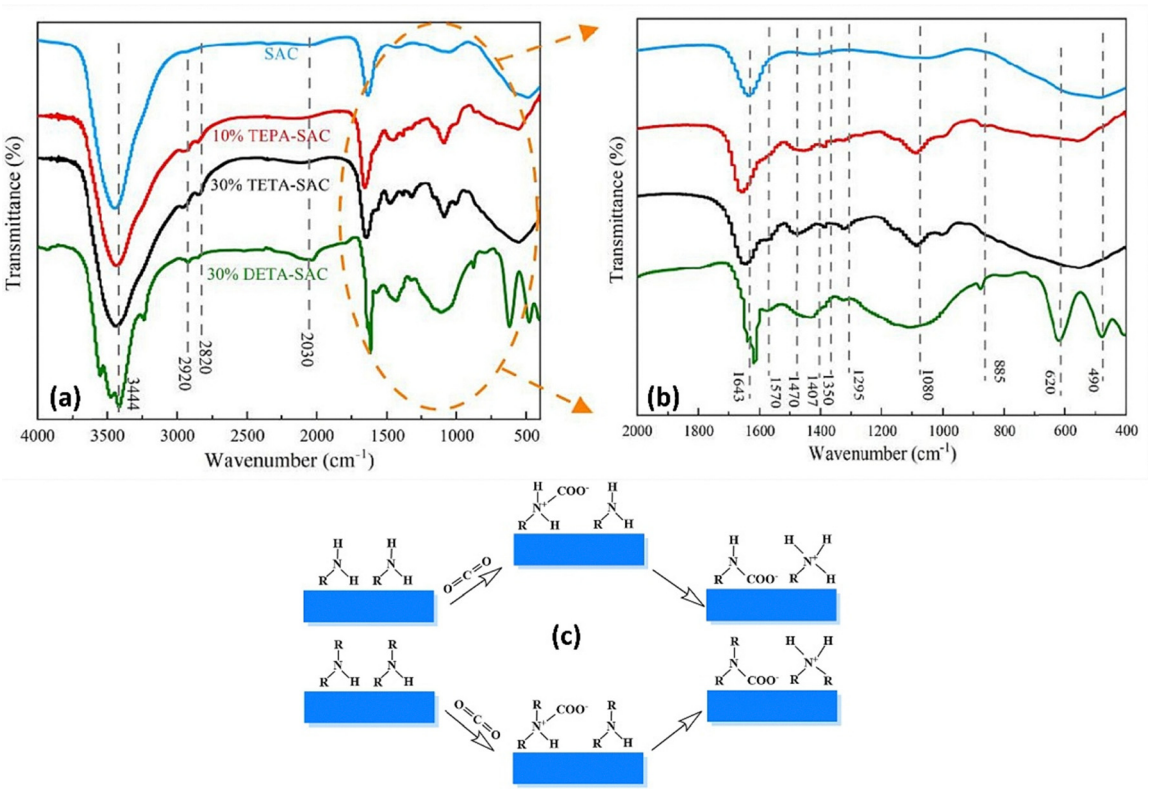

Fig. 10 (a) FT-IR spectra of various carbon materials; (b) magnified view of the region highlighted by the orange dashed circle; (c) schematic illustration of the potential CO_2 adsorption mechanisms on carbon surfaces functionalized with primary and secondary amine groups (reproduced from ref. 189 with permission from [Elsevier], copyright [2024]).

a lot of attention for their use in gas adsorption. DFT tests show that clean MXenes can hold around 0.36 mg g^{-1} of CO_2, mainly because they are very good at transferring charge from the MXene surface to CO_2 molecules. Adding activated carbon to the spaces between the layers of MXenes helps prevent MXenes from restacking, thereby increasing the surface area available for adsorption. Adding just 2.5% MXene to the activated carbon matrix made a significant difference in the amount of CO_2 it could hold, increasing from 46.46 cm^3 g^{-1} to 67.83 cm^3 g^{-1}.

Beyond adsorption capacity, gas selectivity is a critical parameter for separation processes. The MXene–AC composite exhibited superior CO_2 selectivity, with a measured uptake of 67.83 cm^3 g^{-1}, compared to only 13.65 cm^3 g^{-1} for CH_4 and 5.29 cm^3 g^{-1} for N_2. Even pristine AC showed respectable selectivity, adsorbing 46.46 cm^3 g^{-1} of CO_2, *versus* 11.004 cm^3 g^{-1} for CH_4 and 3.992 cm^3 g^{-1} for N_2. Equilibrium adsorption, pure component analysis, and the ideal adsorbed solution theory (IAST) all confirmed the selectivity tests, which showed that $CO_2 > CH_4 > N_2$ was the order of preference. The improved selectivity of the MXene–AC composite is attributed to the chemisorption process facilitated by the presence of titanium carbide functional groups, as indicated by the FTIR signal at 105 cm^{-1}. In a separate investigation, Gorbounov *et al.*[192] produced acid-treated carbon by using a nitration mixture (HNO_3 and H_2SO_4) on physically activated biomass. This one-step treatment enhanced surface oxidation and nitrification, resulting in an adsorption capacity of 0.96 mmol g^{-1} at 50 °C. Combining acid treatment with plasma activation has also been demonstrated to be an effective method for increasing surface area, porosity, and CO_2 collection capability. Zhiping Ye *et al.*[193] used a two-step treatment method, first utilizing HNO_3 acidification and then exposing the sample to cold plasma, as shown in Fig. 11. Adsorption measurements revealed a substantial increase in CO_2 uptake: 81% at 298 K and 64% at 273 K, compared to untreated carbon. Mechanistically, the acid treatment introduced oxygen-rich functional groups (*e.g.*, carboxyl, nitro, and phenolic) that provided active sites for subsequent nitrogen doping, enhancing CO_2 and NO_2 adsorption. The plasma treatment, using N_2/Ar gases, generated high-energy species (ionized N_2 and Ar^+), where Ar^+ ions played a dominant role in etching the AC surface, creating microporous structures. In contrast, reactive N_2 species enabled effective nitrogen doping.

This section highlights that the efficacy of porous carbons in capturing CO_2 is influenced by the interplay between pore structure and surface characteristics, both of which are significantly impacted by the activation and functionalization methods employed. Chemical activation, especially when employing KOH, proves highly efficient in creating ultrahigh surface areas and hierarchical pore structures, thereby facilitating rapid adsorption kinetics and substantial capacities. Nevertheless, these benefits are offset by diminished carbon yields, more demanding processing conditions, and the requirement for extensive post-treatment. Conversely, physical activation utilizing CO_2 or steam presents a more yield-preserving and scalable approach, yielding narrowly distributed ultramicropores (<1 nm) that augment adsorption enthalpy and CO_2/N_2 selectivity through size-sieving effects, thus rendering this method particularly appealing for post-combustion capture under conditions of low CO_2 partial pressures.

Beyond textural optimization, amine functionalization emerges as a powerful strategy to improve low-pressure CO_2 uptake through strong chemisorptive interactions. The incorporation of amines such as PEI or TEPA significantly enhances affinity toward CO_2, particularly under dilute conditions, but at the expense of surface area and pore accessibility due to pore filling and diffusion limitations. Notably, the superior tolerance and, in some cases, enhancement of CO_2 capture performance under humid conditions distinguish amine-functionalized carbons from purely physisorptive systems, highlighting their potential for realistic flue-gas environments. Overall, the insights consolidated in this review emphasize that no single

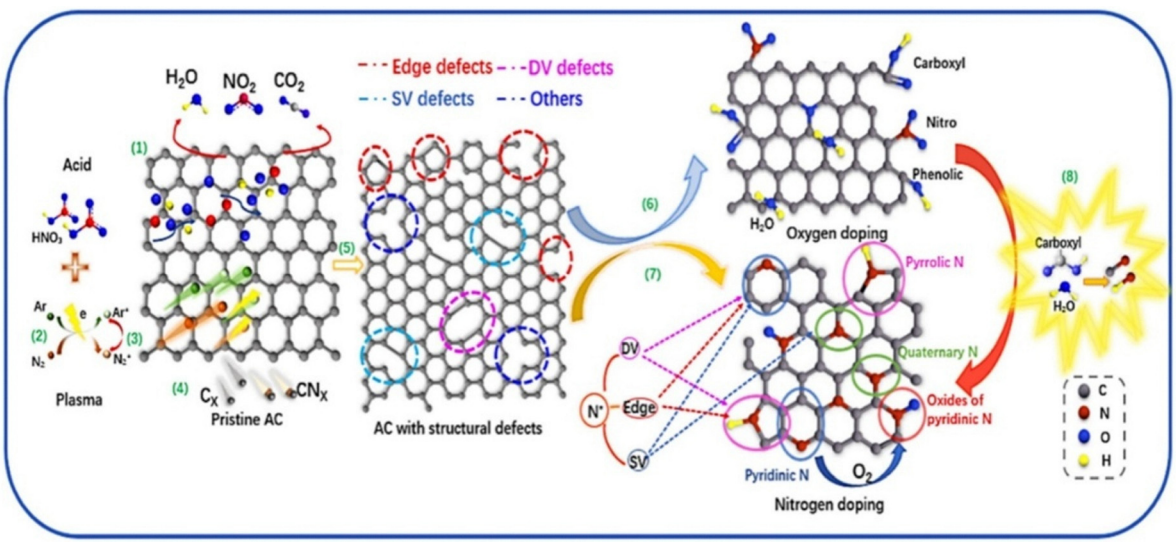

Fig. 11 Schematic illustration of surface modification of activated carbons (ACs) *via* acid treatment and cold plasma techniques, highlighting the introduction of functional groups and enhancement of surface activity (reproduced from ref. 193 with permission from [Elsevier], copyright [2025]).

Table 7 Comparative summary of precursor materials, activation/modification strategies, surface area, and CO_2 adsorption performance parameters of activated carbon-based adsorbents

Precursor material	Activation/modification	Surface area ($m^2\ g^{-1}$)	CO_2 uptake (mmol g^{-1})	Q_{st} (kJ mol^{-1})	Selectivity (CO_2/N_2)	Ref.
Sunflower seed shell	Carbonization and activation by KOH at 773 K	1790	1.46	38–23.5	7.2	179
Indian almond shell	Heat treatment in air (HPC) and nitrogen (HPAC)	244 616	1.7 2.3	43	41.80	182
Commercial AC	1 M HNO_3 + H_2SO_4 and cold plasma treatment	354 (acid) 468 (plasma) 339 (acid+ plasma)	2.7 (298 K) 3.3 (273 K)	14–27	CO_2/N_2 (40.5)	193
AC	Not mentioned	1025	46.46 $cm^3\ g^{-1}$	26.7–31.3	CO_2/N_2 (11.79) CO_2/CH_4 (4.97)	167
Date-palm waste	Activation by KOH	1506.3	6.71 at 0 °C and 4.214 at 25 °C	35	—	194
Starch	N-doped biochars with rich-oxygen functional groups	409.3	1.2 at 0.15 bar CO_2	—	—	195
Waste tyre	TEPA loading (5%)	109.78	43.88 mg g^{-1} CO_2 flow rate of 100 mL min^{-1}	—	—	188
Peanut shell 1	Carbonization and activation of K_2CO_3	1150	5.7 at 273 K	29.7–42.6	—	180
Peanut shell 2	Carbonization and activation at 500 °C	956	1.54	21.5–60	5.6	179
Sawdust	Activation using CO_2 at 1000 °C 1100 °C	1651 1163	10.64 (0 °C) 9.2 (50 °C) 8.6 (50 °C)	—	207.52 (0 °C) 40.2 (25 °C)	177
Date seed	KOH-carbon activation (2 : 1)	786	1.21	—	—	190
Jujube seeds		698	1.16	—	—	
Date seed	KOH activation and N-doping	864	1.31 at 25 C	—	—	190
Walnut shell	CO_2 activation	810	2.1	—	—	166
Olive tree pruning	600 °C, carbon KOH ratio 1:3 KOH activation at 788.5 °C, carbon KOH ratio (1:6.38)	786–1985 3526	265.8 at 0 °C 5.1 at 0 °C and 1 bar	23.8 19.4 (chemical) 24.2 (physical)	— —	183 184
AC	Acid treated (HNO_3 and H_2SO_4)	221	0.96 at 50 °C	30.5	—	192
Chitosan-based AC	N-functionalized	2262	5.3 at 25 °C and 1 bar	20–29	1–10	196
Chestnut shell	Carbonized (500 °C) material, boron-doped/activated with $KBrO_2$	683	3.15 mmol g^{-1} (298 K) 4.22 mmol g^{-1} (273 K)	21–38	—	197
Coconut shell	Carbonized (500 °C) treated with thiourea and KOH (700 °C)	1315	4.38 mmol g^{-1} (298 K) 6.46 (273 K)	—	17	198
Lotus petioles	Carbonised (500 °C) treated with sodium phytate (700 °C)	525	2.51 (298 K) 3.34 (273 K)	15–44	19	199

Note: the gas composition (*e.g.*, purity and mixed-gas environments) and operating pressures used across different studies may differ.

strategy is universally optimal; rather, the rational integration of activation methods and surface functionalization, tailored to specific capture conditions, is essential for the development of next-generation CNM-based adsorbents for efficient and practical CO_2 capture. A thorough comparison of precursor materials, activation and surface modification techniques, textural characteristics (including specific surface area), and the corresponding CO_2 adsorption performance metrics of activated carbon-based adsorbents reported in recent literature is given in Table 7.

6.2. Fullerene-based adsorbents

Fullerene, a zero-dimensional (0D) carbon allotrope, is characterized by its distinctive cage-like structure, typically denoted by its number of carbon atoms, such as C_{60} or C_{70}. Due to their unique geometry and electronic properties, fullerenes have garnered global research interest, particularly for adsorption applications involving fuels and greenhouse gases, such as NO_2 and CO_2.[200] However, the inherent adsorption mechanism of fullerenes is limited primarily to weak physical interactions, which allows only a monolayer of gas molecules to bind to the first layer of active sites. This limitation mainly stems from the absence of intrinsic porosity in pristine fullerenes, rendering surface modification or decoration essential to enhance their adsorption performance.

Studies have shown that pure C_{60} exhibits negligible CO_2 adsorption because of its nonporous nature. Interestingly, when a single CO_2 molecule adsorbs onto a metal-supported fullerene (C_{60}) surface, the process becomes exoergic, with a reported adsorption energy of –1.57 eV. Doping strategies, such as the incorporation of titanium (Ti) or calcium (Ca) atoms onto the fullerene surface, have been reported to significantly enhance CO_2 adsorption capacity.[201,202] This improvement stems from enhanced charge transfer interactions between the dopant and CO_2 molecules, as well as modifications to the adsorption energy and enthalpy profiles compared to undoped (bare) fullerenes. Metal or metal oxide doping thus provides a promising route to transform fullerenes from passive surfaces into highly active materials for CO_2 capture.

Recent advancements in DFT and other computational techniques have highlighted the potential of fullerenes in CO_2 adsorption. Bottani *et al.*[201] conducted a Monte Carlo simulation study,

which suggested that CO_2 can be adsorbed onto fullerene surfaces if voids are present within the structure. Perham Rezaee *et al.*[203] examined the CO_2 adsorption properties of boron (B), phosphorus (P), and nitrogen (N) doped C_{20} fullerenes (C_{20}-*n*X*n*, where X represents B, P, or N). Their findings revealed that boron and nitrogen doping enhanced CO_2 adsorption more effectively than phosphorus doping. These stronger interactions are attributed to the higher concentration of the highest occupied molecular orbitals (HOMO) and lowest unoccupied molecular orbitals (LUMO) associated with B and N, which are primarily localized on the dopant atoms and adjacent carbon atoms, as shown in Fig. 12. Nitrogen doping activates the π-electrons, making the N–C bond a preferred site for electrophilic or nucleophilic attachment.[203] When an electric field was applied, the CO_2 adsorption capacity

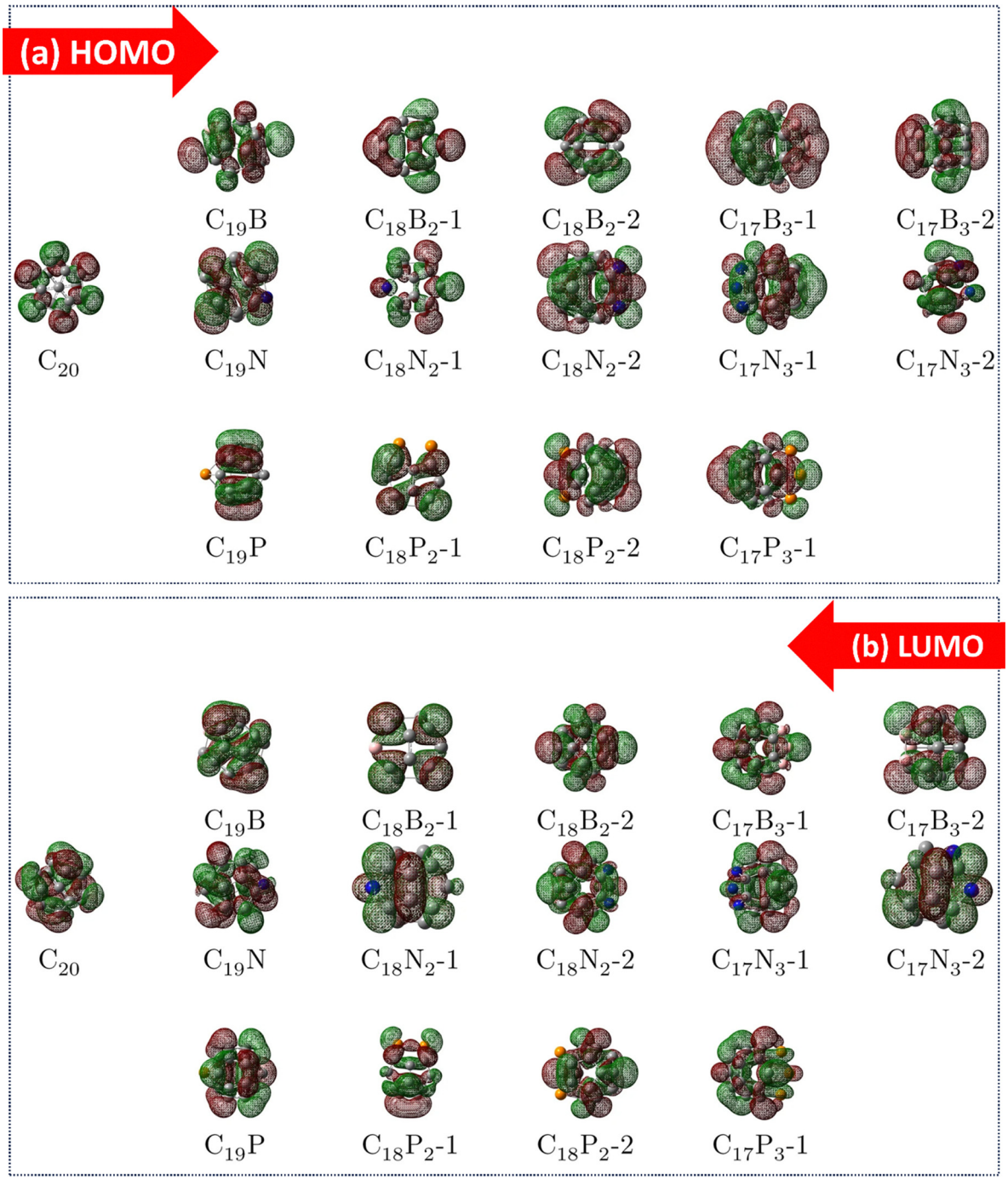

Fig. 12 (a) HOMO plots of pristine C_{20} and doped $C_{20-n}X_n$ structures (n = 1, 2, 3; X = B, N, P), illustrating the spatial distribution of the highest occupied molecular orbitals; (b) LUMO plots of pristine C_{20} and doped $C_{20-n}X_n$ structures (n = 1, 2, 3; X = B, N, P), showing the lowest unoccupied molecular orbitals. In both plots, red and green represent the positive and negative phases of the wave function, respectively. Atom color coding: pink—boron, blue—nitrogen, yellow—phosphorus, grey—carbon (reproduced from ref. 203 under the Creative Commons Attribution (CC BY) license).

of the doped fullerene increased (from −0.53 eV to −0.71 eV) due to chemisorption processes that followed initial physisorption. In a separate study, phosphorus-decorated fullerene (P-$C_{24}N_{24}$) demonstrated selective CO_2 adsorption from a CO_2–N_2 mixture.[204] Using an electric field, in conjunction with DFT calculations, revealed that the binding distance between carbon and oxygen decreased (from 0.012 to 0.013 au) with increasing electric field strength, signalling the onset of chemisorption alongside physisorption. This method allows for controlled desorption of CO_2 by toggling the electric field, providing a potential pathway for CO_2 regeneration. Boron-doped fullerenes (*e.g.*, B_{38}, B_{40}, and B_{80}) have garnered particular interest in CO_2 capture applications. While B_{80} has yet to be experimentally realized, its theoretical potential remains promising. Mahsa Kabiri *et al.* demonstrated the CO_2 capture potential of B_{40} fullerenes, citing their amphoteric nature and practicality in the literature. B_{40} exhibited an impressive CO_2 adsorption capacity of 13.87 mmol g^{-1} and good selectivity.[205]

However, doping with a transition metal is necessary to improve performance due to the energy barrier (1.2 V) associated with CO_2 adsorption and its low dipole moment. Kabiri *et al.* showed that doping B_{40} with yttrium (Y) resulted in a higher adsorption energy (−0.75 eV) for CO_2 molecules compared to pristine B_{40}.[206] Furthermore, CO_2 adsorption in Y-doped B_{40} is dominated by chemisorption, as evidenced by the overlap between Y's 4d orbitals and CO_2's LUMO, confirming the strong interaction between yttrium and CO_2.[206] Esrafili *et al.* explored scandium (Sc)-decorated porphyrin-like fullerene (C_{24}) for efficient CO_2 capture *via* adsorption. Similarly, Sebastian Anila *et al.* prepared imidazolium cation polyanionic fulleride $((IM+)_n\ C_{60}\ (CN)_n)_n^-$ ionic liquids, noting an increase in binding energy with a greater number of CN anions. The molecular electrostatic potential (MESP) analysis revealed that the excess electrons in the complex were delocalized over the unsaturated carbon centers of the fullerene, while the CN groups remained neutral. This increase in CN groups enhanced the interaction with CO_2, converting non-covalent interactions into stronger covalent bonding. Further studies on nitrogen-doped C_{60} fullerene ($C_{60-2n}N_{2n}$) revealed that nitrogen doping increases the electron density of the fullerene molecule, improving the CO_2 interaction.[206] By attaching a CN-group to the carbon center (forming *N*-cyanofulleride), CO_2 adsorption was further enhanced, as confirmed by MESP analysis, which indicated an electron-rich anion facilitating stronger interactions with CO_2.[207] While much of the research on fullerene-based CO_2 adsorption has been theoretical, there is a limited amount of experimental work on its real-world applications. However, the potential for fullerene-based materials in CO_2 capture remains a promising avenue for further investigation.[208] The curvature of the fullerene cage has a significant influence on its interaction with CO_2 molecules. Smaller cages with higher curvature, such as C_{20} and B_{40}, exhibit localized electron density and enhanced Lewis basicity compared to the larger, more diffuse C_{60} cage. This higher charge concentration on the cage surface strengthens the dipole–quadrupole interactions with CO_2, theoretically resulting in higher binding energies and improved capture affinity for highly curved analogues.

In conclusion, CO_2 capture *via* fullerene-based methods is predominantly theoretical. Although experimental realization is limited, advances in density functional theory (DFT) and Monte Carlo simulations have provided critical blueprints for designing next-generation adsorbents. Moreover, the theoretical studies summarized above are not merely abstract calculations; they serve as essential pre-screening and mechanistic guides for experimentalists.

6.3. CNT-based CO_2 adsorbents

CNTs can be classified into two primary types: single-walled carbon nanotubes (SWCNTs) and multi-walled carbon nanotubes (MWCNTs). SWCNTs consist of a single graphene sheet wrapped into a tube form, while MWCNTs comprise multiple graphene sheets wrapped concentrically.[209] The synthesis of CNTs typically involves arc discharge, laser ablation, or CVD. Although arc discharge and laser ablation are known for producing high-quality CNTs, CVD enables the production of large quantities with the potential for alignment.

This section of the review focuses on the role of CNTs in CO_2 capture and discusses the most recent advancements in this area. Over the last two decades, CNTs have garnered significant attention for CO_2 absorption due to their lightweight nature, high surface area, conductive properties, hydrophobicity, and tunable surface chemistry. The hydrophobicity of CNTs minimizes the impact of water interaction, while their hollow tubular structure increases the surface area for adsorption inside and outside the tube. The adsorption mechanism differs fundamentally between pristine and functionalized CNTs. Pristine CNTs rely on weak van der Waals forces (physisorption) and often suffer from low selectivity. In contrast, acid treatment (introducing –COOH groups) enhances surface polarity, while amine functionalization shifts the mechanism toward chemisorption. Primary amines facilitate the formation of carbamates, significantly increasing the heat of adsorption (Q_{st}). However, excessive functionalization can lead to agglomeration and blockage of the inner nanotube channels, reducing the accessibility of internal pore volume to gas molecules.

Cinke *et al.*[210] conducted a temperature-dependent study on SWCNTs synthesized *via* the HiPco process for CO_2 adsorption. They found that the CO_2 adsorption capacity of purified SWCNTs was twice that of activated carbon and raw HiPco at 35 °C. As with other carbon materials, amine functionalization is an effective method to enhance CO_2 adsorption in CNTs. This method also benefits from lower energy requirements for CO_2 desorption compared to traditional amine solutions such as monoethanolamine (MEA).[211,212]

Recently, Khoshraftar *et al.*[213] reported modified MWCNTs, synthesized using Fe–Ni/AC catalysts to achieve exceptional CO_2 adsorption capacity, reaching a maximum of 424.08 mg g^{-1} at 25 °C and 10 bar pressure. The catalyst modification, which reduced the surface area from 240 $m^2\ g^{-1}$ (pristine MWCNTs) to 11 $m^2\ g^{-1}$ (modified M-MWCNTs), paradoxically resulted in an increased adsorption capacity. This was attributed to the introduction of new adsorption sites and favorable interactions

between functional groups, which enhance CO_2 binding at lower temperatures.

Lourenco *et al.*[211] compared pristine CNTs with COOH-functionalized and amine-functionalized MWCNTs, using N1–(3-trimethoxysilylpropyl) diethylenetriamine (DETASi) as the functionalizing agent. They found that pristine MWCNTs and MWCNT-OH could not adsorb CO_2 due to the absence of functional groups. In contrast, COOH-functionalized MWCNTs adsorbed 0.1% CO_2 per gram of material, indicating weak interactions between the carboxylic group and CO_2. However, MWCNTs functionalized with DETASi showed a significant improvement in CO_2 adsorption, reaching 2.11%. Specifically, CO_2 adsorption capacities were 0.48 mmol g^{-1} and 0.43 mmol g^{-1} for CNT-COOH-DETASi and CNT-SD-DETASi, respectively. Due to their high surface area, CNTs also help mitigate amine accumulation issues and aid in the structural arrangement of nanoparticles. Ronghuan Xu *et al.*[214] impregnated CNTs with silica nanoparticles and tetraethylenepentamine (TEPA) to enhance CO_2 adsorption. The composite was heat-treated at 90 °C to remove moisture before CO_2 adsorption. Fig. 13(b–e) reveals that, at 50% amine loading, the TEPA-impregnated CNT–SiO_2 composite exhibited an increased CO_2 adsorption capacity of 2.70 mmol g^{-1}, compared to 2.18 mmol g^{-1} for the TEPA–SiO_2 composite alone. This result highlights the role of CNTs in promoting pore filling and rearranging SiO_2 nanoparticles at higher TEPA viscosities. The study also found that increasing the amine functionalization weight fraction (up to 60%) has further enhanced CO_2 adsorption.

Ying Wang *et al.*[215] incorporated sulfur and nitrogen doping to further improve the CO_2 adsorption capacity of CNTs by introducing dual heteroatoms. The CNTs were *in situ* grown from coal activated by KOH, followed by doping with nitrogen and sulfur atoms (KS-NTC). To enhance nitrogen concentration, dual urea treatment was carried out (KN-NTC). Both KN-NTC and KS-NTC exhibited high surface areas of 1789 m^2 g^{-1} and 1875 m^2 g^{-1}, respectively, due to low pore sizes (<0.7 nm), high pore volumes (~ 0.8 cm^3 g^{-1}), and additional defect structures. These defects were attributed to surface etching mediated by the reduction and activation of CNTs.[215] The formation of g-C_3N_4 at 500 °C enhanced the graphitic character, and at higher temperatures (900 °C), it converted to ammonia, creating a porous structure and introducing N-doping. Fig. 14(a and b) shows TEM images of KS-NTC samples demonstrating a tube-like structure with open and closed end configurations, which shows intact structure integrity of carbon nanotubes formed from coal. The CO_2 adsorption capacities of KN-NTC and KS-NTC were evaluated at 25 °C and 0 °C under 0.15 bar pressure of CO_2 as shown in Fig. 14(c and d). KN-NTC showed capacities of 0.815 mmol g^{-1} at 25 °C and 1.6 mmol g^{-1} at 0 °C, while KS-NTC demonstrated higher adsorption capacities of 0.973 mmol g^{-1} at 25 °C and 1.829 mmol g^{-1} at 0 °C. At 1 bar pressure, both samples exhibited significantly higher adsorption capacities, KN-NTC at 5.81 mmol g^{-1} and KS-NTC at 5.66 mmol g^{-1} at 0 °C. Additionally, CO_2 adsorption was far superior to N_2 adsorption (~ 0.5 mmol g^{-1}), confirming the selectivity of the composite for CO_2 over N_2.

Due to their high surface area and lightweight properties, CNTs are highly effective even in very low quantities, making them cost-effective materials for CO_2 capture. Mohammad Heidari *et al.*[216] explored the use of small amounts of CNTs (2.5, 5, and 10 wt%) as additives in the development of $CaZrO_3$–CaO xerogels, thereby improving their structural and textural properties for CO_2 capture. This study investigated the effects of varying Ca/Zr molar ratios (15/1 and 30/1) on the performance of the xerogels to minimize the use of expensive zirconium precursors while maximizing CO_2 capture efficiency. The inclusion of CNTs led to the formation of highly porous structures, significantly enhancing the durability and efficiency of CaO-based adsorbents during cyclic CO_2 capture processes. The xerogels containing 5 wt% CNTs achieved the highest CO_2 capture capacities: 0.164 g CO_2 per g adsorbent for the 15/1 Ca/Zr ratio and 0.149 g CO_2 per g for the 30/1 ratio, demonstrating substantial improvements over traditional CaO sorbents. After 15 cycles under challenging CO_2 capture conditions, the total amount of captured CO_2 increased from 2.01 g CO_2 per g for the 15/1 ratio to 2.92 g CO_2 per g and from 1.96 g CO_2 per g to 3.01 g CO_2 per g for the 30/1 ratio, reflecting excellent cyclic performance. The incorporation of CNTs reduced the crystallite sizes of CaO by 15.84% and 33.1% for the 15/1 and 30/1 ratios, respectively, contributing to a higher surface area and enhanced CO_2 adsorption. Furthermore, the xerogels exhibited substantial increases in pore volume (50.57% for the 15/1 ratio and 90.55% for the 30/1 ratio), promoting greater CO_2 diffusion and capture efficiency. Yuhang Zhang *et al.*[217] introduced MWCNTs/carbon foam (CF) nanocomposites (MCF), synthesized from liquefied larch sawdust, providing a novel approach to utilizing biomass for the creation of advanced materials. These MCF nanocomposites exhibit a unique hierarchical porous structure with ultra-micropores (0.50–0.80 nm) and mesopores (approximately 3.70–3.90 nm), thereby enhancing their potential for gas adsorption. The MCF-2 sample demonstrated impressive CO_2 adsorption capacities of 4.58 mmol g^{-1} at 0 °C and 3.19 mmol g^{-1} at 25 °C, indicating its effectiveness in CO_2 capture. At 25 °C, MCF-2 exhibited a CO_2/N_2 selectivity ratio of 23.71, highlighting its potential for CO_2 separation from nitrogen in practical applications. The MCF nanocomposites showed high isosteric heats of adsorption, ranging from 23.32 to 36.48 kJ mol^{-1}, suggesting strong interactions between CO_2 molecules and the material, which is beneficial for efficient capture. Furthermore, MCF-2 demonstrated excellent recyclability, maintaining its CO_2 capture capacity over multiple adsorption–desorption cycles, indicating low energy requirements for regeneration. Incorporating MWCNTs also significantly enhanced the mechanical strength of the carbon foam, resulting in a 113% increase in compressive strength compared to traditional biomass-based carbon foams. Kavitha Ramadass *et al.*[26] highlighted the potential of naturally occurring materials, such as halloysite nanotubes, for creating advanced carbon nanostructures with superior properties for CO_2 capture. Activated halloysite nanocarbon (AHNC) exhibited an impressive CO_2 adsorption capacity of 25.7 mmol g^{-1} at 0 °C and 30 bar pressure, significantly outperforming other materials, such as mesoporous carbon, activated carbon, and MWCNTs.

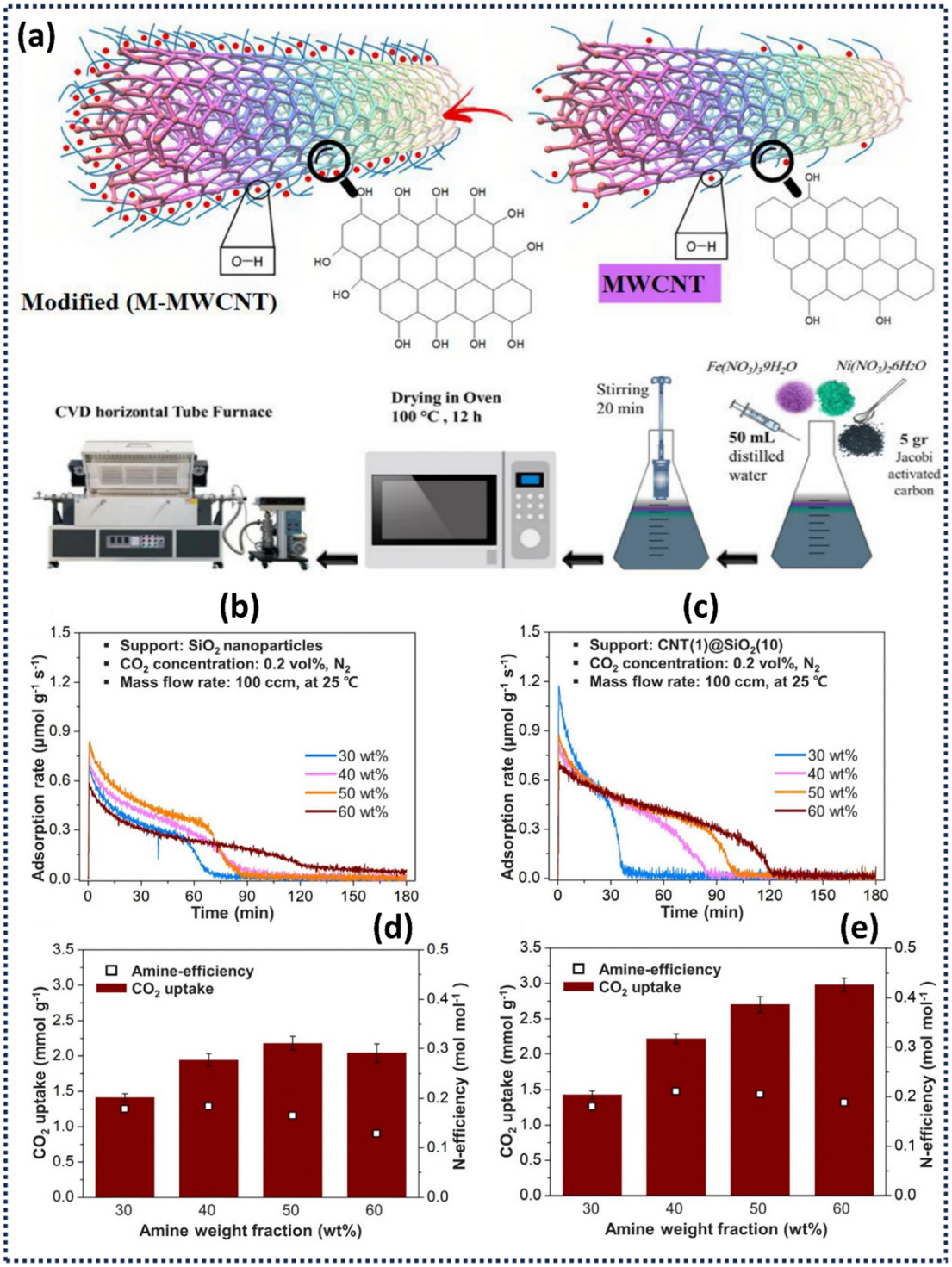

Fig. 13 (a) Experimental setup for the fabrication of M-MWCNTs (reproduced from ref. 213 under the Creative Commons Attribution (CC BY) license); effect of amine loading and support type on CO_2 capture performance; (b) and (c) illustrate the CO_2 adsorption rate, while (d) and (e) present the total CO_2 uptake and amine efficiency, respectively, with experimental conditions: 0.2 vol% CO_2 in N_2, a gas flow rate of 100 ccm, and a temperature of 25 °C (reproduced from ref. 214 with permission from [Elsevier], copyright [2025]).

This high capacity is attributed to the material's large surface area and unique pore structure. The AHNC exhibited a specific surface area of 1646 $m^2\ g^{-1}$, 74 times greater than the raw halloysite's surface area (22.5 $m^2\ g^{-1}$). Additionally, the AHNC exhibited excellent cycling stability, retaining its CO_2 capture efficiency over multiple adsorption–desorption cycles. It is highly suitable for practical applications, as it suggests that the material can be reused without significant performance loss.[26] Immobilizing

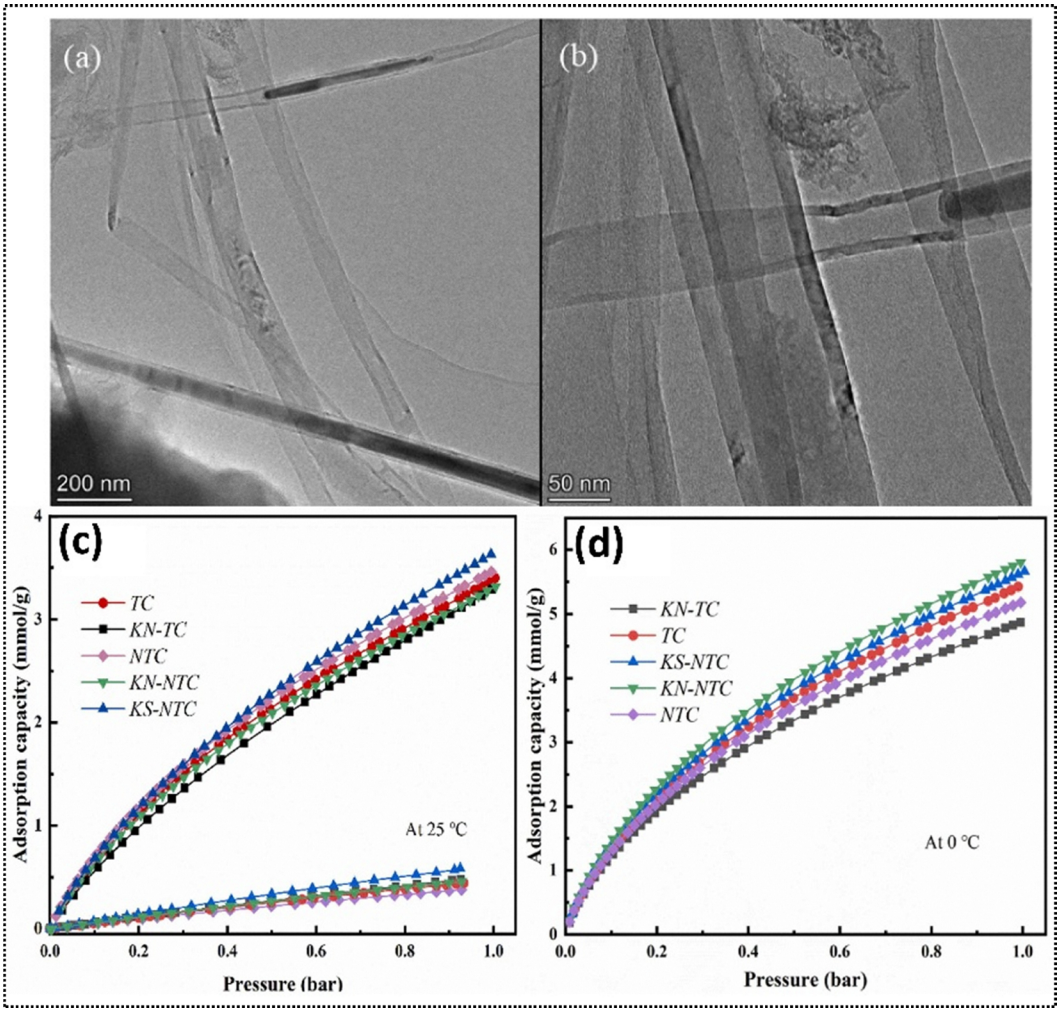

Fig. 14 (a and b) TEM images of the KS-NTC sample; (c) CO_2 and N_2 adsorption capacities of the carbon nanotube composite measured at 25 °C; (d) CO_2 and N_2 adsorption capacities at 0 °C (reproduced from ref. 215 with permission from [Elsevier], copyright [2024]).

active materials on high-surface-area materials, particularly porous ones, can provide many active sites for CO_2 capture. Yingjun Li *et al.*[218] proposed a core–shell material composed of CNTs with ionic polymers and a porous structure, featuring activated epoxide rings for enhanced catalytic activity. They prepared bipyridine-functionalized Zn(II) ionic polymers, which showed enhanced performance in CO_2 capture. Table 8 summarizes the functionalization strategies, specific surface areas, and corresponding CO_2 adsorption performance parameters of CNT-based adsorbents reported in the literature. This comparison clarifies how surface functionalization affects adsorption capacity, selectivity, and kinetics, providing critical insights into structure–property relationships and guiding the rational design of high-efficiency CNT-based sorbents for advanced CO_2 capture applications.

6.4. Graphene-based adsorbents

Graphene, a 2D carbon material, is considered one of the most explored allotropes of carbon due to its unique structure, which is sp^2-hybridized and consists of a single atomic-thick layer of carbon atoms.[220–223] Single- or bilayer graphene can be synthesized using CVD, but the top-down wet chemical method is often preferred for large-scale production. This approach produces GO, which can be reduced and exfoliated to yield multilayer or few-layer graphene.[224,225] The presence of defects in graphene or GO enhances their CO_2 adsorption properties. Additionally, the 2D structure of graphene provides a high surface area, and its properties can be tuned to optimize CO_2 capture.

This section focuses on recent advancements in CO_2 capture using graphene-based materials. Graphene and GO are widely studied for CO_2 adsorption, infiltration, and capture.[226–229] However, pure graphene with few layers tends to have low CO_2 adsorption capacity due to its multi-layered structure, which acts as a diffusion barrier. Furthermore, its hydrophobic and non-polar nature results in low selectivity towards CO_2.[230] To improve CO_2 capture, several strategies have been employed, including tuning the surface defects and increasing the surface area of GO and reduced graphene oxide (rGO).[231] Techniques including physical activation, hydrothermal treatment, chemical treatment,

Table 8 Comparative summary of functionalization, surface area, and CO_2 adsorption performance parameters of CNT-based adsorbents

CNT type	Functionalization/treatment	Surface area (m^2 g^{-1})	CO_2 capacity (mmol g^{-1})	Q_{st} (kJ mol^{-1})	Selectivity (CO_2/N_2)	Ref.
MWCNTs	Produced *via* CVD and modified by Fe–Ni/AC catalysts	240, but after modification, it was reduced to 11	424.08 mg g^{-1} at 25 °C and 10 bar	—	—	213
f-MWCNTs	Functionalized MWCNTs by a simultaneous combination of two amines	155	2.35 (modified MWCNTs) and 1.48 (MWCNT–COOH)	—	—	219
f-MWCNTs	Functionalized MWCNTs with 1,6-diaminohexane	262.69	253.99 mg g^{-1} at 30 °C and 17 bar	21–17		212
Silica particle - MWCNT	TEPA impregnation	—	2.70 (Si-MWCNT-TEPA) 2.18 (Si-TEPA)	—	—	214
Heteroatom doping	N(KN-NTC), doped carbon nanotubes	1789	3.31 (25 °C) and 5.81 (0 °C) at 1 bar	27–34	19	215
Heteroatom doping	N-S(KS-NTC) doped carbon nanotubes	1875	3.63 (25 °C) and 5.66 (0 °C) at 1 bar	31–27	18	
COOH-functionalized	Commercial	121	0.1% CO_2 g^{-1}	—	0%	211
CNT-COOH-DETASi	Reflux for 16 h	74	0.48	—	1.46%	
CNT-SD-DETASi	Reflux for 16 h	88	0.25	—	1.89%	
MWCNT (5%)-$CaZrO_3$-CaO xerogels	Heat treatment and dessication at 150 °C (3 h) and 850 °C (1.5 h)	17.83 20.63	0.164 g (CO_2 g^{-1}) (Ca/Zr 15) 0.149 g (CO_2 per g) Ca/Zr 30)	—	—	216

Note: the gas composition (*e.g.*, purity and mixed-gas environments) and operating pressures used across different studies may vary.

thermal treatment, and plasma treatment have been explored to enhance their adsorption properties. Graphene derivatives can adsorb CO_2 through physisorption and chemisorption, and the adsorption route is primarily governed by the pore structure, surface area, and functional groups (oxygen, nitrogen, and sulfur) present on the graphene sheets. GO, being oxygen-rich, can support chemisorption, whereas rGO's defect structure favours physisorption.[232] However, chemisorption is most effective under low CO_2 pressures or when sufficient adsorption sites are available; otherwise, physisorption predominates.

Surface modification of GO through UV activation has been reported by Anish Mathai Varghese *et al.*[233] to improve CO_2 adsorption. In their study, a Cu-BTC MOF/GO composite was developed, and it was observed that the surface area of the pure Cu-BTC MOF decreased after growth on GO. However, the surface area was restored when the GO was subjected to UV irradiation for 10 minutes. The Cu-BTC MOF/UV-GO composite exhibited a 45% increase in CO_2 adsorption capacity, reaching 5.14 mmol g^{-1} at 25 °C and 1 bar, compared to 3.55 mmol g^{-1} for the pure Cu-BTC MOF.[233] At 0 °C, the adsorption capacity increased to 9.5 mmol g^{-1}. Additionally, the CO_2/N_2 selectivity for UV-activated GO was 21, compared to 19.32 for the pure Cu-BTC MOF.

Similar to other carbon-based adsorbents, graphene-based materials have been functionalized with amine groups to further enhance CO_2 adsorption.[234–236] Amination of graphene is challenging due to the lack of oxygenated groups, but GO, with its abundant oxygen-containing functional groups, offers more opportunities for functionalization. rGO, depending on the production method, can retain these oxygenated groups while also maintaining conductivity, making it more suitable for amine linkage. Polyethyleneimine (PEI) is often used as an amine precursor to form composites with rGO. These PEI–rGO composites have demonstrated high CO_2 uptake at low pressures, with one study reporting an uptake of 0.61 mmol g^{-1} at 4 pK_a of CO_2. At higher CO_2 pressures (101 kPa), the adsorption capacity increased to 1.03 mmol g^{-1}. Interestingly, at 50 °C, the adsorption capacity at low pressure decreased by 72%, but at high pressure, it increased by 50%, reaching 1.55 mmol g^{-1}. This behavior is attributed to an increase in the number of available CO_2 adsorption sites at higher temperatures and pressures.[226]

Due to their stability, primary amines such as 3-aminopropyltrimethoxysilane (APTES) are particularly effective for amine linkage.[237] MP Jerome *et al.*[238] explored the functionalization of cellulose-coated GO with APTES to create a composite with a 3D porous structure and abundant oxygen functionalities. Waste white paper was used to extract cellulose (84.9%) through bleaching and alkali treatment. The cellulose-coated GO was then functionalized with APTES and freeze-dried to form an aerogel. Fig. 15 presents SEM images of paper, extracted cellulose, cellulose aerogel, GO aerogel, CGO, CGO-0.25 APTES, and CGO-1.5 APTES.

The rough surface of the paper is attributed to residual impurities from the papermaking process, such as lignin, calcite, and other additives. After alkali and bleaching treatments, the cellulose fibers become fibrillated and free from contaminants. Notably, extracted cellulose exhibits increased porosity along its fiber walls, likely due to the removal of lignin and hemicellulose, which enhances the flexibility of the fibers. Some pores may also be intrinsic, aiding plant fiber physiology. The native cellulose aerogel exhibits a 3D porous network, potentially offering a higher surface area than compact fibers, though this depends on cellulose content. In contrast, the GO aerogel shows a wrinkled, sheet-like morphology. The CGO aerogel combines these features with GO flakes anchored to cellulose fibrils in a porous matrix. Strong cellulose–GO interactions and high GO content (33.3 wt%) result in loosely layered pore walls rather than a rigid fibrous structure. APTES modification induces subtle morphological changes (Fig. 15f–g). With increasing APTES concentration, the GO sheets and cellulose fibrils appear

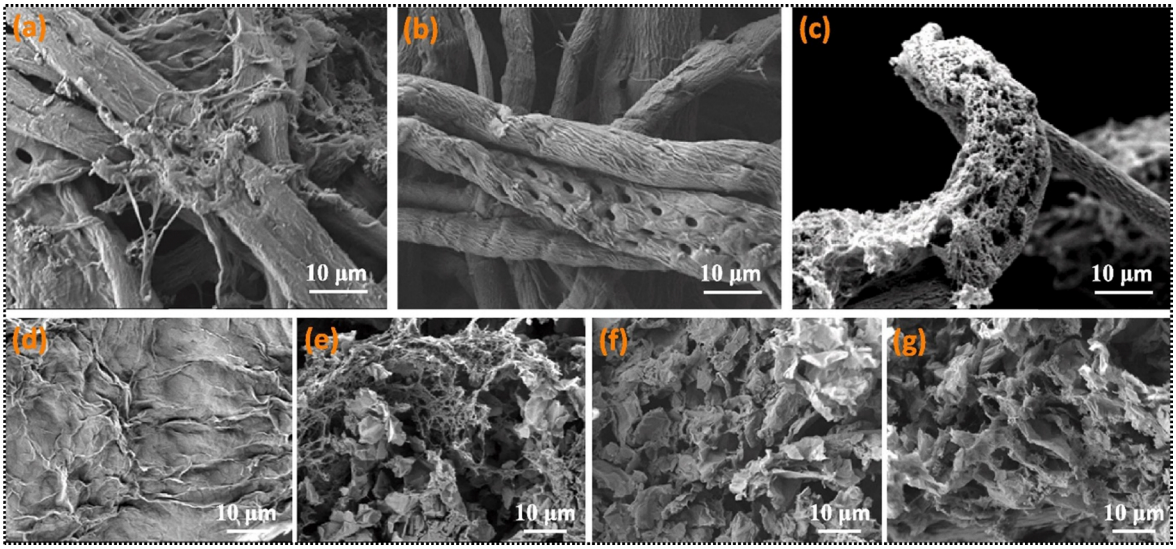

Fig. 15 SEM images of (a) raw paper, (b) extracted cellulose, (c) the cellulose aerogel, (d) the graphene oxide (GO) aerogel, (e) the cellulose–GO (CGO) aerogel, (f) the CGO aerogel modified with 0.25% APTES, and (g) the CGO aerogel modified with 1.5% APTES (reproduced from ref. 238 with permission from [Elsevier], copyright [2025]).

more compact and integrated. The FTIR peak at 1565 cm^{-1} confirmed the successful formation of an amine linkage. Plain GO exhibited a CO_2 capture capacity of 0.57 mmol g^{-1}, higher than plain cellulose (0.2 mmol g^{-1}). The cellulose–GO composite functionalized with APTES showed a remarkable increase in adsorption capacity, reaching 2.52 mmol g^{-1} at 0.25% APTES and 1.34 mmol g^{-1} at 1.5% APTES, significantly outperforming both cellulose and GO. This enhancement is attributed to the increased basicity of the amine groups, which facilitates chemisorption. The chemisorption mechanism is explained through specific equations detailing the interaction between CO_2 and the amine groups on the surface.

$$RNH_2 + CO_2 \leftrightarrow RNH_2^+COO^- \quad (a)$$

$$RNH_2 + RNH_2^+COO^- \leftrightarrow RNHCOO^- + NH_3^+ \quad (b)$$

Further adsorption of CO_2 in the pores of graphene derivatives occurs through physisorption. However, pore blocking and self-polymerization can occur at higher concentrations of amine groups, as seen in the case of 1.5% APTES, which reduces the surface area and decreases performance. The plasma technique (cold plasma) is another non-chemical method that has gained attention. This technique utilizes various gases, such as nitrogen (N_2), argon (Ar), ammonia (NH_3), and hydrogen (H_2), to induce pore formation, functionalization, and morphological improvements in graphene without altering its primary structure. Navik *et al.*[239] applied cold plasma surface modification to graphene-based aerogels using a N_2/H_2 mixture (0.5 mL min^{-1}) at treatment times ranging from 2.5 to 10 minutes. The plasma treatment introduced C=C vacancies and functionalized the graphene surface with amine groups, creating nanovoids and edges. This process occurs due to highly energized nitrogen ions, atoms, or molecules interacting with the graphene surface, replacing carbon atoms with N–H groups. The CO_2 adsorption capacity of the treated graphene increased significantly, from 1.6 mmol g^{-1} to 3.3 mmol g^{-1} (when exposed to simulated flue gas) and 1.3 mmol g^{-1} (DAC). Additionally, the selectivity for CO_2 improved dramatically from 42 to 87 after just 5 minutes of plasma treatment. The treatment also enhanced the load-bearing capacity of the graphene aerogel.

In recent years, there has been growing interest in using waste materials to synthesize graphene for CO_2 capture.[225] Bryan E. Arango Hoyos *et al.* synthesized graphene oxide (GO) foam from commercial bamboo using double thermal decomposition. The GO foam was carbonized at varying temperatures (873 K, 973 K, and 1073 K), resulting in different oxidation levels, as determined by XPS analysis. The degree of oxidation varied from 9% at 873 K (GO 873 K) to 3% at 1073 K (GO 1073 K). The results showed that a higher degree of oxidation led to increased surface area, with GO 873 K reaching 570.9 m^2 g^{-1}. GO foam exhibited superior CO_2 retention performance compared to traditional adsorbents, such as zeolite and silica gel. After 2500 seconds of CO_2 adsorption, no desorption was observed even after 18 000 seconds, demonstrating the material's ability to retain CO_2 at room temperature. Complete desorption occurred at 673 K, making the GO foam highly reusable. The CO_2 adsorption efficiency was the highest for GO 1073 K (92.20%), followed by GO 973 K (89.38%) and GO 873 K (86.28%).[227] While the 2D structure of graphene offers a high surface area, it can also limit gas transport when used in pellet form. Researchers have explored the use of one-dimensional graphene nanoribbons (GNRs) to address this issue. These nanoribbons enable enhanced gas transport due to their complex structure. Fau-type zeolites (faujasites) combined with graphene oxide (GO) nanoribbons have shown an advantage in pelletization without structure-directing agents. CO_2 adsorption tests, using a CO_2:N_2 mixture (15:85), showed that zeolite pellets with 12% GO nanoribbons exhibited a CO_2 uptake of 4.61 mmol g^{-1} with high selectivity for CO_2 (76.5)

Table 9 Overview of structure–property–performance relationships of GO-based adsorbents for CO_2 capture, including surface area, adsorption capacity, Q_{st}, and selectivity

Type of material	Treatment	Surface area ($m^2\ g^{-1}$)	CO_2 adsorption (mmol g^{-1})	Q_{st} (kJ mol^{-1})	Selectivity	Ref.
Cu-BTC MOF/GO	UV activation	1323.49	5.14 (25 °C) 9.5 (0 °C)	22.5	21 (0.1 bar) 14.35 (1 bar) CO_2/N_2	233
PEI–rGO composite	Amine functionalization (71%)	—	0.61 at 4 pK_a 1.03 at 101 pK_a 1.55 (50 °C)	—	—	226
Holey graphene (HPhG)	Li, Na, K, Mg, Ca doped	—	11.51 (Ca-HPhG)	43.37	~2385 (CO_2/CH_4) ~1366 (CO_2/N_2) at 298 K 1 bar	147
Graphene nanoribbon (GNR)	Fau-zeolite + GNR (12%) pellet	613	4.61	—	76.5 (CO_2/N_2)	228
Graphene oxide	Ionic liquid and C_4mimBF_4	—	247.99 GPU permeation	—	13.58 (CO_2/H_2) 44.82 (CO_2/N_2) 75.45 (CO_2/CH_4)	229

Note: the gas composition (*e.g.*, purity and mixed-gas environments) and operating pressures used across different studies may vary.

compared to N_2.[228] Furthermore, CO_2 desorption occurred in the 125–150 °C temperature range, allowing for complete material regeneration. Nitrogen flow during the regeneration process also made the process energy-efficient.

A novel 2D allotrope of carbon, known as holey penta-hexagonal graphene (HPhG), was also investigated for CO_2 adsorption due to its ample pores and superior stability. Although bare HPhG exhibits a CO_2 adsorption capacity of 2.46 mmol g^{-1}, researchers have been working on composites of HPhG to enhance its performance. Tiantian Quio *et al.* developed holey GO composites doped with alkali earth metals (Li, Na, K, Ca, and Mg) to improve the adsorption capacity of HPhG. Among the doped composites, Ca-doped HPhG exhibited the highest CO_2 adsorption capacity of 11.51 mmol g^{-1}, followed by Li-doped HPhG (10.84 mmol g^{-1}), Na-doped HPhG (9.73 mmol g^{-1}), K-doped HPhG (9.73 mmol g^{-1}), and Mg-doped HPhG (9.67 mmol g^{-1}). This enhancement is attributed to the strong van der Waals and coulombic interactions between CO_2 and the metal-doped HPhG surface. The intense quadrupole moment and polarizability of the CO_2 molecules contribute to the high selectivity of the doped composite towards CO_2, especially in the presence of methane and nitrogen gases. A thorough summary of the structure–property–performance relationships of GO-based adsorbents for CO_2 capture is presented in Table 9, which includes key factors such as specific surface area, adsorption capacity, selectivity, and isosteric heat of adsorption (Q_{st}). This comparative study provides important insights for the logical design and optimization of high-performance GO-based sorbents by highlighting how customized structural engineering and surface functionalization control adsorption thermodynamics, affinity, and separation efficiency.[147]

6.5. Carbon foam

Carbon foam is a porous 3D carbon material characterized by interconnected pores, lightweight properties, and high compressive strength.[240] It can be synthesized using various methods, including the template method or by incorporating surfactants, foaming agents, and catalysts. Carbon foam is typically produced from resins and polymers such as phenolic resin, coal tar pitch, and other synthetic polymers.

Diego Fernando *et al.*[241] synthesized carbon foam using novolac-type phenolic resin. In their process, *n*-pentane and dichloromethane were used as foaming agents, while NaOH, NH_3, and phosphoric acid served as catalysts. The presence of the –OH bond (900–3650 cm^{-1}) indicated the phenolic group, and two peaks near 2980 cm^{-1} and 3000 cm^{-1} confirmed the formation of a methylene bridge during the polymerization of the resin to form a carbon foam. Carbon foam synthesized at 600 °C using phosphoric acid and DCM exhibited the highest surface area (984 cm^2) and, consequently, the highest adsorption capacity (103.3 mg g^{-1}). Recently, the thermal transformation of biowaste has also been explored as a method to produce carbon foam, offering both structural benefits and the added advantage of waste recycling. Beizhang *et al.*[242] used palm kernel shells to prepare a multiporous carbon foam. Fig. 16(a–c) illustrates the schematic representation of the synthesis process for lignin-based carbon foam derived from palm kernel shells, along with the proposed reaction mechanism. The carbon foam obtained through this method was subjected to high-temperature heat treatment (600 °C), which increased CO_2 adsorption. This improvement was attributed to the foam's multiporous structure (macro- and mesoporous), which enhanced CO_2 accommodation by increasing diffusion capacity.

Hoyos *et al.*[227] investigated the potential of eco-friendly GO foams, produced from bamboo waste, as effective adsorbents for carbon capture. The GO foams were synthesized as shown in Fig. 16(d–e) *via* a double thermal decomposition process, with varying temperatures employed to regulate oxidation levels. The foams were subsequently assessed through experimental CO_2 adsorption tests and DFT simulations. The results indicated that the GO foams exhibited significantly enhanced CO_2 capture efficiency, ranging from 86.28% to 92.20%, compared to traditional adsorbents such as zeolite and silica gel. The foam with 3% oxidation showed the best adsorption efficiency, while the foam oxidized at 9% had the highest material yield. DFT calculations indicate that CO_2 capture primarily occurs through physisorption. This process is driven by weak van der

Fig. 16 (a) Schematic representation of the synthesis process for lignin-based carbon foam derived from palm kernel shells; (b and c) proposed reaction mechanism illustrating the key steps involved in the formation of the carbon foam structure (reproduced from ref. 242 with permission from [Elsevier], copyright [2022]); GO foams obtained employing the DTD and characterization methods, (d) 873.15 K (GO 9.00%), (e) 973.15 K (GO 5.25%) (reproduced from ref. 227 under the Creative Commons Attribution (CC BY) license).

Waals forces, with hydroxyl (–OH) groups playing a key role. In addition, the GO foams demonstrated excellent regenerability, completely regaining their adsorption capacity after thermal desorption at 673.15 K.

Zhou *et al.*[243] developed hierarchically porous N-doped carbon foams (HPNCFs) for efficient CO_2 capture by maximizing nitrogen content and microporous surface area through precise control of carbonization temperature and the PBC/His

molar ratio. Among the samples, HPNCF-1.0–700 exhibits optimal performance, delivering CO_2 adsorption capacities of 3.06 mmol g^{-1} (25 °C) and 4.13 mmol g^{-1} (0 °C) at 760 torr, along with high uptake under flue–gas conditions (0.81 mmol g^{-1} at 114 torr) and an exceptional CO_2/N_2 selectivity of 24. Raising the carbonization temperature from 700 °C to 900 °C increases the total surface area but sharply reduces nitrogen content, micropore surface area, CO_2 capacity, and selectivity. This trend highlights the dominant role of micropores (0.77–1.9 nm) and nitrogen functionalities, particularly pyrrolic N, in CO_2 adsorption, which outweighs the benefits of increased macroporosity. The relatively high isosteric heat of adsorption (26.5 kJ mol^{-1}) indicates strong yet reversible physisorption driven by dipole–π interactions.

A study conducted by Vorokhta *et al.*[244] reveals a clear trade-off between nitrogen doping and porosity in carbon foams, where increasing nitrogen content enhances CO_2 affinity but progressively suppresses pore development, necessitating careful optimization. Among the samples, the triethanolamine-derived nitrogen-doped carbon foam (NCF-TEA, ~7 at% N) delivered the highest CO_2 uptake (5.14 mmol g^{-1} at 273 K, 100 kPa), outperforming the undoped foam despite possessing a substantially lower surface area. In contrast, further nitrogen enrichment (~13 at% in NCF-MEA) severely reduced micropore volume and specific surface area, leading to diminished adsorption capacity due to pore blockage during pyrolysis. The enhanced performance at optimal doping arises from a synergistic interplay between pore architecture and surface chemistry. CO_2 uptake is governed by ultra-micropores (<0.7 nm), where overlapping adsorption potentials maximize confinement, while nitrogen functionalities (pyridinic, pyrrolic, and amine groups) act as Lewis base sites that strengthen CO_2 binding *via* acid–base and hydrogen-bonding interactions. This chemical enhancement compensates for surface area loss up to the optimal nitrogen level.

In advanced CNM-based adsorbents, the way pores are connected hierarchically, rather than just the total surface area, has become the most important factor in determining how quickly substances are adsorbed, how selective the process is, and how easily the adsorbent can be reused.[245] By seamlessly integrating macropores and mesopores with microporous areas, diffusion limitations are reduced, mass transport is accelerated, and the active adsorption sites are used almost completely.[246,247] In this structural context, macropores serve as pathways for transport, while the selectivity for CO_2 is largely determined by the distribution of micropore sizes (less than 2 nm) and the surface chemistry, specifically the presence of nitrogen-containing functional groups that increase affinity *via* Lewis acid–base interactions.[248] Because CO_2 uptake occurs quickly and can be easily reversed through physisorption, these materials require less energy to regenerate and exhibit excellent stability over multiple cycles, which is superior to traditional chemisorbents.

In addition to how well they adsorb, the mechanical and thermal stability of materials are crucial for their practical use. Carbon foams provide a clear engineering advantage over fragile aerogels and loose powders, which are prone to wear, compaction, and inefficient heat transfer.[248] The interconnected strut network, which is rigid, ensures structural integrity while also allowing for a quick thermal response. This is crucial for temperature swing adsorption (TSA) processes. Because carbon foams conduct heat so effectively, they can withstand repeated heating and cooling cycles without degrading. Experimental studies demonstrate that hierarchical porous carbons and foams can retain over 95% of their capacity after more than 50 cycles of adsorption and desorption, supporting these benefits.[244,249] The combined results underscore the importance of hierarchical pore connectivity, along with structural and thermal stability, as key design principles for the next generation of multifunctional CO_2 capture systems The structure–property–performance correlations of various carbon-form-based adsorbents for CO_2 capture are summarized in Table 10, highlighting the effects of material type and post-treatment techniques on specific surface area, CO_2 adsorption capacity, and CO_2/N_2 selectivity. To optimize carbon-based sorbents for high-efficiency, selective CO_2 separation, this comparative analysis clarifies key structure-function relationships and provides useful design guidelines.

6.6. Carbon dots

Carbon dots (CDs) are zero-dimensional nanomaterials with ultra-low sizes (1–10 nm) and multifunctional properties, positioning them as promising candidates for CO_2 capture applications. While their potential has been recognized, CDs have historically been underutilized compared to their carbon-based counterparts. Recent advances demonstrate substantial progress in optimizing their performance through composite architectures, heteroatom doping, and pilot-scale validation.

The foundational work of Sahoo *et al.*[250] utilized amine-doped carbon dots for CO_2 capture from a 30 L automated pilot plant. They synthesized CDs from citric acid and ethylenediamine and then blended them with methyl diethanolamine, piperazine, and 2-amino-2-methyl-1-propanol as amine precursors. The CO_2 source was flue gas (10% CO_2). The solvent

Table 10 Summary of structure–property performance correlations of various carbon form-based adsorbents for CO_2 capture, highlighting the influence of material type and treatment on specific surface area, CO_2 adsorption capacity, and CO_2/N_2 selectivity

Type of material	Treatment	Surface area (m^2 g^{-1})	CO_2 adsorption (mmol g^{-1})	Selectivity	Ref.
Novalac-type phenolic resin	600 °C using phosphoric acid and DCM	984 m^2 g^{-1}	103.3 mg g^{-1}	—	241
Palm kernel shells	Hydrothermal carbonization and acid-alkali treatment	335.97 m^2 g^{-1}	1.25 mmol g^{-1} (35 °C 1 bar) 0.86 mmol g^{-1} (50 °C 1 bar)	34	242

Note: the gas composition (*e.g.*, purity and mixed-gas environments) and operating pressures used across different studies may vary.

system consisting of amine-blended CDs exhibited enhanced CO_2 adsorption, with the capacity increasing as the concentration of CDs increased to 100 mg L^{-1}. This improvement is attributed to enhanced Brownian motion, which increases the mass transfer rate. However, agglomeration occurs at higher concentrations, which inhibits mass transfer and diminishes performance. Despite this, the CDs maintained stable CO_2 capture efficiency for over 200 hours without significant degradation. Samandari *et al.*[251] used lignin-derived carbon dots functionalized with oxygen and nitrogen groups for CO_2 capture. Simulation studies revealed that in a single gas environment, the CO_2/N_2 and CO_2/O_2 selectivity ratios were 3.6 and 6.7, respectively, at 300 K. Additionally, Broud *et al.*[252] also observed the effectiveness of amine-functionalized CDs, with selectivity values of 4.1 for CO_2/N_2 and 3.1 for CO_2/O_2. Notably, it was found that in the case of flue gas, the selectivity for CO_2 was higher compared to pure gas mixtures. This is attributed to CO_2 having a higher displacement for N_2 and O_2 compared to CO_2 itself. Although CO_2 preference is higher than that for N_2 and O_2, the selectivity toward N_2 and O_2 depends on the positioning of the functionalities, with interior hydroxyl functionalization increasing the preference for N_2 over O_2. The performance drop observed at higher CD concentrations is primarily attributed to particle agglomeration.[253] As the concentration increases, strong van der Waals forces and hydrogen bonding between surface groups cause the 0D dots to cluster. This aggregation not only reduces the effective surface area available for gas interaction but can also mask active amine/functional sites buried within the clusters (Fig. 17).[254]

In summary, recent advances reveal the transformative potential of CDs as a scalable, highly selective, and previously underexploited platform for CO_2 capture. Moving beyond laboratory-scale demonstrations, the pilot-scale validation reported by Sahoo *et al.*[250] represents a pivotal milestone toward industrial implementation. The study shows that amine-blended CD systems significantly enhance gas–liquid mass transfer while maintaining structural and functional stability for over 200 hours under realistic flue gas conditions containing 10% CO_2. Complementary investigations by Samandari *et al.*[251] and Broud *et al.*[252] further establish the chemical tunability of CDs, demonstrating that targeted oxygen and nitrogen-based functionalization, and, critically, the spatial distribution of these groups, can be precisely engineered to achieve high CO_2 selectivity over N_2 and O_2. This level of control over surface chemistry positions CDs as a uniquely adaptable class of adsorbents and absorbents, capable of bridging molecular-scale interactions with process-level performance.

Although both carbon dots and fullerenes (*e.g.*, C_{60}) belong to the family of zero-dimensional carbon allotropes, CDs offer several decisive advantages for CO_2 capture applications. Most notably, CDs are intrinsically hydrophilic, owing to abundant surface hydroxyl, carboxyl, and amine functionalities. This property enables their seamless dispersion in aqueous amine solvents, forming efficient CD-based nanofluids that enhance CO_2 absorption kinetics without requiring the complex surface modifications typically necessary for hydrophobic fullerenes, which often rely on toxic organic solvents for processing.[250] From a manufacturing perspective, CDs are inherently more scalable and cost-effective. They can be synthesized *via* simple, low-temperature bottom-up routes using inexpensive and renewable precursors such as citric acid or lignin.[255] In contrast, fullerene production typically involves energy-intensive arc-discharge methods, followed by costly purification steps, which limit its economic feasibility at scale.[256,257] Finally, the structurally disordered and defect-rich surfaces of CDs facilitate versatile heteroatom doping (N, S, and P), allowing fine-tuning of CO_2 binding strength and selectivity.[251] Fullerenes, while chemically robust, possess rigid and stoichiometric structures that are far less amenable to the flexible surface engineering required for optimized CO_2 capture. Collectively, these advantages position carbon dots as a practically superior and industrially relevant alternative to other zero-dimensional carbon materials for next-generation CO_2 capture technologies.

7. Techno-economic analysis of CNMs for CO_2 capture technologies

Aqueous amine-based absorption technology for CO_2 capture is currently at a Technology Readiness Level (TRL) of 9 and is a well-established method. Nevertheless, the primary challenges associated with this technology stem from its thermodynamic and economic limitations. Solvent regeneration presents a considerable challenge, driven by substantial energy costs (3.5–4.5 GJ per tonne CO_2), thermal breakdown, and the production of hazardous byproducts. Consequently, the materials science field has focused on enhancing this technology through the application of CNMs as innovative adsorbents. This section will examine the various research and techno-economic data published over the last five years.

CNM-based CO_2 capture adsorbents, which are produced from agricultural and animal waste, present a promising avenue for value-added applications. The reported production costs for these materials range from USD 1.44 to 3.12 per kg, depending on the specific characteristics of the feedstock and the activation method employed.[258–260] A key factor influencing both cost and efficacy is the selection of either physical or chemical activation, with the associated trade-offs being significantly dependent on the precursor material. Pricing analyses reveal that physically activated carbons typically demonstrate lower and more stable market prices across a diverse array of raw materials, approximately USD 0.96 to 1.92 per kilogram.[261] This cost advantage is attributable to the streamlined process flows, the lack of corrosive chemical reagents, and the reduced need for extensive post-treatment procedures. Therefore, physical activation is particularly well-suited for large-scale, cost-sensitive applications, especially when utilizing waste-derived materials such as used tires and carbon black.

In contrast, chemical activation usually results in higher product costs, particularly for fossil fuel-derived precursors such as petroleum coke (USD 5.76 kg^{-1}), lignite (USD 4.22 kg^{-1}), and charcoal (USD 3.84 kg^{-1}).[261] These increased costs are mainly

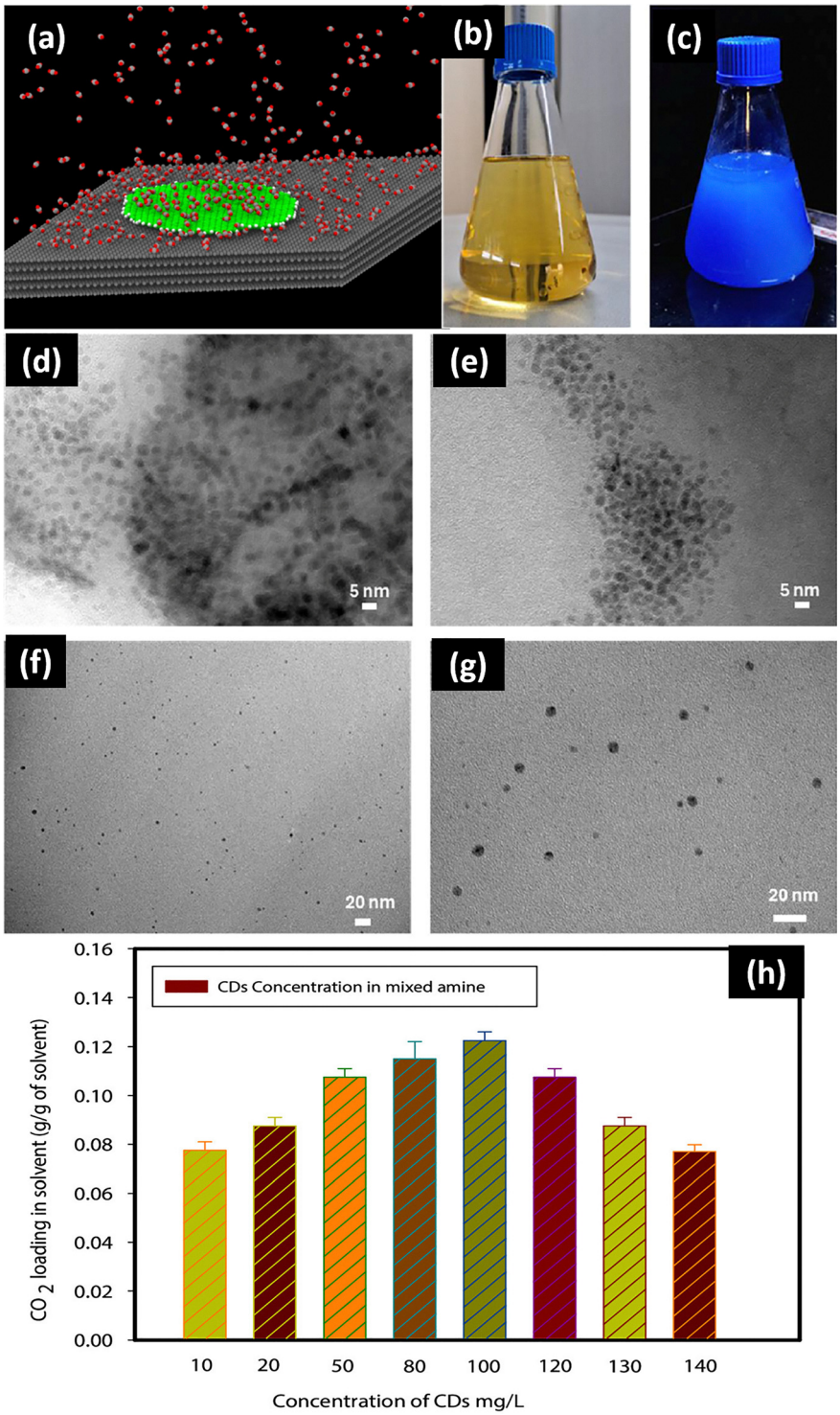

Fig. 17 (a) Representative snapshot from molecular simulation illustrating CO_2–carbon interactions. Color scheme: carbon atoms of graphite and CO_2 (gray), carbon atoms of carbon quantum dots (CQDs, green), oxygen (red), and hydrogen (white) (reproduced from ref. 251 with permission from [American Chemical Society], copyright [2024]); photographic images of amine-stable carbon dots under (b) visible light and (c) UV irradiation, demonstrating their optical response. TEM micrographs of (d and e) water-stable carbon quantum dots and (f, g) amine-stable carbon quantum dots; (h) Effect of CD loading on CO_2 absorption capacity in a mixed amine solution (reproduced from ref. 250 with permission from [Elsevier], copyright [2025]).

due to reagent use (*e.g.*, H_3PO_4 and KOH), the need for corrosion-resistant reactors, extensive washing steps, and wastewater treatment. However, chemical activation often yields better textural properties, including a larger surface area, increased microporosity, and a higher carbon yield at lower activation temperatures. These performance enhancements can justify the increased

expense in high-value applications, such as gas separation, energy storage, and catalysis. It is significant that biomass-derived precursors, such as wood, exhibit similar product costs for both activation methods (approximately USD 1.54 kg^{-1}), implying that advantageous feedstock chemistry can, to some extent, mitigate the cost disadvantages linked to chemical activation. Consequently, these observations suggest that physical activation is most suitable for commodity-grade, high-throughput production, while chemical activation is strategically beneficial for performance-focused markets, thereby underscoring the need to select a precursor-specific and application-oriented process.[261]

Furthermore, enhancing the commercial feasibility of activated carbons derived from biomass and waste necessitates a combination of process intensification and targeted market positioning. Scaling up production to large-capacity facilities (>50 t day^{-1}) can significantly reduce unit costs through improved thermal efficiency, bulk procurement, and streamlined logistics. In parallel, upgrading existing activation routes through energy recovery and chemical recycling has the potential to lower production costs by 15–25%. Additional savings can be achieved by reducing capital expenditure through shared utilities, co-locating carbon production with existing industrial infrastructure, and prioritizing locally available feedstocks to stabilize supply chains and transportation costs. Furthermore, hybrid activation strategies that combine steam and chemical activation warrant attention, as they enable a more balanced trade-off between pore development, reagent consumption, and overall cost–performance metrics. Finally, integrating life cycle assessment (LCA) into process design is essential for identifying emission hotspots, quantifying environmental benefits, and substantiating sustainability claims, including eligibility for carbon credits and compliance with emergent regulatory frameworks.

8. Comparative analysis of CNMs over commercial MOFs for CO_2 capture

This section presents a comparative evaluation of MOFs and CNMs for CO_2 capture technologies, highlighting their comparative features in Table 11. MOFs are already being used commercially because they possess a dual adsorption mechanism that combines open metal sites with framework-specific binding, offering a capacity of up to 12 mmol g^{-1}.[262,263] CNMs, on the other hand, primarily utilize physisorption, which is reinforced by interactions with heteroatoms. They also exhibit excellent chemical and thermal stability in harsh flue gas environments, maintaining structural integrity even in the presence of moisture, SO_x, NO_x, and elevated temperatures. CNMs are inexpensive ($0.01–50 per kg), readily available, and can be produced in bulk quantities, compared to MOFs, which are more expensive ($10–200 per kg).[125] However, CNMs currently have a lower capacity, but their performance is significantly improving through four primary engineering approaches. Heteroatom doping introduces active sites, such as pyridinic, pyrrolic, and graphitic nitrogen, which increases CO_2 affinity by nearly 35%.[264,265] Dual N, S-doping in graphene results in a good adsorption capacity for CO_2 capture under mild conditions (<100 °C, 1 atm) due to extra charge transfer from graphene to CO_2.[266] It is expected that the N–B co-doped systems will be available for sale in the next 5 years. Hierarchical pore engineering further enhances the adsorption kinetics of CNM-based adsorbents by combining micropores (<1 nm) for high-density uptake with mesopores (2–50 nm) for rapid diffusion, allowing for 95–98% retention after 100 cycles using optimized KOH activation strategies.[267] Amine functionalization creates a chemisorption pathway, resulting in the highest CO_2 capacities (5–8 mmol g^{-1}).[268] Grafted amine systems are more durable and drop less than 6% of their capacity over five cycles. But they remain sensitive to moisture. New strategies, such as tri-doping (N + B + O), the addition of single-atom metal sites, and operando electrochemical doping, are expected to further enhance performance and adsorption capacities up to 5–7 mmol g^{-1}.[269] These combined engineering methods provide an emerging pathway toward scalable, industrial-grade CNMs for next-generation CO_2 capture systems. Hybrid systems that combine carbon supports with MOF coatings offer the best features of both materials, significantly enhancing performance. For instance, two hybrid materials composed of MOFs with MWCNTs exhibit an increase in adsorption capacity, from 64% to 76% (*i.e.*, 5.8 to 9.52 mmol g^{-1} and from 4.53 to 8 mmol g^{-1}), respectively, at 298 K and 18 bar. This increment has been attributed to the increase in micropore volume of MOFs by the incorporation of MWCNTs.[270] Hence, it can be concluded that MOFs are the most effective performers and are employed commercially. However, engineered CNMs are rapidly improving and becoming strong candidates for scalable, next-generation CO_2 capture solutions.

9 Challenges and probable solutions in CNM-based CO_2 capture technologies

Using CNM-based materials to absorb CO_2 is very promising, as they can be tailored to have different levels of porosity, possess

Table 11 Comparative summary of various features of CNM-based and commercial MOFs for CO_2 capture and conversion

Feature	CNM-based	Commercial MOFs
Primary mechanism	Physisorption (physical)	Physisorption and chemisorption
CO_2 capacity	Moderate (3 to 8 mmol g^{-1})	High (5 to 9 mmol g^{-1})
Selectivity	Moderate (improved with N-doping)	High (intrinsic to structure)
Moisture stability	High (hydrophobic)	Low (hydrophilic/degrades)
Heat of adsorption	Low/moderate (20–30 kJ mol^{-1})	Moderate/high (25–50 kJ mol^{-1})
Regeneration energy	Low (energy efficient)	High (energy intensive)
Cost	Low (biomass/waste precursors)	High (metals/ligands)

a large surface area, are thermally stable, and are relatively inexpensive. However, several important scientific and technical issues still need to be addressed before they can be used on a large scale. The main problems are discussed here, along with possible solutions. CNM-based materials often exhibit limited CO_2/N_2 selectivity due to their primarily non-polar surfaces and the absence of specialized binding sites, which complicates the efficient separation of CO_2 from mixed gas streams, such as flue gases that contain N_2 or O_2. Their efficacy is further impaired by moisture sensitivity, as water vapor contends with CO_2 for active sites and may destroy oxygen-containing functional groups, resulting in a loss of stability and adsorption capacity. Another significant issue is that CO_2 does not absorb well at low partial pressures, which is often the case in post-combustion situations. CNMs that mainly depend on physisorption do not interact well with CO_2 in these circumstances, which means they do not collect it well enough. Additionally, CNM-based adsorbents modified with amines or heteroatoms often lose their integrity when heated and cooled repeatedly, leading to structural breakdown and a decline in their adsorption capacity over time. The pore structure of carbon materials derived from biomass or waste is also a concern, as they often exhibit uneven distributions across micro-, meso-, and macropores, which renders their adsorption performance unreliable. Additionally, the high expense of synthesis and functionalization, particularly in techniques such as amine grafting or KOH activation, makes it more challenging to generate revenue and creates hazardous waste, posing a significant safety and environmental issue. Finally, scaling up and integrating into the industry are still significant challenges. Even though lab tests have shown encouraging results, it is challenging to scale up these materials into large-scale systems, as they are not very strong, may easily lose pressure, and are not always compatible with current CCUS technology. For CNM-based CO_2 collection systems to function effectively in real-world applications, these problems must be addressed.

The suggested portable solution to the above highlighted challenges is described below:

To address the constraints inherent in non-polar surfaces, heteroatom doping approaches will focus on optimizing pyridinic nitrogen functionalities. These functionalities feature a localized lone pair, which facilitates robust Lewis acid-base interactions with CO_2, thereby substantially improving selectivity for CO_2 over N_2, surpassing the capabilities of simple physisorption.[271] Moreover, the functionalization of CNMs with amines will be strategically designed to influence the moisture-enhanced chemisorption mechanism. In this mechanism, the presence of water vapor within flue gas alters the reaction stoichiometry from 2:1 (carbamate) to 1:1 (bicarbonate), effectively doubling the theoretical efficiency of the amine.[272] To make them less sensitive to moisture, hydrophobic coatings such as fluorinated or alkylsilane layers will be used to keep water out while still allowing CO_2 to pass through. Additionally, moisture-resistant features such as sterically hindered amines and ionic-liquid grafted surfaces will be employed to ensure that CO_2 affinity remains constant under humid conditions. This chemical modification will be integrated with ultra-micropore engineering, specifically targeting pores smaller than 0.7 nm, to maximize adsorption potential through the overlapping of van der Waals fields. This chemical modification will be integrated with ultra-micropore engineering, specifically targeting pores smaller than 0.7 nm, to maximize adsorption potential through the overlapping of van der Waals fields. Consequently, this approach will ensure a high uptake capacity, even under conditions of low partial pressure. Chemisorption-active sites, including metal–nitrogen coordination centers, will also be added to increase binding energy while yet allowing for reversible desorption for cyclic usage. Using thermally stable linkers, such as pyridine and imidazole, can help address the issue of low regeneration stability. These linkers will hold functional groups in place and stop them from coming loose as the temperature rises over 100 °C. Long-term stability will be achieved through a comprehensive strategy that addresses moisture, oxidation, and contaminants. To prevent capillary condensation and water competition, hydrophobic functionalization will be applied to physisorbents using fluorinated alkylsilanes. For amine-based systems, oxidative degradation will be reduced by shifting from thermal swing to Vacuum Swing Adsorption (VSA) or Electrical Swing Adsorption (ESA). This change will help avoid the high temperatures that can deactivate amines by catalyzing their breakdown.[58] Furthermore, the irreversible binding of SOx and NOx will be managed by using sterically hindered amines and tertiary amine functionalities. These materials have lower binding energies for CO_2 molecules, allowing for some regeneration and extending the lifespan of the adsorbent in real-world flue gas environments.[273]

Template-assisted synthesis using silica templates or block copolymers will be used to ensure that the pores are evenly spaced and that the best pore architecture is achieved. To create hierarchical micro- and mesoporous networks, we will utilize controlled activation methods, such as steam or CO_2 activation, combined with programmable heating. Using sustainable precursors, such as biochar, lignocellulosic biomass, or agricultural byproducts, can lower the cost and environmental impact of synthesis. Green activation technologies, such as H_3PO_4 treatment, CO_2 activation, or one-pot activation–doping processes, will facilitate processing and reduce chemical waste. For use in factories, CNM-based adsorbents will be formed into strong structural shapes, such as pelletization or structured packings, including those utilizing 3D-printed supports, which are necessary. However, these methods often block the pores, thereby reducing the available surface area. As a means of process intensification, CNMs' adsorbents might be more efficiently utilized within rotating packed beds, where centrifugal forces alleviate pressure-drop constraints and substantially improve mass transfer compared to traditional static beds. This will allow the use of CNM-based CO_2 capture technologies on a larger scale. Table 12 briefly summarizes the key challenges in commercial-scale CO_2 capture and conversion, their primary causes, and potential solutions, providing critical insights into technological, material, and process bottlenecks to support scalable and economically viable industrial implementation.

Table 12 Summary of the key challenge, its primary cause, and possible solutions for efficient commercial-scale CO_2 capture and conversion

Key challenge	Primary cause	Possible solutions
Low CO_2/N_2 selectivity	Weak physisorption, non-polar surfaces	N-doping, amine functionalization
Sensitivity to humidity	Hydrophilic surface groups	Hydrophobic pore design, stable functionalities
Low CO_2 uptake at low pressure	Lack of ultra-micropores, weak adsorption forces	Ultra-micropore tuning, chemical adsorption sites
Poor regeneration stability	Functional group degradation	Robust chemistry, low-energy regeneration methods
Inconsistent pore structure	Variability in synthesis	Template methods, advanced activation control
High synthesis/functionalization cost	Expensive precursors or chemicals	Biomass sources, green chemistry approaches
Scale-up and integration difficulties	Lack of pilot studies or structured forms	Engineering design, modular reactors, performance validation

10. Future directions: from nanoscale design to industrial deployment

Despite remarkable advances in the nanoscale design of CNMs, their large-scale deployment in CCUS remains constrained by challenges related to process integration, manufacturability, and real-world operating conditions. Future research must therefore evolve beyond material-centric performance metrics and adopt a systems-oriented, application-driven paradigm. A central direction is the development of multifunctional and integrated materials that combine capture, conversion, and transport within a single platform. Rather than treating adsorption and utilization as isolated steps, next-generation CNMs should enable seamless process coupling to minimize energy penalties and improve overall process efficiency. Equally critical is addressing the form factor challenge. Translating nanoscale advantages into industrially viable architectures will require advances in shaping, compaction, and structuring of CNMs into mechanically robust, structured adsorbents that ensure low pressure drop, fast mass transfer, and compatibility with cyclic operation.

CCUS strategies will also focus on hybrid process integration, in which CNMs operate within membranes, solvents, or other capture technologies as high-performance polishing or intensification units, enabling stringent purity targets while reducing the burden on primary separation stages. To ensure practical relevance, material design must increasingly account for realistic gas environments, including moisture and trace contaminants. Improving chemical and structural resilience under these conditions through targeted surface engineering will be crucial for sustaining long-term performance and stability. Given the large design space of CNMs, machine learning and AI-guided frameworks are expected to identify optimal process–structure relationships tailored to specific operating conditions, thereby reducing reliance on empirical trial-and-error methods. Finally, the transition from laboratory success to industrial credibility will depend on rigorous techno-economic and life-cycle assessments. Future studies should benchmark CNMs against incumbent materials using standardized metrics, such as energy penalty, capture cost, and environmental footprint, to ensure that performance gains translate into tangible system-level benefits. Hence, the future of CNM-based CCUS lies in shifting the guiding question from maximum adsorption capacity to maximum system efficiency under industrially relevant conditions. The convergence of multifunctional material design, scalable architectures, hybrid process integration, data-driven optimization, and transparent economic validation will ultimately determine the viability of CNMs in next-generation CCUS technologies.

11. Conclusion

In conclusion, this review presents a comprehensive and critical examination of the importance of CNM-based adsorbents as scalable and cost-effective solutions for mitigating rising CO_2 emissions. Substantial advancements in CNMs have been achieved over the past few decades, underscoring sustained efforts to enhance capture efficiency with long-term sustainability while reducing environmental and energy penalties. The effective CO_2 mitigation relies not only on maximizing the specific surface area, but also on the precise engineering of pore topology and surface energetics. Low-dimensional allotropes, including 0D and 1D, exhibit distinctive electronic properties and transport pathways. However, 3D hierarchical carbon structures stand out as the most promising materials for industrial use. These frameworks strike an ideal balance between capacity and kinetics by integrating ultra-micropores (<0.7 nm) for high-density CO_2 molecular storage, along with mesoporous channels that reduce diffusion resistance during rapid pressure changes. Moreover, the various strategies for heteroatom functionalization, including nitrogen doping and amine grafting, carefully adjust adsorption enthalpies to make capture reversible and achieve long-term cycling stability. From a physics perspective, the core scientific insight derived from this review is that the good performance adsorbent based on CNMs must operate within this thermodynamic window defined by the isosteric heat of adsorption, Q_{ST}, which must be tuned to a value of 35–50 kJ mol^{-1}. In this window, CNMs adsorb strongly enough to capture CO_2 from dilute flue gas streams (chemisorption-like affinity) yet weak enough to allow for complete desorption below 100 °C (physisorption-like regenerability). The amine functionalization yields the highest capacities through carbamate formation, resulting in nitrogen-doped carbons that offer superior long-term stability and moisture tolerance, thereby mitigating the degradation issues often observed in amine-grafted composites. However, optimisation of heteroatom doping is necessary to maintain the ultramicroporous structure. To effectively translate laboratory-scale advances into industrially viable retrofitting solutions, future adsorbent materials must meet stringent

performance criteria under realistic post-combustion conditions, including a CO_2 uptake of ≥ 3 mmol g^{-1} at low partial pressure (0.15 bar), a CO_2/N_2 selectivity exceeding 20 to ensure high-purity separation from flue gas, and a regeneration energy penalty of ≤ 50 kJ mol^{-1}, thereby maintaining clear economic and energetic advantages over conventional aqueous amine-based capture systems.

To summarize, this review provides valuable insights for advancing CO_2 capture strategies using CNMs as state-of-the-art materials, offering excellent metrics for effective and large-scale deployment in mitigating greenhouse gas emissions.

Author contributions

JS: conceptualization, acquisition of data, investigation, analysis and interpretation, writing – original draft, writing – review and editing, visualization, validation, software, resources; AG: writing – original draft, writing – review and editing, validation; ZZ and SKT: writing – review & editing, validation; ASD: writing – review and editing, proof-reading; all authors have read and agreed to the published version of the manuscript.

Conflicts of interest

The authors declare that they have no known competing financial interests or personal relationships that could have appeared to influence the work reported in this paper.

Abbreviations

CCUS	Carbon capture, utilization, and storage
CO_2	Carbon dioxide
CNMs	Carbon nanomaterials
CNTs	Carbon nanotubes
IPCC	Intergovernmental Panel on Climate Change
IEA	International Energy Agency
EOR	Enhanced oil recovery
DAC	Direct air capture
MOFs	Metal–organic frameworks
GO	Graphene oxide
rGO	Reduced graphene oxide
SWCNTs	Single-walled carbon nanotubes
MWCNTs	Multi-walled carbon nanotubes
Q_{st}	Heat of adsorption (isosteric heat)
ACs	Activated carbons
TEPA	Tetraethylenepentamine
DETA	Diethylenetriamine
TETA	Triethylenetetramine
DFT	Density functional theory
BET	Brunauer–Emmett–Teller (surface area analysis)
NLDFT	Non-linear density functional theory
SEM	Scanning electron microscopy
FTIR	Fourier transform infrared spectroscopy
IAST	Ideal adsorbed solution theory
MESP	Molecular electrostatic potential
PEI	Polyethyleneimine
APTES	3-Aminopropyltrimethoxysilane
AHNC	Activated halloysite nanocarbon

Data availability

No primary research results, software, or code have been included, and no new data were generated or analysed as part of this review.

Acknowledgements

J. Singh gratefully acknowledges the Department of Physics and Materials Science and the authorities of Thapar Institute of Engineering and Technology (TIET), Patiala, for providing state-of-the-art research infrastructure, advanced technical support, and a highly conducive academic environment that collectively enabled the successful execution and completion of this work. SKT also thanks the SPARC project (P3808) under the Indo-UK scheme for its help. Additionally, the authors express gratitude to all the researchers in this field who are mentioned in this paper.

References

1 D. J. Soeder, *Fracking and the environment: A scientific assessment of the environmental risks from hydraulic fracturing and fossil fuels*, 2020.
2 R. Heede and N. Oreskes, *Glob. Environ. Chang.*, 2016, **36**, 12–20.
3 S. Paraschiv and L. S. Paraschiv, *Energy Reports*, 2020, **6**, 237–242.
4 J. Singh, A. S. Dhaliwal, K. Sharma, R. Sehgal and V. Kumar, Conjugated Polymers for Next-Generation Applications, *Synthesis, Properties and Optoelectrochemical Devices*, Vol. 1, 2022, pp. 505–538.
5 Y. Liu, J. Liu, M. Chang and C. Zheng, *Fuel*, 2012, **95**, 521–527.
6 Y. Liu, J. Liu, Y. S. Lin and M. Chang, *J. Phys. Chem. C*, 2014, **118**, 6744–6751.
7 A. Majumdar and J. Deutch, *Joule*, 2018, **2**, 805–809.
8 M. R. Raupach, G. Marland, P. Ciais, C. Le Quéré, J. G. Canadell, G. Klepper and C. B. Field, *Proc. Natl. Acad. Sci. U. S. A.*, 2007, **104**, 10288–10293.
9 M. Wang, J. Liu, J. Hu and F. Liu, *Ind. Eng. Chem. Res.*, 2015, **54**, 9805–9812.
10 A. Kumar, S. Ogita and Y. Y. Yau, *Biofuels: Greenhouse gas mitigation and global warming: Next generation biofuels and role of biotechnology*, 2018.
11 Intergovernmental Panel on Climate Change (IPCC), Climate Change 2021 – The Physical Science Basis, 2023.
12 T. R. Anderson, E. Hawkins and P. D. Jones, *Endeavour*, 2016, **40**, 178–187.
13 V. Ramanathan and Y. Feng, *Atmos. Environ.*, 2009, **43**, 37–50.

14 M. Jarraud and A. Steiner, Managing the Risks of Extreme Events and Disasters to Advance Climate Change Adaptation, *Special Report of the Intergovernmental Panel on Climate Change*, 2012, vol. 9781107025, pp. 3–22.
15 International Energy Agency, Glob. Energy Rev. 2021, 2021, 1–32.
16 M. Yuan, G. Gao, X. Hu, X. Luo, Y. Huang, B. Jin and Z. Liang, *Ind. Eng. Chem. Res.*, 2018, **57**, 6189–6200.
17 P. Wienchol, A. Szlęk and M. Ditaranto, *Energy*, 2020, **198**, 117352.
18 N. Mac Dowell, P. S. Fennell, N. Shah and G. C. Maitland, *Nat. Clim. Chang.*, 2017, **7**, 243–249.
19 P. D. Sutrisna, S. Kawi, K. Khoiruddin, P. C. W. B. Mustika, N. Prasetya and I. G. Wenten, *Carbon Capture Sci. Technol.*, 2025, **14**, 100366.
20 Y. Song, Z. Hu, X. Yang, Y. An and Y. Lu, *Environ. Res.*, 2025, **274**, 121271.
21 M. Bui, C. S. Adjiman, A. Bardow, E. J. Anthony, A. Boston, S. Brown, P. S. Fennell, S. Fuss, A. Galindo, L. A. Hackett, J. P. Hallett, H. J. Herzog, G. Jackson, J. Kemper, S. Krevor, G. C. Maitland, M. Matuszewski, I. S. Metcalfe, C. Petit, G. Puxty, J. Reimer, D. M. Reiner, E. S. Rubin, S. A. Scott, N. Shah, B. Smit, J. P. M. Trusler, P. Webley, J. Wilcox and N. Mac Dowell, *Energy Environ. Sci.*, 2018, **11**, 1062–1176.
22 R. Stuart Haszeldine, *Science*, 2009, **325**, 1647–1652.
23 A. Thorbjörnsson, H. Wachtmeister, J. Wang and M. Höök, *Energy Strateg. Rev.*, 2015, **7**, 18–28.
24 I. Global CCS, GLOBAL STATUS OF CCS 2025, 2025.
25 M. Atif, H. Z. Haider, R. Bongiovanni, M. Fayyaz, T. Razzaq and S. Gul, *Surf. Interfaces*, 2022, **31**, 102080.
26 K. Ramadass, C. I. Sathish, S. Mariaruban, G. Kothandam, S. Joseph, G. Singh, S. Kim, W. Cha, A. Karakoti, T. Belperio, J. B. Yi and A. Vinu, *ACS Appl. Mater. Interfaces*, 2020, **12**, 11922–11933.
27 J. Singh and A. S. Dhaliwal, *J. Phys. Chem. Solids*, 2022, **160**, 110358.
28 H. Sharma and A. Dhir, *Environ. Chem. Lett.*, 2021, **19**, 851–873.
29 *Materials for Carbon Capture*, ed. D. E. Jiang, S. M. Mahurin, S. Dai, 2019, p. 376.
30 J. Wang, L. Huang, R. Yang, Z. Zhang, J. Wu, Y. Gao, Q. Wang, D. O'Hare and Z. Zhong, *Energy Environ. Sci.*, 2014, **7**, 3478–3518.
31 K. Tian, Z. Wu, F. Xie, W. Hu and L. Li, *Energy Fuels*, 2017, **31**, 12477–12486.
32 P. Mehra and A. Paul, *ACS Omega*, 2022, **7**, 34538–34546.
33 R. Shi, B. Liu, Y. Jiang, X. Xu, H. Wang, Z. Zeng and L. Li, *ACS Omega*, 2021, **6**, 30716–30725.
34 A. Das, S. D. Peu, M. S. Hossain, M. M. A. Nahid, F. R. Bin Karim, H. Chowdhury, M. H. Porag, D. B. P. Argha, S. Saha, A. R. M. T. Islam, M. M. Salah and A. Shaker, *Heliyon*, 2023, **9**, e22341.
35 D. Bonenfant, M. Kharoune, P. Niquette, M. Mimeault and R. Hausler, *Sci. Technol. Adv. Mater.*, 2008, **9**, 013007.
36 J. Singh, Z. Zhu, S. Han, N. Wang and S. K. Tiwari, *J. Alloys Compd.*, 2025, **1042**, 183755.
37 Y. J. Park, H. Lee, H. L. Choi, M. C. Tapia, C. Y. Chuah and T. H. Bae, *npj 2D Mater. Appl.*, 2023, **7**, 61.
38 B. Dziejarski, J. Serafin, K. Andersson and R. Krzyżyńska, *Mater. Today Sustainability.*, 2023, **24**, 100483.
39 J. Singh, S. K. Tiwari, S. Bhowmik, K. S. Hada and A. S. Dhaliwal, *Curr. Appl. Phys.*, 2025, **75**, 50–62.
40 G. Singh, J. Lee, A. Karakoti, R. Bahadur, J. Yi, D. Zhao, K. Albahily and A. Vinu, *Chem. Soc. Rev.*, 2020, **49**, 4360–4404.
41 M. S. Khosrowshahi, M. A. Abdol, H. Mashhadimoslem, E. Khakpour, H. B. M. Emrooz, S. Sadeghzadeh and A. Ghaemi, *Sci. Rep.*, 2022, **12**, 8917.
42 A. H. Farmahini, S. Krishnamurthy, D. Friedrich, S. Brandani and L. Sarkisov, *Chem. Rev.*, 2021, **121**, 10666–10741.
43 V. Georgakilas, J. A. Perman, J. Tucek and R. Zboril, *Chem. Rev.*, 2015, **115**, 4744–4822.
44 W. Al-Hajri, Y. De Luna and N. Bensalah, *Energy Technol.*, 2022, **10**, 2200498.
45 U. H. Bhatti, M. S. Alivand, F. Barzagli, M. G. Sanku, J. Gascon and K. A. Mumford, *ACS Sustainable Chem. Eng.*, 2023, **11**, 11955–11964.
46 K. Gong, F. Du, Z. Xia, M. Durstock and L. Dai, *Science*, 2009, **323**, 760–764.
47 L. Spessato, V. A. Duarte, J. M. Fonseca, P. A. Arroyo and V. C. Almeida, *J. CO_2 Util.*, 2022, **61**, 102013.
48 N. Rao, M. Wang, Z. Shang, Y. Hou, G. Fan and J. Li, *Energy Fuels*, 2018, **32**, 670–677.
49 L. Wang, S. Fan, X. Li, M. O. Tadé and S. Liu, *ACS Omega*, 2022, **7**, 40184–40194.
50 L. B. Hamdy, C. Goel, J. A. Rudd, A. R. Barron and E. Andreoli, *Mater. Adv.*, 2021, **2**, 5843–5880.
51 M. Crippa, D. Guizzardi, M. Banja, E. Solazzo, E. Schaaf, F. Pagani, F. Monforti-Ferrario, J. J. G. Olivier, R. Quadrelli, M. Risquez Martin, P. Moharamli, Taghavi, G. Grassi, S. Rossi, D. Oom, A. Branco, J. San Miguel, E. Vignati, M. Muntean, E. Schaaf, E. Solazzo, F. Monforti-Ferrario, J. J. G. Olivier and E. Vignati, *Fossil CO2 emissions of all world countries - 2020 Report*, 2022.
52 J. Chen, Y. Xu, P. Liao, H. Wang and H. Zhou, *Carbon Capture Sci. Technol.*, 2022, **4**, 100052.
53 J. Artz, T. E. Müller, K. Thenert, J. Kleinekorte, R. Meys, A. Sternberg, A. Bardow and W. Leitner, *Chem. Rev.*, 2018, **118**, 434–504.
54 F. Almomani, A. Abdelbar and S. Ghanimeh, *Sustainability*, 2023, **15**, 10438.
55 T. M. McDonald, W. R. Lee, J. A. Mason, B. M. Wiers, C. S. Hong and J. R. Long, *J. Am. Chem. Soc.*, 2012, **134**, 7056–7065.
56 B. Olfe-Kräutlein, T. Strunge and A. Chanin, *Front. Energy Res.*, 2021, **9**, DOI: 10.3389/fenrg.2021.742709.
57 F. Raganati and P. Ammendola, *Energy Fuels*, 2024, **38**, 13858–13905.
58 F. Raganati, F. Miccio and P. Ammendola, *Energy Fuels*, 2021, **35**, 12845–12868.
59 J. Hack, N. Maeda and D. M. Meier, *ACS Omega*, 2022, **7**, 39520–39530.
60 S. Vaz, A. P. Rodrigues de Souza and B. E. Lobo Baeta, *Clean. Eng. Technol.*, 2022, **8**, 100456.
61 S. Kammerer, I. Borho, J. Jung and M. S. Schmidt, *Int. J. Environ. Sci. Technol.*, 2023, **20**, 8087–8104.

62 A. S. Joel and Y. M. Isa, *J. Chem. Technol. Biotechnol.*, 2023, **98**, 838–855.
63 D. Alalaiwat and E. Khan, *Rev. Environ. Sci. Biotechnol.*, 2023, **22**, 799–822.
64 H. Liu, H. Lu and H. Hu, *Renew. Sustain. Energy Rev.*, 2024, **189**, 113908.
65 D. Obi, S. Onyekuru and A. Orga, *Int. J. Sustain. Energy*, 2024, **43**, 2317137.
66 A. Yagmur Goren, D. Erdemir and I. Dincer, *Environ. Res.*, 2024, **240**, 117503.
67 S. Arrhenius and Futur Nat, *Doc. Glob. Chang.*, 2013, **9**, 303–312.
68 J. D. Figueroa, T. Fout, S. Plasynski, H. McIlvried and R. D. Srivastava, *Int. J. Greenh. Gas Control*, 2008, **2**, 9–20.
69 M. Z. Jacobson, *Energy Environ. Sci.*, 2009, **2**, 148–173.
70 S. Iijima, *Nature*, 1991, **354**, 56–58.
71 M. Isah, R. Lawal and S. A. Onaizi, *Green Chem. Eng.*, 2025, **6**, 305–334.
72 F. Xu, Y. Yu, J. Yan, Q. Xia, H. Wang, J. Li and Z. Li, *Chem. Eng. J.*, 2016, **303**, 231–237.
73 D. G. Boer, J. Langerak and P. P. Pescarmona, *ACS Appl. Energy Mater.*, 2023, **6**, 2634–2656.
74 J. S. Zou, Z. P. Wang, Y. H. Andaloussi, J. Xue, W. Zhang, B. E. G. Lucier, Z. Zhang, Y. Jia, X. C. Wu, J. Li, Y. Huang, M. J. Zaworotko, G. Chen, S. Chen and Y. L. Peng, *Nat. Commun.*, 2025, **16**, 2598.
75 M. S. Lee, M. Park, H. Y. Kim and S. J. Park, *Sci. Rep.*, 2016, **6**, 23224.
76 B. Yuan, G. Zhan, Z. Chen, Y. Li, L. Wang, C. You and J. Li, *Int. J. Greenh. Gas Control*, 2022, **118**, 103673.
77 C. Chen, M. Kosari, M. Jing and C. He, *Environ. Funct. Mater.*, 2022, **1**, 253–266.
78 S. Gaikwad, Y. Kim, R. Gaikwad and S. Han, *J. Environ. Chem. Eng.*, 2021, **9**, 105523.
79 R. V. Siriwardane, M. S. Shen, E. P. Fisher and J. Losch, *Energy Fuels*, 2005, **19**, 1153–1159.
80 R. L. Siegelman, E. J. Kim and J. R. Long, *Nat. Mater.*, 2021, **20**, 1060–1072.
81 Y. M. Abdellatif, R. Surkatti, R. Muhammad, A. Sodiq, N. Nassar, T. Al-Ansari and A. I. Amhamed, *Energy Convers. Manag.*, 2026, **347**, 120544.
82 M. M. Devadiga, S. Sarangi, A. S. Bhat, M. Osial, K. Joseph, S. Olusegun, J. Singh, N. Wang, L. A. Ribeiro, Jr. and S. K. Tiwari, *Energy Environ. Sci.*, 2026, DOI: 10.1039/d6ee00134c.
83 L. Espinal, D. L. Poster, W. Wong-Ng, A. J. Allen and M. L. Green, *Environ. Sci. Technol.*, 2013, **47**, 11960–11975.
84 J. W. Park, S. Heo, J. G. Yeo, S. Lee, J. K. Kim and J. H. Lee, *Membranes*, 2025, **15**(7), 200.
85 M. H. Jenab, M. Vahidi and M. Mehrabi, *J. Chinese Chem. Soc.*, 2006, **53**, 283–286.
86 R. Idem, M. Wilson, P. Tontiwachwuthikul, A. Chakma, A. Veawab, A. Aroonwilas and D. Gelowitz, *Ind. Eng. Chem. Res.*, 2006, **45**, 2414–2420.
87 G. T. Rochelle, *Science*, 2009, **325**, 1652–1654.
88 B. Aghel, S. Janati, S. Wongwises and M. S. Shadloo, *Int. J. Greenh. Gas Control*, 2022, **119**, 103715.
89 W. Emori, I. I. Udoh, O. O. Ekerenam, A. I. Ikeuba, I. I. N. Etim, C. N. Njoku, E. F. Daniel, D. I. Njoku, P. C. Uzoma, S. K. Kolawole and O. S. Olanrele, *Greenh. Gases Sci. Technol.*, 2023, **13**, 876–904.
90 A. K. Sleiti, W. A. Al-Ammari, L. Vesely and J. S. Kapat, *J. Energy Resour. Technol. Trans. ASME*, 2022, **144**, 092106.
91 F. M. Orr, *Energy Environ. Sci.*, 2009, **2**, 449–458.
92 M. Cao, L. Zhao, D. Xu, R. Ciora, P. K. T. Liu, V. I. Manousiouthakis and T. T. Tsotsis, *J. Memb. Sci.*, 2020, **605**, 118028.
93 D. Jansen, M. Gazzani, G. Manzolini, E. Van Dijk and M. Carbo, *Int. J. Greenh. Gas Control*, 2015, **40**, 167–187.
94 A. Skorek-Osikowska, K. Janusz-Szymańska and J. Kotowicz, *Energy*, 2012, **45**, 92–100.
95 F. Dai, S. Zhang, Y. Luo, K. Wang, Y. Liu and X. Ji, *Processes*, 2023, **11**, 1765.
96 A. A. Olajire, *Energy*, 2010, **35**, 2610–2628.
97 A. Kather and G. Scheffknecht, *Naturwissenschaften*, 2009, **96**, 993–1010.
98 D. Y. C. Leung, G. Caramanna and M. M. Maroto-Valer, *Renew. Sustain. Energy Rev.*, 2014, **39**, 426–443.
99 B. J. P. Buhre, L. K. Elliott, C. D. Sheng, R. P. Gupta and T. F. Wall, *Prog. Energy Combust. Sci.*, 2005, **31**, 283–307.
100 S. Yadav and S. S. Mondal, *Fuel*, 2022, **308**, 122057.
101 I. Pfaff and A. Kather, *Energy Procedia*, 2009, **1**, 495–502.
102 S. M. Carpenter and H. A. Long, *Integr. Gasif. Comb. Cycle Technol.*, 2017, 445–463.
103 T. Burdyny and H. Struchtrup, *Energy*, 2010, **35**, 1884–1897.
104 A. Mukherjee, J. A. Okolie, A. Abdelrasoul, C. Niu and A. K. Dalai, *J. Environ. Sci.*, 2019, **83**, 46–63.
105 M. Kanniche, R. Gros-Bonnivard, P. Jaud, J. Valle-Marcos, J. M. Amann and C. Bouallou, *Appl. Therm. Eng.*, 2010, **30**, 53–62.
106 D. Loachamin, J. Casierra, V. Calva, A. Palma-Cando, E. E. Ávila and M. Ricaurte, *ChemEngineering*, 2024, **8**, 129.
107 H. A. Alalwan and A. H. Alminshid, *Sci. Total Environ.*, 2021, **788**, 147850.
108 D. Obi, S. Onyekuru and A. Orga, *Energy Sci. Eng.*, 2025, **13**, 980–994.
109 J. Singh and A. S. Dhaliwal, *Int. J. Environ. Sci. Technol.*, 2023, **20**, 11483–11500.
110 K. J. Hughes, K. A. Iyer, R. E. Bird, J. Ivanov, S. Banerjee, G. Georges and Q. A. Zhou, *ACS Appl. Nano Mater.*, 2024, **7**, 18695–18713.
111 M. Pardakhti, T. Jafari, Z. Tobin, B. Dutta, E. Moharreri, N. S. Shemshaki, S. Suib and R. Srivastava, *ACS Appl. Mater. Interfaces*, 2019, **11**, 34533–34559.
112 R. Morales-Ospino, L. Reinert, M. T. Izquierdo, A. Celzard, L. Duclaux and V. Fierro, *Environ. Res.*, 2025, **273**, 121211.
113 A. N. Shafawi, A. R. Mohamed, P. Lahijani and M. Mohammadi, *J. Environ. Chem. Eng.*, 2021, **9**, 106869.
114 H. E. Ashkanani, R. Wang, W. Shi, N. S. Siefert, R. L. Thompson, K. Smith, J. A. Steckel, I. K. Gamwo, D. Hopkinson, K. Resnik and B. I. Morsi, *Int. J. Greenh. Gas Control*, 2020, **101**, 103135.
115 P. Pourhakkak, A. Taghizadeh, M. Taghizadeh, M. Ghaedi and S. Haghdoust, *Interface Sci. Technol.*, 2021, **33**, 1–70.

116 M. E. Majchrowicz, D. W. F. Wim Brilman and M. J. Groeneveld, *Energy Proc.*, 2009, **1**, 979–984.
117 Y. Liu and J. Wilcox, *Environ. Sci. Technol.*, 2012, **46**, 1940–1947.
118 M. Sai Bhargava Reddy, D. Ponnamma, K. K. Sadasivuni, B. Kumar and A. M. Abdullah, *RSC Adv.*, 2021, **11**, 12658–12681.
119 S. K. Tiwari, M. Bystrzejewski, A. De Adhikari, A. Huczko and N. Wang, *Prog. Energy Combust. Sci.*, 2022, **92**, 101023.
120 E. Fleming, I. Kholmanov and L. Shi, *Carbon*, 2018, **136**, 380–386.
121 L. Zou, Y. Sun, S. Che, X. Yang, X. Wang, M. Bosch, Q. Wang, H. Li, M. Smith, S. Yuan, Z. Perry and H. C. Zhou, *Adv. Mater.*, 2017, **29**, 1700229.
122 Y. Hou, Y. Chen, X. He, F. Wang, Q. Cai and B. Shen, *Chem. Eng. J.*, 2024, **490**, 151424.
123 M. Gorbounov, P. Halloran and S. Masoudi Soltani, *J. CO_2 Util.*, 2024, **86**, 102908.
124 A. P. Khedulkar, R. G. Bobade, R. An Doong, B. Pandit, N. M. Ky, R. C. Ambare, T. D. Hoang and K. J. Kumar, *Mater. Today Chem.*, 2025, **46**, 102688.
125 V. Ramar and A. Balraj, *Energy Fuels*, 2022, **36**, 13479–13505.
126 C. H. Yu, C. H. Huang and C. S. Tan, *Aerosol Air Qual. Res.*, 2012, **12**, 745–769.
127 R. Singh, L. Wang, K. Ostrikov and J. Huang, *Adv. Mater. Interfaces*, 2024, **11**, 2202290.
128 I. Khan, A. Altaf, S. Sadiq, S. Khan, A. Khan, S. Khan, M. Humayun, A. Khan, R. A. Abumousa and M. Bououdina, *Chem. Eng. J. Adv.*, 2025, **21**, 100691.
129 Z. Zhu and B. Xu, *Separations*, 2022, **9**, 307.
130 H. Ma, H. Fu, Y. Tong, A. Umar, Y. M. Hung and X. Wang, *Carbon Capture Sci. Technol.*, 2025, **15**, 100441.
131 S. Kundu, T. Khandaker, M. A. A. M. Anik, M. K. Hasan, P. K. Dhar, S. K. Dutta, M. A. Latif and M. S. Hossain, *RSC Adv.*, 2024, **14**, 29693–29736.
132 D. A. Kang, C. Murphy and H. K. Jeong, *Microporous Mesoporous Mater.*, 2024, **369**, 113038.
133 L. Yang, W. Rui, Z. Qingmin, Z. Yuanlong, F. Xin and X. Zhaojie, *Unconv. Resour.*, 2024, **4**, 100096.
134 O. Awogbemi and D. A. Desai, *Discov. Nano*, 2025, **20**, 29.
135 D. Gendron and M. Zakharova, *Appl. Chem.*, 2024, **4**, 236–269.
136 Y. K. Leong, Y. J. Huang and J. S. Chang, *Int. J. Hydrogen Energy*, 2024, 998–1007.
137 T. Iglina, P. Iglin and D. Pashchenko, *Sustainability*, 2022, **14**, 3801.
138 J. Zhang, Z. Xia and L. Dai, *Sci. Adv.*, 2015, **1**, 1500564.
139 J. Wu, S. Ma, J. Sun, J. I. Gold, C. Tiwary, B. Kim, L. Zhu, N. Chopra, I. N. Odeh, R. Vajtai, A. Z. Yu, R. Luo, J. Lou, G. Ding, P. J. A. Kenis and P. M. Ajayan, *Nat. Commun.*, 2016, **7**, 13869.
140 Y. Song, W. Chen, C. Zhao, S. Li, W. Wei and Y. Sun, *Angew. Chem., Int. Ed.*, 2017, **56**, 10840–10844.
141 Y. Liu, Y. Zhang, K. Cheng, X. Quan, X. Fan, Y. Su, S. Chen, H. Zhao, Y. Zhang, H. Yu and M. R. Hoffmann, *Angew. Chem., Int. Ed.*, 2017, **56**, 15607–15611.
142 X. Liu, P. V. Kumar, Q. Chen, L. Zhao, F. Ye, X. Ma, D. Liu, X. Chen, L. Dai and C. Hu, *Appl. Catal., B*, 2022, **316**, 121618.
143 Y. Li, S. Zheng, H. Liu, Q. Xiong, H. Yi, H. Yang, Z. Mei, Q. Zhao, Z. W. Yin, M. Huang, Y. Lin, W. Lai, S. X. Dou, F. Pan and S. Li, *Nat. Commun.*, 2024, **15**, 176.
144 Y. Zhu, L. Chen, J. Pan, S. Jiang, J. Wang, G. Zhang and K. Zhang, *Prog. Mater. Sci.*, 2025, **148**, 101373.
145 M. S. Mohtasim and B. K. Das, *Renew. Sustain. Energy Rev.*, 2025, **218**, 115779.
146 A. M. Afridi, M. Aktary, S. Shaheen Shah, S. I. Mitu Sheikh, G. Jahirul Islam, M. Nasiruzzaman Shaikh and M. Abdul Aziz, *Chem. Rec.*, 2024, **24**, e202400144.
147 T. Qiao, H. Pan, Z. Han, Z. Zhang, S. Zhou, X. Lu and Y. Li, *Fuel*, 2025, **394**, 135129.
148 S. Assyl, S. Botakoz and Z. Saule, *Discov. Nano*, 2025, **20**, 115.
149 T. Zhao, Q. Wang, Y. Kawazoe and P. Jena, *Carbon*, 2018, **132**, 249–256.
150 A. J. Clancy, M. K. Bayazit, S. A. Hodge, N. T. Skipper, C. A. Howard and M. S. P. Shaffer, *Chem. Rev.*, 2018, **118**, 7363–7408.
151 S. K. Gebremariam, A. M. Varghese, S. Ehrling, Y. Al Wahedi, A. AlHajaj, L. F. Dumée and G. N. Karanikolos, *ACS Appl. Mater. Interfaces*, 2024, **16**, 50785–50799.
152 J. Serafin and B. Dziejarski, *Environ. Sci. Pollut. Res.*, 2024, **31**, 40008–40062.
153 S. K. Verma, P. Tripathi and A. Bhatnagar, *Nanomater. Carbon Dioxide Capture Convers. Technol.*, 2022, 245–260.
154 R. Balasubramanian and S. Chowdhury, *J. Mater. Chem. A*, 2015, **3**, 21968–21989.
155 B. Cui, X. Ju, H. Ma, S. Meng, Y. Liu, J. Wang, D. Wang and Z. Yang, *Sep. Purif. Technol.*, 2025, **354**, 128794.
156 S. Wang, Y. Xu, M. Yan, L. Zhang and Z. Liu, *J. Non. Cryst. Solids*, 2018, **499**, 101–106.
157 D. Gang, Z. Uddin Ahmad, Q. Lian, L. Yao and M. E. Zappi, *Chem. Eng. J.*, 2021, **403**, 126286.
158 S. Jung, Y. K. Park and E. E. Kwon, *J. CO2 Util.*, 2019, **32**, 128–139.
159 H. Ma, X. Ju, B. Cui, S. Meng, Y. Liu, J. Li, D. Wang and Z. Yang, *ACS Appl. Mater. Interfaces*, 2025, **17**, 13836–13850.
160 M. T. Dunstan, F. Donat, A. H. Bork, C. P. Grey and C. R. Müller, *Chem. Rev.*, 2021, **121**, 12681–12745.
161 Y. Shen, *Fuel Process. Technol.*, 2022, **236**, 107437.
162 M. Umar, B. O. Yusuf, M. Aliyu, I. Hussain, A. M. Alhassan, M. M. Awad, O. A. Taialla, B. Ali, K. R. Alhooshani and S. A. Ganiyu, *Coord. Chem. Rev.*, 2025, **526**, 216380.
163 Y. Mochizuki, J. Bud, E. Byambajav and N. Tsubouchi, *Carbon Resour. Convers.*, 2024, 100237.
164 M. S. Khosrowshahi, H. Mashhadimoslem, H. Shayesteh, G. Singh, E. Khakpour, X. Guan, M. Rahimi, F. Maleki, P. Kumar and A. Vinu, *Adv. Sci.*, 2023, **10**, 2304289.
165 P. Devi, A. Gupta and A. Kumar, *J. Energy Storage*, 2024, **97**, 102506.
166 M. K. Al Mesfer, *Environ. Sci. Pollut. Res.*, 2020, **27**, 15020–15028.
167 M. Aliyu, B. O. Yusuf, A. H. S. Abdullahi, A. I. Bakare, M. Umar, A. S. Hakeem and S. A. Ganiyu, *Sep. Purif. Technol.*, 2024, **340**, 126737.
168 O. F. Cruz, I. Campello-Gómez, M. E. Casco, J. Serafin, J. Silvestre-Albero, M. Martínez-Escandell, D. Hotza and C. R. Rambo, *Carbon Lett.*, 2023, **33**, 727–735.
169 C. Jin, J. Sun, Y. Chen, Y. Guo, D. Han, R. Wang and C. Zhao, *Sep. Purif. Technol.*, 2021, **276**, 119270.

170 S. Wang, Y. R. Lee, Y. Won, H. Kim, S. E. Jeong, B. Wook Hwang, A. Ra Cho, J. Y. Kim, Y. Cheol Park, H. Nam, D. H. Lee, H. Kim and S. H. Jo, *Chem. Eng. J.*, 2022, **437**, 135378.
171 X. L. Zhu, P. Y. Wang, C. Peng, J. Yang and X. Bin Yan, *Chin. Chem. Lett.*, 2014, **25**, 929–932.
172 A. D. Igalavithana, S. W. Choi, J. Shang, A. Hanif, P. D. Dissanayake, D. C. W. Tsang, J. H. Kwon, K. B. Lee and Y. S. Ok, *Sci. Total Environ.*, 2020, **739**, 139845.
173 K. Kumaraguru, P. Saravanan, L. Nagarajan, V. Saravanan, R. Rajeshkannan and M. Rajasimman, *Biomass Convers. Biorefinery*, 2023, 30447–30466.
174 K. Li, X. Niu, D. Zhang, H. Guo, X. Zhu, H. Yin, Z. Lin and M. Fu, *Environ. Pollut.*, 2022, **306**, 119399.
175 K. Li, D. Zhang, X. Niu, H. Guo, Y. Yu, Z. Tang, Z. Lin and M. Fu, *Sci. Total Environ.*, 2022, **826**, 154133.
176 H. Patel, H. Weldekidan, A. Mohanty and M. Misra, *Carbon Capture Sci. Technol.*, 2023, **8**, 100128.
177 S. Foorginezhad, M. M. Zerafat, M. Asadnia and G. Rezvannasab, *Mater. Chem. Phys.*, 2024, **317**, 129177.
178 A. Koli, R. Dhabbe, J. Shen, R. K. Motkuri and S. Sabale, *Biomass Convers. Biorefinery*, 2024, **14**, 18789–18801.
179 S. Deng, B. Hu, T. Chen, B. Wang, J. Huang, Y. Wang and G. Yu, *Adsorption*, 2015, **21**, 125–133.
180 Y. Xu, Y. Liu, W. Zhan, D. Zhang, Y. Liu, Y. Xu and Z. Wu, *Biomass Bioenergy*, 2024, **183**, 100339.
181 A. E. Ogungbenro, D. V. Quang, K. A. Al-Ali, L. F. Vega and M. R. M. Abu-Zahra, *J. Environ. Chem. Eng.*, 2018, **6**, 4245–4252.
182 A. Koli, A. K. Battu, R. K. Motkuri and S. Sabale, *Biomass Convers. Biorefinery*, 2024, **14**, 10177–10188.
183 P. B. Ramos, F. Jerez, M. Erans, A. Mamaní, M. F. Ponce, M. F. Sardella, E. S. Sanz-Pérez, R. Sanz, A. Arencibia and M. A. Bavio, *Biomass Bioenergy*, 2025, **194**, 107669.
184 P. B. Ramos, A. Mamaní, M. Erans, F. Jerez, M. F. Ponce, M. F. Sardella, A. Arencibia, M. A. Bavio, E. S. Sanz-Pérez and R. Sanz, *Energy Fuels*, 2024, **38**, 6102–6115.
185 P. B. Ramos, A. Mamani, M. F. Sardella, A. Arencibia, R. Sanz, E. S. Sanz-Pérez, M. A. Bavio and M. Erans, *Energy Fuels*, 2025, **39**, 5442–5452.
186 A. Okhovat, A. Ahmadpour, F. Ahmadpour and Z. Khaki Yadegar, *ISRN Chem. Eng.*, 2012, **2012**, 1–10.
187 M. Sevilla, N. Alam and R. Mokaya, *J. Phys. Chem. C*, 2010, **114**, 11314–11319.
188 P. Toh-ae, N. Timasart, D. Tumnantong, T. Bovornratanaraks and S. Poompradub, *Sci. Rep.*, 2024, **14**, 17100.
189 Y. Yang, Y. Liu, S. Liu, Y. Zhao, Q. Zhang, L. Su, Z. Chen and M. Zhao, *Chem. Eng. Sci.*, 2024, **292**, 119968.
190 M. Lotfinezhad, M. Tahmasebpoor and C. Pevida, *Environ. Res.*, 2024, **263**, 120017.
191 R. Morales-Ospino, A. Taurbekov, J. Castro-Gutiérrez, M. T. Izquierdo, M. Atamanov, Z. Mansurov, A. Celzard and V. Fierro, *Carbon*, 2025, **234**, 119978.
192 M. Gorbounov, L. Hecquet-Perrot, S. Ignatova, P. Hewitson and S. M. Soltani, *Next Mater.*, 2025, **6**, 100321.
193 Z. Ye, C. Han, M. Pan, L. Zhao, N. Liu, A. Nikiforov, K. Leus, N. De Geyter, R. Morent, J. Chen and J. Li, *Chem. Eng. J.*, 2025, **507**, 160530.
194 E. H. Al-Ghurabi, M. M. Boumaza, W. Al-Masry and M. Asif, *Sci. Rep.*, 2025, **15**, 17132.
195 Y. Long, H. Tian, C. H. Lee, H. Li, Z. Zeng, Z. Yang, G. Zhu, X. Chen and L. Liu, *Sep. Purif. Technol.*, 2025, **359**, 130476.
196 J. A. O. Chagas, B. P. Pinto, A. L. de Lima and C. J. A. Mota, *Energy Fuels*, 2025, **39**, 15039–15050.
197 J. Wang, Y. Yin, X. Liu, Y. Liu, Q. Xiao, L. Zhao, M. Demir, M. Ö. Alaş Çolak, L. Wang and X. Hu, *Sep. Purif. Technol.*, 2025, **376**, 134079.
198 J. Shao, Y. Wang, M. Che, Q. Xiao, M. Demir, M. K. Al Mesfer, L. Wang, X. Hu and Y. Liu, *J. Energy Inst.*, 2025, **123**, 102273.
199 Y. Zhi, J. Shao, J. Wang, X. Liu, Q. Xiao, M. Demir, U. B. Simsek, L. Wang and X. Hu, *Molecules*, 2025, **30**, 3990.
200 Z. Zhang, Z. P. Cano, D. Luo, H. Dou, A. Yu and Z. Chen, *J. Mater. Chem. A*, 2019, **7**, 20985–21003.
201 A. Martínez-Alonso, J. M. D. Tascón and E. J. Bottani, *J. Phys. Chem. B*, 2001, **105**, 135–139.
202 N. Kuganathan, *Fuels*, 2022, **3**, 176–183.
203 P. Rezaee, S. A. Asl, M. H. Javadi, S. Rezaee, R. Morad, M. Akbari, S. S. Arab and M. Maaza, *Sci. Rep.*, 2024, **14**, 12388.
204 A. A. Khan, R. Ahmad, I. Ahmad and X. Su, *J. Mol. Graph. Model.*, 2021, **103**, 107806.
205 H. Dong, B. Lin, K. Gilmore, T. Hou, S. T. Lee and Y. Li, *Curr. Appl. Phys.*, 2015, **15**, 1084–1089.
206 M. Kabiri and A. Bahrami, *Comput. Theor. Chem.*, 2024, **1233**, 114482.
207 S. Anila and C. H. Suresh, *New J. Chem.*, 2023, **47**, 3047–3054.
208 A. S. Palakkal and R. S. Pillai, *Sep. Purif. Technol.*, 2023, **325**, 124650.
209 J. Singh and A. S. Dhaliwal, *Polym. Bull.*, 2024, **81**, 13155–13182.
210 M. Cinke, J. Li, C. W. Bauschlicher, A. Ricca and M. Meyyappan, *Chem. Phys. Lett.*, 2003, **376**, 761–766.
211 M. A. O. Lourenço, M. Fontana, P. Jagdale, C. F. Pirri and S. Bocchini, *Chem. Eng. J.*, 2021, **414**, 128763.
212 N. Salehi Ardali, S. Riahi, M. Abbasi and N. Mohammadpour, *Fuel*, 2023, **338**, 127213.
213 Z. Khoshraftar, A. Ghaemi and A. Hemmati, *Sci. Rep.*, 2024, **14**, 5130.
214 R. Xu, S. Kim, H. Ahn, H. S. Kim, M. Kim and Y. T. Kang, *Sep. Purif. Technol.*, 2025, **356**, 129922.
215 Y. Wang, C. Zhang, M. Tang, J. Liu, J. Yuan, Y. Zhao and G. Zhang, *J. Environ. Chem. Eng.*, 2024, **12**, 114452.
216 M. Heidari, S. Borhan Mousavi, F. Rahmani, P. T. Clough and S. Ozmen, *Energy Convers. Manag.*, 2022, **274**, 116461.
217 Y. Zhang, J. Sun, J. Tan, C. H. Ma, S. Luo, W. Li and S. Liu, *Fuel*, 2021, **305**, 121622.
218 Y. Li, W. Zha, J. Zhang, W. Chen, Q. Yang, S. Zhong and Y. Z. Lei, *Fuel*, 2025, **382**, 133809.
219 T. S. Mirmiran, S. Riahi, M. Abbasi and M. Mohammadi-Khanaposhtani, *J. Environ. Chem. Eng.*, 2025, **13**, 119213.
220 M. I. Katsnelson, *Mater. Today*, 2007, **10**, 20–27.
221 K. Bansal, J. Singh and A. S. Dhaliwal, *Fullerenes, Nanotubes Carbon Nanostruct.*, 2024, **32**, 651–663.
222 K. Bansal, J. Singh and A. S. Dhaliwal, *Inorg. Nano-Metal Chem.*, 2024, **54**, 1145–1153.

223 K. Bansal, J. Singh and A. S. Dhaliwal, *Fullerenes, Nanotubes Carbon Nanostruct.*, 2023, **31**, 277–287.
224 A. K. Pathak, M. Borah, A. Gupta, T. Yokozeki and S. R. Dhakate, *Compos. Sci. Technol.*, 2016, **135**, 28–38.
225 C. Kumar, A. Gupta, P. Saharan, M. Singh and S. R. Dhakate, *Diam. Relat. Mater.*, 2023, **140**, 110433.
226 J. Ai, Z. Bacsik, K. Hallstensson, J. Yuan, A. Sugunan and N. Hedin, *Chem. Eng. J.*, 2025, **506**, 159963.
227 B. E. Arango Hoyos, H. F. Osorio, E. K. Valencia Gómez, J. Guerrero Sánchez, A. P. Del Canto Palominos, F. A. Larrain and J. J. Prías Barragán, *Sci. Rep.*, 2023, **13**, 14476.
228 W. Choi, Y. Ho Cho, T. Kim, C. H. Lee, J. Y. Kim, S. H. So, K. Eum, C. H. Lee and D. W. Kim, *Sep. Purif. Technol.*, 2025, **354**, 129270.
229 H. Dong, Y. Wang, W. Ding, Y. Qiu and H. He, *Sep. Purif. Technol.*, 2025, **354**, 129158.
230 Y. Wang, H. Wang, T. C. Zhang, S. Yuan and B. Liang, *J. Power Sources*, 2020, **472**, 228610.
231 M. He, H. Zhao, J. Jia, W. Zhou, Z. Wang, K. An, Y. Jiao, X. Yang, X. Zhang and T. Fan, *Environ. Res.*, 2025, **267**, 120701.
232 S. Chakraborty, R. Saha and S. Saha, *Environ. Sci. Pollut. Res.*, 2023, **31**, 67633–67663.
233 A. M. Varghese, K. S. K. Reddy, N. Bhoria, S. Singh, J. Pokhrel and G. N. Karanikolos, *Chem. Eng. J.*, 2021, **420**, 129677.
234 Z. Zhou, E. Davoudi and B. Vaferi, *J. Environ. Chem. Eng.*, 2021, **9**, 106202.
235 Y. Hosseini, M. Najafi, S. Khalili, M. Jahanshahi and M. Peyravi, *Mater. Chem. Phys.*, 2021, **270**, 124788.
236 V. V. Chaban and N. A. Andreeva, *Phys. Chem. Chem. Phys.*, 2022, **24**, 25801–25815.
237 Y. Nan, D. Gomez-Maldonado, K. Zhang, H. Du, D. C. Whitehead, M. Li, X. Zhang and M. S. Peresin, *Carbohydr. Polym. Technol. Appl.*, 2024, **8**, 100585.
238 M. P. Jerome, A. Mathai Varghese, S. Kuppireddy, G. N. Karanikolos and N. Alamoodi, *Sep. Purif. Technol.*, 2025, **360**, 131089.
239 R. Navik, E. Wang, X. Ding, H. Yunyi, Y. Liu and J. Li, *J. Energy Chem.*, 2025, **100**, 653–664.
240 A. Sharma, R. Kumar, A. Gupta, P. R. Agrawal, N. Dwivedi, D. P. Mondal, A. K. Srivastava and S. R. Dhakate, *Mater. Today Commun.*, 2022, **30**, 103055.
241 D. F. Maquíñez-Buitrago, J. M. Ramos-Rincón, L. Giraldo and J. C. Moreno-Piraján, *Hybrid Adv.*, 2024, **6**, 100219.
242 B. Zhang, Y. Jiang and R. Balasubramanian, *Resour. Conserv. Recycl.*, 2022, **185**, 106453.
243 M. Zhou, Y. Lin, H. Xia, X. Wei, Y. Yao, X. Wang and Z. Wu, *Nano-Micro Lett.*, 2020, **12**, 58.
244 M. Vorokhta, M. I. M. Kusdhany, D. Vöröš, M. Nishihara, K. Sasaki and S. M. Lyth, *Chem. Eng. J.*, 2023, **471**, 144524.
245 L. F. Cai, J. M. Zhan, J. Liang, L. Yang and J. Yin, *Sci. Rep.*, 2022, **12**, 3118.
246 X. Liu, C. Wang, C. Chen, Z. Pan, C. Gao, W. Lai, J. Zhao, T. Tian and W. Xiao, *Coord. Chem. Rev.*, 2025, **544**, 216927.
247 L. Estevez, D. Barpaga, J. Zheng, S. Sabale, R. L. Patel, J. G. Zhang, B. P. McGrail and R. K. Motkuri, *Ind. Eng. Chem. Res.*, 2018, **57**, 1262–1268.
248 L. Wang, Y. Ma, H. Liu, Y. Guo, B. Yang and B. Chang, *Sep. Purif. Technol.*, 2025, **354**, 128910.
249 L. Zheng, W. B. Li and J. L. Chen, *RSC Adv.*, 2018, **8**, 29767–29774.
250 P. C. Sahoo, R. Singh, P. Sivagurunathan, D. Singh, M. Kumar, R. P. Gupta and U. Srivastava, *Int. J. Greenh. Gas Control*, 2025, **142**, 104340.
251 M. Samandari, M. T. Broud, D. P. Harper and D. J. Keffer, *J. Phys. Chem. B*, 2024, **128**, 8530–8545.
252 M. T. Broud, M. Samandari, L. Yu, D. P. Harper and D. J. Keffer, *J. Phys. Chem. C*, 2023, **127**, 13639–13650.
253 Y. Ru, G. I. N. Waterhouse and S. Lu, *Aggregate*, 2022, **3**, e296.
254 Y. Liu, D. Zhong, L. Yu, Y. Shi and Y. Xu, *Nanomaterials*, 2023, **13**, 437.
255 A. Khayal, V. Dawane, M. A. Amin, V. Tirth, V. K. Yadav, A. Algahtani, S. H. Khan, S. Islam, K. K. Yadav and B. H. Jeon, *Polymers*, 2021, **13**, 3190.
256 C. Wang, A. Inazaki, T. Shirai, Y. Tanaka, T. Sakuta, H. Takikawa and H. Matsuo, *Thin Solid Films*, 2003, **425**, 41–48.
257 R. Dubrovsky, V. Bezmelnitsyn and A. Eletskii, *Carbon*, 2004, **42**, 1063–1066.
258 C. Ng, W. E. Marshall, R. M. Rao, R. R. Bansode and J. N. Losso, *Ind. Crops Prod.*, 2003, **17**, 209–217.
259 I. M. Lima, A. McAloon and A. A. Boateng, *Biomass Bioenergy*, 2008, **32**, 568–572.
260 C. A. Toles, W. E. Marshall, M. M. Johns, L. H. Wartelle and A. McAloon, *Bioresour. Technol.*, 2000, **71**, 87–92.
261 G. G. Stavropoulos and A. A. Zabaniotou, *Fuel Process. Technol.*, 2009, **90**, 952–957.
262 D. A. Yang, H. Y. Cho, J. Kim, S. T. Yang and W. S. Ahn, *Energy Environ. Sci.*, 2012, **5**, 6465–6473.
263 M. Ding, R. W. Flaig, H. L. Jiang and O. M. Yaghi, *Chem. Soc. Rev.*, 2019, **48**, 2783–2828.
264 Y. Li, Y. Wang, N. Liu, B. Wang and R. Dong, *Colloids Surf., A*, 2023, **658**, 130732.
265 N. Kostkova, M. Vorokhta, M. Kormunda, R. Pilar, G. Sadovska, P. Honcova, E. Mikyskova, J. Moravkova and P. Sazama, *Microporous Mesoporous Mater.*, 2024, **379**, 113286.
266 J. Li, M. Hou, Y. Chen, W. Cen, Y. Chu and S. Yin, *Appl. Surf. Sci.*, 2017, **399**, 420–425.
267 H. Li, J. Bin Niu, K. J. Tay, M. C. Tan and H. Y. Low, *ACS Sustainable Chem. Eng.*, 2024, **12**, 2911–2920.
268 H. J. Esfahani, A. Ghaemi and S. Shahhosseini, *Sci. Rep.*, 2024, **14**, 18871.
269 Y. Gong and T. He, *Small Methods*, 2023, **7**, 2300702.
270 F. Eshraghi, M. Anbia and S. Salehi, *J. Environ. Chem. Eng.*, 2017, **5**, 4516–4523.
271 H. Kiuchi, R. Shibuya, T. Kondo, J. Nakamura, H. Niwa, J. Miyawaki, M. Kawai, M. Oshima and Y. Harada, *Nanoscale Res. Lett.*, 2016, **11**, 127.
272 R. Ben Said, J. M. Kolle, K. Essalah, B. Tangour and A. Sayari, *ACS Omega*, 2020, **5**, 26125–26133.
273 F. Rezaei and C. W. Jones, *Ind. Eng. Chem. Res.*, 2013, **52**, 12192–12201.